UNIVERSITY OF WAH

5th Pak-Turk
ETSE
2022

5th Pak-Turk International Conference
on Emerging Technologies in the Field of Sciences and Engineering

1st and 2nd December, 2022

CONFERENCE PROCEEDINGS

The Pak-Turk Conference series is the technical event which focuses on the advances in new technologies in engineering sciences, computer sciences and natural sciences. The series of event was initiated in 2018 and since then these conferences have been successfully organized every year. The purpose of this conference is to provide a platform for researchers, academicians and practitioners to make them familiar with recent advancements in the various fields of engineering and sciences. The conference accepts wide range of abstracts/papers from Turkish and Pakistani participants to encourage young and experienced researches to present their work and also the possibility of initiating mutual collaboration with international repute researchers and industry personals.

5th Pak-Turk International Conference

on Emerging Technologies in the field of Sciences and Engineering

1st and 2nd, December 2022

CONFERENCE PROCEEDINGS

Editors:
Dr Syed Waqas Hassan
Ms Zeenat Haq

Published and Organized by University of Wah, Wah Cantt, Pakistan

TABLE OF CONTENTS

Sr. No.	Research Article	Page No.
1.	Numerical Investigation of Dual Flow Integral Fin Mini Channels Using Nano Fluid	1-6
2.	Thermal Investigation of Rectangular Header Normal Channel Facile Heat Sink Using Hybrid Nano Fluids	7-12
3.	A Data Mining Perspective on Polio Eradication in Pakistan	13-22
4.	Finite Element Modeling of Residual Stress and Distortion in Dissimilar TIG Welded Joints of Aluminum 2024 and Stainless Steel 304	23-30
5.	Tribological Analysis of Ionic Liquid as an Additive to the Bio Based Oils	31-42
6.	A Statistical Framework for Optimization of Cylindrical Grinding Parameters on AISI-D6 Steel	43-51
7.	Design and Development of Speed Bumps System for Energy Scavenging	52-58
8.	Thermal analysis and the optimum pin fin configuration for a heat sink design for a central processor unit (CPU)	59-64
9.	Mechanical and durability properties of 3D printing concrete A-Review	65-72
10.	Comparatively Study Between Monocrystalline and Polycrystalline Photovoltaic Panel Based on PCM	73-79
11.	Comparative Analysis of Software Development Process Models	80-90
12.	A Short Review on Latest Technologies for the Pretreatment of Lignocellulosic Biomass	91-105
13.	Gender Classification Using Novel Acoustics Deviated Local Ternary Patterns	106-111

Numerical Investigation of Dual Flow Integral Fin Mini Channels Using Nano Fluid

Taha Baig [1,2, a], Amna Adil [1,2, b], S. Manzoor [1, b]*, Ebrahem Khalid[1, d], Abid Hussain[1, e] and Muzaffar Ali [1, f]
[1]*Department of Mechanical Engineering, University of Engineering and Technology Taxila*
[2] *Department of Mechanical Engineering, Wah Engineering College, University of Wah, Wah Cantt, Pakistan*
*Correspondence: sherry.manzoor@gmail.com

Email address: [a)] tahabaig893@gmail.com, [b)] amnaadil2022@gmail.com, [c)] sherry.manzoor@gmail.com, [d)] ebrahem.khalid@uettaxila.edu, [e)] abid.hussain@uettaxila.edu.pk, [f)] muzaffar.ali@uettaxila.edu.pk

***Abstract*—To meet today's technological demand, performance of the electronic devices needs to increases at a faster rate. High performance electronic devices generate more heat which eventually becomes a bottle neck problem for the IT industry. The generated heat flux needs to be timely removed to maintain the temperature within a safe threshold range. Water cooled mini channels have gained significance because of better thermal conductivity as compared with air. In the current investigation, the thermal performance of the mini channels is enhanced using nano fluids. Results are discussed in terms of base temperature reduction, enhancement in heat transfer, decrement in the thermal resistance and increment in pressure drop.**

Keywords—Integral fins, Dual flow heat sinks, Nano fluids

I. INTRODUCTION

With the rapid advancement in technology, high flux generation inside electronic devices becomes a significant issue. The air-cooling technique has now reached its limit which is able to remove a maximum flux of 100W/cm^2. For management of higher flux, attention is focused on the water-based cooling systems. Jajja et al [1] performed experimental investigations on mini channel heat sink with single inlet and single outlet, using water as the base fluid. They reported that decrement in fin spacing causes an increment in heat transfer. Baig et al [2] performed numerical investigations on slotted mini channel heat sink and reported maximum heat transfer recorded for 0.5mm fin spacing as 1.6% compared with straight integral mini channel heat sink. Tariq et al [3] performed numerical investigation on mini-channel heatsink. It was reported that by using double flow configuration better base temperature distribution was observed as compared to single flow configuration. Literature review of different studies on Nano fluids is mentioned in TABLE 1.

Evidently from the literature; nano fluids play a significant role in effective thermal management. For the current investigation, thermal behavior of a dual integral mini-channel heat sink is enhanced using nano fluids. SiO_2-H_2O nano fluid is used in a straight integral fin dual flow mini channel heat sink as the focus of the current study.

II. NUMERICAL MODEL

A. Methodology for Numerical Model

ANSYS / Fluent is used in this study. To solve the numerical model for steady, absolute velocity formulation, k-ε realizable model, semi-implicit method model was used. For multiphase mixture model two number of Eulerian phases were used i.e., one for water and second for nano fluids. Second order upwind scheme is used for momentum discretization and turbulence in kinetic energy.

TABLE I: LITERATURE REVIEW OF DIFFERENT STUDIES ON NANO FLUIDS

Sr. No	Types of Nano fluids	Type of study	Literature
01	Copper Oxide (CuO-H_2O)	Numerical	Mohsen et al [4], Anwar et al [5]
		Experimental	Afzal et al [6], Sivasubramanian et al [7], Rimbault et al [8], Ali et al [9], Siddiqui et al [10], Tariq et al [11]
02	Titanium oxide (TiO_2-H_2O)	Numerical	Tariq et al [12]
		Experimental	Miry et al [13], Roshani et al [14], Tariq et al [12]
03	Aluminum oxide (Al_2O_3-H_2O)	Numerical	Saeed and kim [15]
		Experimental	Siddiqui et al [10], Miry et al [13], Neyestani et al [16], Roshani et al [14], Tariq et al [11], Itankar et al [17]
04	Silicon oxide (SiO_2-H_2O)	Numerical	Fazeli et al[18]
		Experimental	Fazeli et al[18]

B. Assumptions for Numerical Model

Incompressible and steady flow, no viscous heating, heat generation, and radiation heat transfer, while constant thermal properties throughout the heat sink have been considered.

C. Boundary Conditions for Numerical Model:

Zero-gauge pressure at outlet, fixed heat flux of 325W (supplied from the bottom of heatsink), and uniform inlet velocity. The right left and the top surfaces are considered adiabatic, inlet fluid temperature is considered to be constant ($T_i = 27$℃). For multiphase flow volumetric concentration (∅) 0.005% and 0.01% have been investigated.

D. Governing Equations for Single Phase Flow:

Mass momentum and energy equations used for single phase flow are as,

$$\frac{\partial}{\partial x_i}(\rho u_i) = 0 \tag{1}$$

$$\frac{\partial}{\partial x_i}(\rho u_i u_j) = -\frac{\partial \rho}{\partial x_j} + \frac{\partial}{\partial x_i}\left[(\mu + \mu_t)\frac{\partial u_j}{\partial x_i}\right] + \frac{\partial}{\partial x_i}\left[(\mu + \mu_t)\frac{\partial u_i}{\partial x_j}\right], \mathrm{j} = 1, 2, 3 \tag{2}$$

$$\frac{\partial}{\partial x_i}(\rho u_i T) = \frac{\partial}{\partial x_i}\left[\left(\frac{\lambda}{c_p} + \frac{\mu_t}{\sigma_t}\right)\frac{\partial T}{\partial x_i}\right] \tag{3}$$

E. Governing Equations for Multi-Phase Flow:

Many researchers extensively utilized multiphase model for simulations of the nano fluids Minea et al [19] and Saadoon et al [20].

Mass, momentum, energy and volumetric fraction are written below,

$$\nabla.\left(\rho_m \overrightarrow{V_m}\right) = 0 \tag{4}$$

$$\nabla.\left(\rho_m \overrightarrow{V_m}\,\overrightarrow{V_m}\right) = -\nabla p + \nabla.\left(\mu_m \nabla \overrightarrow{V_m}\right) + \rho_m \vec{g} + \nabla.\left(\sum_{k=1}^{n} \varphi_k \rho_k \overrightarrow{V_{dr,k}}\,\overrightarrow{V_{dr,k}}\right) \tag{5}$$

$$\nabla.\sum_{k=1}^{n}(\varphi_k\,\overrightarrow{v_k}(\rho_k H_k + p_m)) = \nabla.(k_m \nabla T) \tag{6}$$

$$\nabla.\left(\varphi_{np}\rho_{np}\overrightarrow{V_m}\right) = -\nabla.\left(\varphi_{np}\rho_{np}\overrightarrow{V_{dr,k}}\right. \tag{7}$$

III. INDEPENDENT MESH STUDY

To check authenticity of the numerical results, sensitivity analysis is performed. Tetrahedral mesh with an aspect ratio of unity and element size of 2.9 x 10^{-4} is used. Six different cases of varying number of elements as shown in Fig. 1(a) were analyzed. Difference in temperature (of base and inlet) recorded for 2.9 million and 3.1 million is found to be less than 0.5% so to save computation power and time, mesh with 2.9 million elements is selected for the entire study.

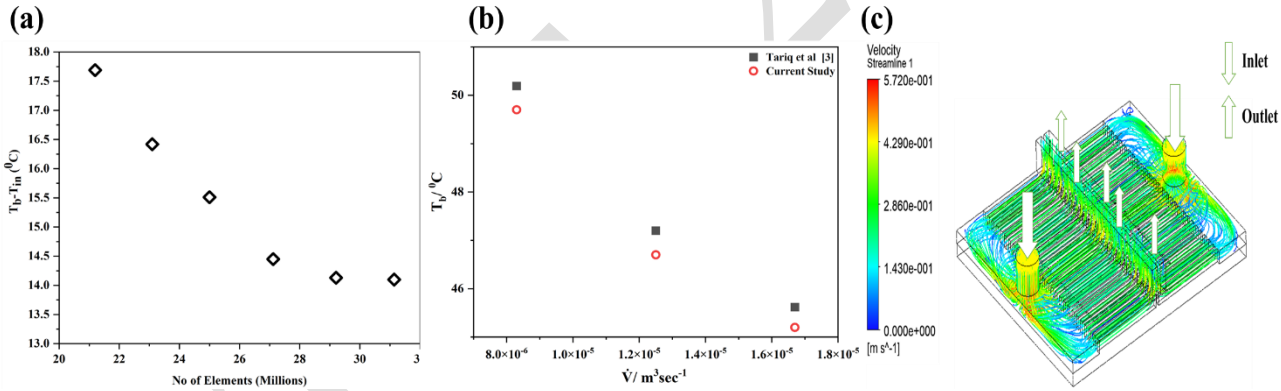

Fig. 1 : *(a) Independent Mesh, (b) Numerical model validation (c) Flow propagation*

IV. VALIDATION OF NUMERICAL MODEL

The base temperature of straight integral fin Mini channel heat sink is compared with literature Tariq et al [3]. All the data points are plotted against the volumetric flow rate as shown in Fig. 1(b) and quite good agreement was found between the current study and the literature Tariq et al [3].

V. HEAT SINK FLOW DESCRIPTION

Fig. 1 (c) shows the flow propagation inside the heat sink. Heat sink is divided equally into two parts. Dual circular channels are provided as inlet and rectangular channels are provided as outlet. A square chip of 28.7mm ×28.7mm is made at the bottom of the heat to provide uniform heat flux.

VI. DATA REDUCTION

Heat transfer, log mean temperature difference (LMTD) and thermal resistance is calculated as,

$$\dot{Q}=\dot{m}C_p(T_O - T_i) \quad (8)$$

$$LMTD = \frac{(T_b-T_{in})-(T_b-T_o)}{ln\left(\frac{(T_b-T_{in})}{(T_b-T_o)}\right)} \quad (9)$$

$$R_{th} = \frac{LMTD}{\dot{Q}} \quad (10)$$

VII. RESULTS AND DISCUSSION

A. *Base Temperature*

Fig. 2 (a) shows the temperature recorded at the base of the heat sink for different volumetric flow rates**.** Decrement in base temperature is observed by increment in volumetric flow rate. The trend reflects that the SiO_2-H_2O nano fluid plays a significant role in maintaining the base temperature of the mini channel heat sink. It is observed that minimum base temperature is recorded at volumetric concentration ($\emptyset = 0.01\%$). Also, increment in volumetric concentration causes decrement in base temperature. The percentage reduction in thermal resistance recorded at volumetric concentration ($\emptyset = 0.01\%$) was 8.32%,5.61% and 4.31% as compared with Tariq *et al* [3] and 16%,13.49% and 11.42% respectively as compared with Jajja et al [1] at varying volumetric flow rates.

B. *Thermal Resistance*

Thermal resistance recoded for the heat sink is shown in Fig. 2 (b). By increment in volumetric flow rate, thermal resistance decreases. Minimum thermal resistance is observed at volumetric concentration of 0.01%. Also, by increasing the volumetric concentration, the thermal resistance decreases. Percentage reduction in thermal resistance was recorded as 30.3%,22.68% and 19.02% as compared with Tariq et al [3] and 33.5%,25.25% and 20.37% as compared with Jajja et al [1] at varying volumetric flow rates.

C. *Pressure Drop*

The plot for the pressure drop is shown in Fig. 2 (c). It was observed that by using the nano fluid and by increasing the volumetric concentration, the pressure drops increases. Percentage increment in pressure drop recorded at volumetric concentration of 0.01% was 18.22%,10.89% and 6.53% as compared with Tariq et al [3] at varying volumetric flow rates.

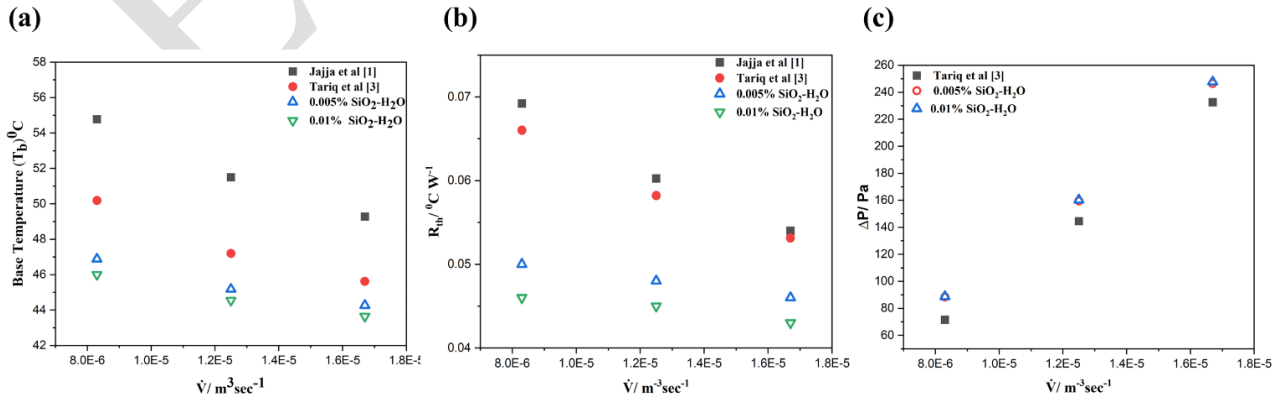

Fig. 2: *(a) Base Temperature, (b) Thermal resistance, (c) Pressure drop*

VIII. CONCLUSIONS

Findings of the current numerical investigation have been presented in the form of base temperature, thermal resistance and pressure drop. By increasing volumetric concentration, base temperature and thermal resistance decrease while the pressure drops increases. Maximum reduction in base temperature was observed as 8.32% and 16%, reduction in thermal resistance was recorded as 30.3% and 33.5% at a volumetric flow rate of 8.3×10^{-6} m^3s^{-1}. The maximum increment in pressure drop was observed as 18%. This is because the nano fluid increases the fluid viscosity which causes an increment in pressure drop.

ACKNOWLEDGMENT

This work is supported by Mechanical Engineering Department, UET Taxila and Wah Engineering College, University of Wah, which is gratefully acknowledged.

REFERENCES

[1] S. A. Jajja, W. Ali, H. M. Ali, and A. M. Ali, "Water cooled minichannel heat sinks for microprocessor cooling: Effect of fin spacing," *Appl. Therm. Eng.*, vol. 64, no. 1–2, pp. 76–82, 2014, doi: 10.1016/j.applthermaleng.2013.12.007.

[2] T. Baig *et al.*, "Thermal performance investigation of slotted fin minichannel heat sink for microprocessor cooling," *Energies*, vol. 14, no. 19, pp. 1–15, 2021, doi: 10.3390/en14196347.

[3] H. A. Tariq, M. Anwar, H. M. Ali, and J. Ahmed, "Effect of dual flow arrangements on the performance of mini-channel heat sink: numerical study," *J. Therm. Anal. Calorim.*, vol. 143, no. 3, pp. 2011–2027, 2021, doi: 10.1007/s10973-020-09617-8.

[4] S. A. A. Al-Mohsen, I. M. Abed, and F. H. Ali, "A numerical comparison of circular and corrugation heat sink for laminar CuO–water nano-fluid flow and heat transfer enhancement," *Appl. Nanosci.*, pp. 1–28, 2021.

[5] M. Anwar, H. A. Tariq, A. A. Shoukat, H. M. Ali, and H. Ali, "Numerical study for heat transfer enhancement using cuo-water nanofluids through mini-channel heat sinks for microprocessor cooling," *Therm. Sci.*, vol. 24, no. January, pp. 2965–2976, 2020, doi: 10.2298/TSCI180722022A.

[6] A. Afzal, A. D. M. Samee, and R. K. A. Razak, "Experimental thermal investigation of CuO-W nanofluid in circular minichannel," *Model Meas Control B*, vol. 86, no. 2, pp. 335–344, 2017.

[7] M. Sivasubramanian, T. Theivasanthi, and R. Manimaran, "Experimental investigation on heat transfer enhancement in a minichannel using CuO-water nanofluid," *Int. J. Ambient Energy*, vol. 40, no. 8, pp. 847–853, 2019.

[8] B. Rimbault, C. T. Nguyen, and N. Galanis, "Experimental investigation of CuO–water nanofluid flow and heat transfer inside a microchannel heat sink," *Int. J. Therm. Sci.*, vol. 84, pp. 275–292, 2014.

[9] M. Ali, A. A. Shoukat, H. A. Tariq, M. Anwar, and H. Ali, "Header design optimization of mini-channel heat sinks using CuO–H2O and Al2O3–H2O nanofluids for thermal

management," *Arab. J. Sci. Eng.*, vol. 44, no. 12, pp. 10327–10338, 2019.

[10] N. S. Al-Zubaidi, A. A. Alwasiti, and D. Mahmood, "A comparison of nano bentonite and some nano chemical additives to improve drilling fluid using local clay and commercial bentonites," *Egypt. J. Pet.*, vol. 26, no. 3, pp. 811–818, 2017, doi: 10.1016/j.ejpe.2016.10.015.

[11] H. A. Tariq, A. A. Shoukat, M. Hassan, and M. Anwar, "Thermal management of microelectronic devices using micro-hole cellular structure and nanofluids," *J. Therm. Anal. Calorim.*, vol. 136, no. 5, pp. 2171–2182, 2019, doi: 10.1007/s10973-018-7852-0.

[12] H. A. Tariq, M. Anwar, A. Malik, and H. M. Ali, "Hydro-thermal performance of normal-channel facile heat sink using TiO2-H2O mixture (Rutile–Anatase) nanofluids for microprocessor cooling," *J. Therm. Anal. Calorim.*, vol. 145, no. 5, pp. 2487–2502, 2021, doi: 10.1007/s10973-020-09838-x.

[13] S. Z. Miry, M. Roshani, P. Hanafizadeh, M. Ashjaee, and F. Amini, "Heat Transfer and Hydrodynamic Performance Analysis of a Miniature Tangential Heat Sink Using Al2O3-H2O and TiO2-H2O Nanofluids," *Exp. Heat Transf.*, vol. 29, no. 4, pp. 536–560, 2016, doi: 10.1080/08916152.2015.1046016.

[14] M. Roshani, S. Z. Miry, P. Hanafizadeh, and M. Ashjaee, "Hydrodynamics and heat transfer characteristics of a miniature plate pin-fin heat sink utilizing Al2O3-Water and TiO2-water nanofluids," *J. Therm. Sci. Eng. Appl.*, vol. 7, no. 3, pp. 1–12, 2015, doi: 10.1115/1.4030103.

[15] M. Saeed and M. H. Kim, "Heat transfer enhancement using nanofluids (Al2O3-H2O) in mini-channel heatsinks," *Int. J. Heat Mass Transf.*, vol. 120, pp. 671–682, 2018, doi: 10.1016/j.ijheatmasstransfer.2017.12.075.

[16] M. Neyestani, M. Nazari, M. M. Shahmardan, M. Sharifpur, M. Ashouri, and J. P. Meyer, "Thermal characteristics of CPU cooling by using a novel porous heat sink and nanofluids: Comparative experimental study," *J. Therm. Anal. Calorim.*, vol. 138, no. 1, pp. 805–817, 2019, doi: 10.1007/s10973-019-08256-y.

[17] M. S. Itankar, P. Walke, and M. Basavaraj, "To study heat transfer analysis of heat sink Minichannel using nanofluids," vol. 2, pp. 36–41, 2017.

[18] S. A. Fazeli, S. M. H. Hashemi, H. Zirakzadeh, and M. Ashjaee, "Experimental and numerical investigation of heat transfer in a miniature heat sink utilizing silica nanofluid," *Superlattices Microstruct.*, vol. 51, no. 2, pp. 247–264, 2012.

[19] A. Minea, A.Alina, B.Buonomo, J.Burggraf, D.Ercole, K.R.Karpaiya, A D Pasqua, G.Sekrani, J.Steffens, J.Tibaut, N.Wichmann, "NanoRound: A benchmark study on the numerical approach in nanofluids' simulation," *Int. Commun. Heat Mass Transf.*, vol. 108, p. 104292, 2019.

[20] Z. H. Saadoon, F. H. Ali, H. K. Hamzah, A. M. Abed, and M. Hatami, "Improving the performance of mini-channel heat sink by using wavy channel and different types of nanofluids," *Sci. Rep.*, vol. 12, no. 1, pp. 1–22, 2022.

Thermal Investigation of Rectangular Header Normal Channel Facile Heat Sink Using Hybrid Nano Fluids

Amna Adil [1,2, a], Taha Baig [1,2, b], Shehryar Manzoor [1, c]*, Furqan Jamil [3, d], Muzaffar Ali [1, e] and Abid Hussain[1, f]

[1] *Department of Mechanical Engineering, University of Engineering and Technology Taxila, Pakistan*
[2] *Department of Mechanical Engineering, Wah Engineering College, University of Wah, Wah Cantt, Pakistan*
[3] *School of engineering, Edith Cowan University, 270 Joondalup drive, Joondalup, Perth, WA 6027, Australia*
*Correspondence: sherry.manzoor@gmail.com

Email address: [a)] amnaadil2022@gmail.com, [b)] tahabaig893@gmail.com and [c)] sherry.manzoor@gmail.com, [d)] f.jamil@ecu.edu.au [e)] muzaffar.ali@uettaxila.edu.pk [f)] abid.hussain@uettaxila.edu.pk

***Abstract*—In today's era the thermal management of microelectronic devices has become a challenging task because of high flux generation. Hybrid nano fluid is the new class of nano fluids which is used as a coolant for better thermal performance. In the current work, numerical investigation of rectangular header normal channel facile heat sink is performed. Thermal performance of the heat sink is enhanced by using hybrid nano fluids (mixture of SiO_2-TiO_2 / H_2O). Effects of varying volumetric concentrations of the nano particles are also noted. It is observed that by increasing the volumetric concentration of silicon oxide nano particles thermal performance is enhanced. Results are reported in the form of reduction in base temperature, thermal resistance and pressure drop.**

Keywords—*Hydrothermal performance, Facile heat sink, Hybrid Nano fluids*

I. INTRODUCTION

Modernization and miniaturization of electronic equipment is the foundation of the fourth industrial revolution. Usage of electronic devices increased more during the pandemic 2019, as the modes of earning and learning shifted online. Online earning is expected to increase further in the future [1]. At first electronic cooling was done using air [2], which was considered to be efficient for moderate powers [3]. Considering high power densities, researchers moved to liquid cooling which has been proven to be better compared to air [4], [5]. After water, addition of nanoparticles was introduced by the researchers in base fluid to make nanofluids, in order to further improve the cooling of electronic devices [6]. Two different nanoparticles combined or mixed together in various ratios are known as hybrid nanoparticles. Addition of hybrid nanoparticle in base fluid makes it a hybrid nano fluid. Researchers have been working on the importance of hybrid nano fluids in electronic cooling [7]–[9]. In this work, hybrid of TiO_2 and SiO_2 nano fluid is investigated numerically using different ratios, in a rectangular header normal channel facile heat sink. This specific heat sink is chosen given its simplicity and ease of manufacturing. Thermal conductivity of SiO_2 is higher and it is combined with TiO_2 to assess further improvements.

II. METHODOLOGY

ANSYS / Fluent is used for numerical analysis of the heat sink. Realizable k-ε model, semi implicit model is used, second order spatial discretization scheme, turbulent K.E. and dissipation rate, 2nd order upwind scheme is applied. Convergence criteria for water and hybrid nanofluids is set to be 10^{-8} and 10^{-12} respectively.

A. Boundary Conditions for Numerical Model

Adiabatic sink walls with no slip at the surface have been considered. During the whole process of fluid flow, thermal properties don't change, fluid enters the heat sink with uniform velocity while fluid is steady and incompressible. Radiation heat transfer, viscous heating and heat generation is negligible. Gauge pressure and velocity have been considered to be zero everywhere inside heat sink and at outlet of fluid domain respectively. A constant 325W of flux is provided from the bottom.

B. Governing Equations for Numerical Model

Mass, momentum, and energy conservation equations (11-12) are used for single phase while (13-14) are used for multiphase fluid flow:

$$\frac{\partial}{\partial x_i}(\rho u_i) = 0 \quad (15)$$

$$\frac{\partial}{\partial x_i}(\rho u_i u_j) = -\frac{\partial \rho}{\partial x_j} + \frac{\partial}{\partial x_i}\left[(\mu + \mu_t)\frac{\partial u_j}{\partial x_i}\right] + \frac{\partial}{\partial x_i}\left[(\mu + \mu_t)\frac{\partial u_i}{\partial x_j}\right], \; j = 1, 2, 3 \quad (16)$$

$$\frac{\partial}{\partial x_i}(\rho u_i T) = \frac{\partial}{\partial x_i}\left[\left(\frac{\lambda}{c_p} + \frac{\mu_t}{\sigma_t}\right)\frac{\partial T}{\partial x_i}\right] \quad (17)$$

$$\nabla.\left(\rho_m \overrightarrow{V_m}\right) = 0 \quad (18)$$

$$\nabla.\left(\rho_m \overrightarrow{V_m}\,\overrightarrow{V_m}\right) = -\nabla p + \nabla.\left(\mu_m \nabla \overrightarrow{V_m}\right) + \rho_m \vec{g} + \nabla.\left(\sum_{k=1}^{n} \varphi_k \rho_k \overrightarrow{V_{dr,k}}\,\overrightarrow{V_{dr,k}}\right) \quad (19)$$

$$\nabla.\sum_{k=1}^{n}(\varphi_k \overrightarrow{v_k}(\rho_k H_k + p_m)) = \nabla.(k_m \nabla T) \quad (20)$$

III. MESH SENSITIVITY STUDY

The mesh independence or sensitivity analysis specifies the legitimacy of numerical model. Size of element for study was 3.8 x 10^{-4} in case-5, which was chosen to save the time it takes for computation as deviation of change in base and inlet temperature (T_b - T_i) is calculated to be under 1%. Mesh sensitivity study curve is shown in

Fig. 1 (a).

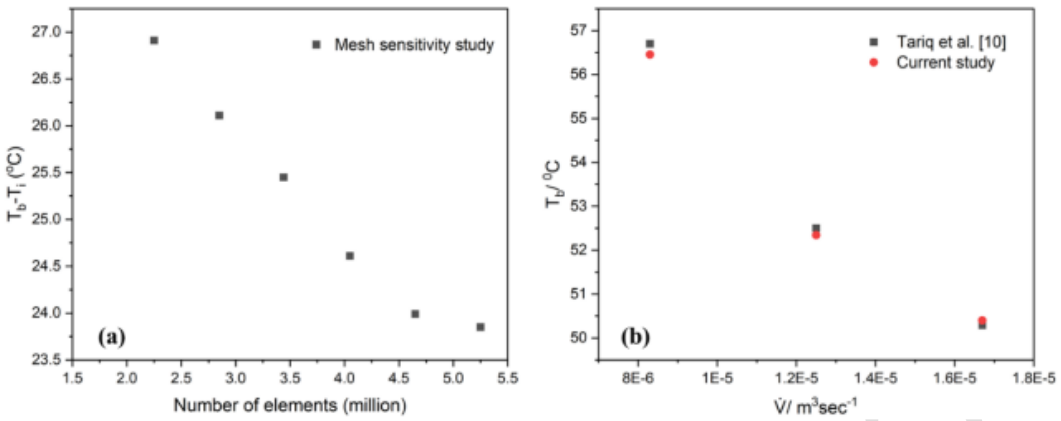

Fig. 1: *(a) Mesh sensitivity study (b) Confirmation of numerical model*

IV. VALIDATION OF NUMERICAL MODEL

Numerical model is validated by reproducing the base temperature results produced by Tariq et al. [10] using water as a cooling fluid. Results have been found to be accurate with less than 1% deviation as shown in Fig. 1 (b).

V. HEAT SINK DESCRIPTION

A rectangular header normal channel facile heat sink is modeled in ANSYS. Flow propagates from circular channels inside heat sink as shown in Fig. 2 (a). A chip at the base of heat sink is made to simulate flux.

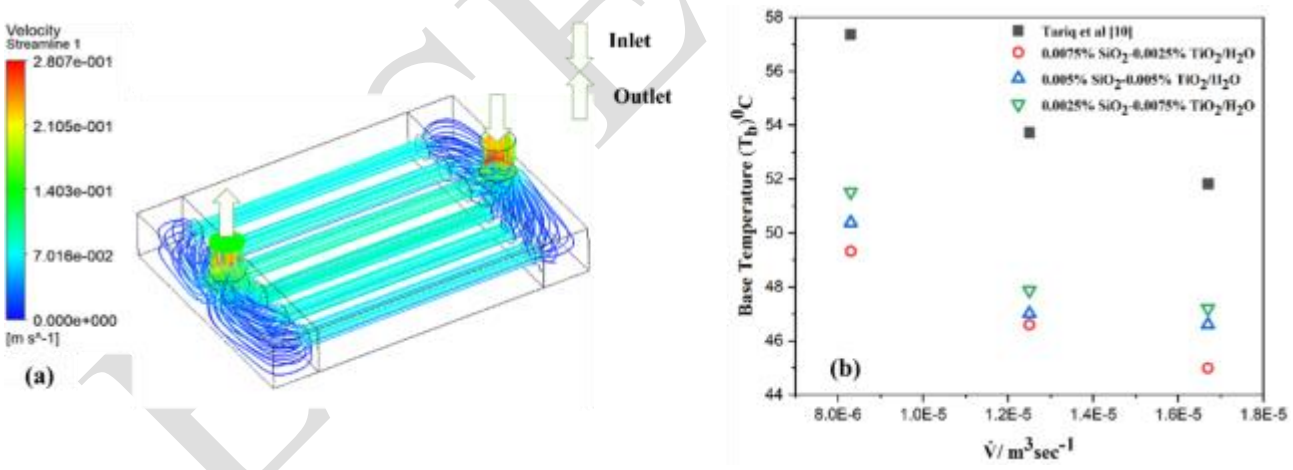

Fig. 2: *(a) Fluid flow in Normal channel facile heat sink (b) Base temperature*

VI. DATA REDUCTION

Heat transfer rate, $\dot{Q}=\dot{m}C_p(T_O - T_i)$, log mean temperature difference, $LMTD=\frac{(T_b-T_{in})-(T_b-T_o)}{ln\left(\frac{(T_b-T_{in})}{(T_b-T_o)}\right)}$ and thermal resistance are calculated as, $R_{th} = \frac{LMTD}{\dot{Q}}$ to deduce results.

VII. RESULTS AND DISCUSSION

A. *Base Temperature*

While the flow increased as illustrated in Fig. 2, data points show a decline in temperature at base at all the volumetric flow rates. Temperature decrement is significant for different volumetric concentrations of hybrid nanofluids as compared with Tariq et al [10]. It may be noted that by increasing the volumetric concentration of silicon dioxide nano particles in hybrid combinations as listed in TABLE the base temperature decreases. The maximum decrement in base temperature is found for hybrid nano fluid combination (0.0075% SiO2-0.0025%TiO2/H2O) as 14.05%, 14%, and 13.6% at varying flow rates as compared with Tariq et al [10]. This shows that hybrid nano fluid can play a significant role in maintaining the base temperature of the heat sink.

TABLE I: DIFFERENT VOLUMETRIC CONCENTRATIONS OF HYBRID NANO FLUID

Sr. No	SiO_2 Nano particle (%)	TiO_2 Nano particle (%)	Hybrid (SiO_2-TiO_2) (%)
01	0.0075	0.0025	0.0075 SiO_2-0.0025 TiO_2
02	0.005	0.005	0.005 SiO_2-0.005 TiO_2
03	0.0025	0.0075	0.025SiO_2-0.0075 TiO_2

B. *Thermal Resistance*

The thermal resistance recoded for rectangular header normal channel facile heat sink is shown in

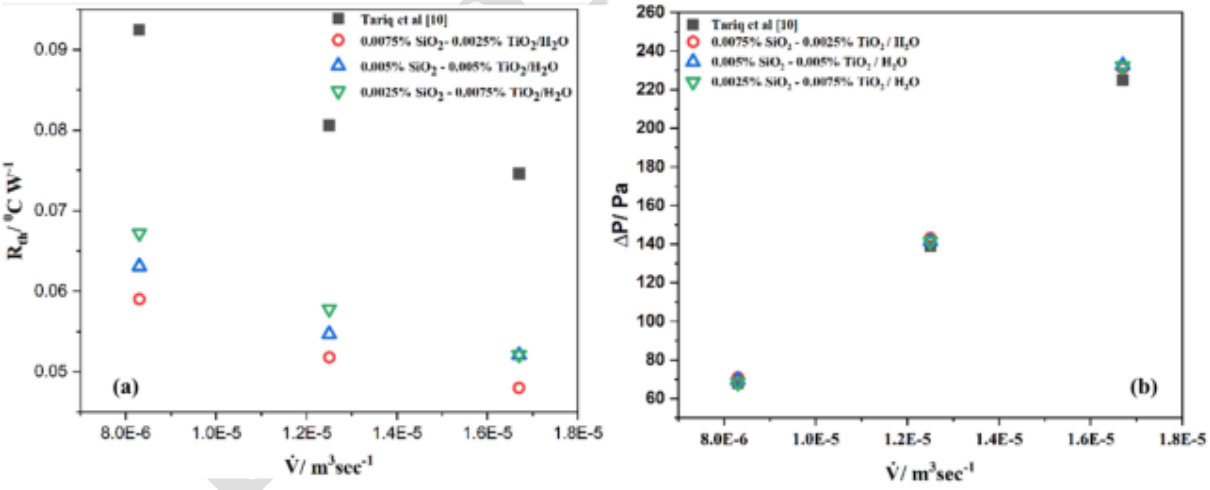

Fig. 3 (a). Results show that thermal resistance decreases by increasing the volumetric flow rates that result in increment in heat transfer. Minimum value of thermal resistance is noted to be 0.048 ºC/W for Hybrid nano fluid (0.0075% SiO2-0.0025%TiO2/H2O) at 1.67 x 10-5 m3/s. Maximum decrement in thermal resistance is observed for hybrid nano fluid (0.0075% SiO2-0.0025% TiO2/H2O) as 36.2%, 35.7%, and 35.6% at varying volumetric flow rates as compared with Tariq et al. [10].

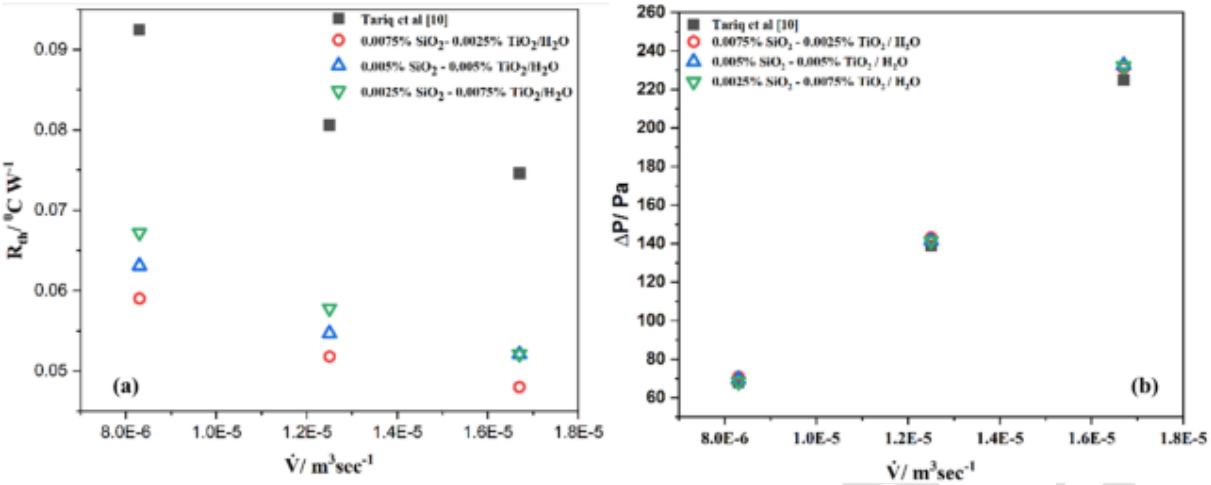

Fig. 3: *(a) Thermal Resistance (b) Pressure Drop*

C. Pressure Drop

Pressure drop was observed to be increasing with increment in volumetric flow rates. Utilizing hybrid nanofluids in the heat sink under discussion, caused the slight increase in pressure drop because the addition of two distinct nanoparticles causes the viscosity to increase. Trend of pressure drop at different volumetric flow rates is shown in

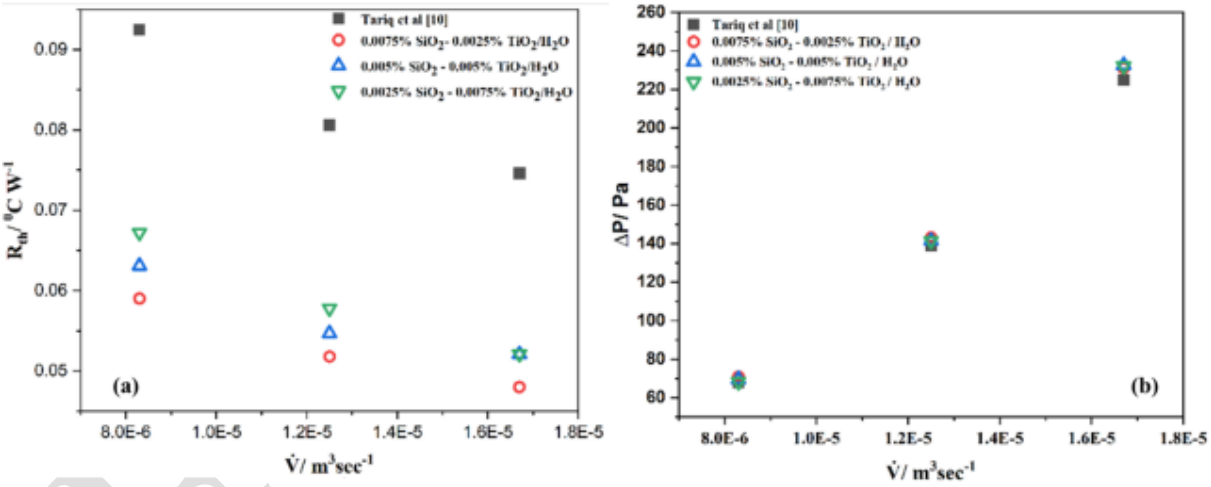

Fig. *3* (b). The maximum pressure drops recorded for hybrid nano fluid (0.0075% SiO2-0.0025% TiO2/H2O) as 231Pa at 1.67 x 10-5 m3/sec. By using different combinations of hybrid nano fluids pressure drop increases. Percentage increment in pressure drop observed for hybrid nano fluid (0.0075% SiO2-0.0025% TiO2/H2O) was 4.11%, 2.95% and 2.67% respectively at varying volumetric flow rates as compared with Tariq et al. [10].

VIII. CONCLUSIONS

Various parameters are calculated for the evaluation of heat sink's performance including temperature observed at base, the amount of resistance it offers to heat produced and pressure drop. As volumetric flow rate increased, base temperature and thermal resistance decreased while pressure drop increased. It was observed that better thermal performance can be achieved by increasing the

volumetric concentration of silicon oxide nano particle in the hybrid nano fluid combinations. The maximum decrement in base temperature and thermal resistance is observed as 14.05% and 36.2% respectively at 8.25 x $10^{-5}m^3/s$. It is noted that the pressure drop increases for the hybrid nano fluids but this enhancement was not more than 4.11%.

AKNOWLEDGEMENT

Support of Mechanical Engineering Department, UET Taxila, and WEC is appreciatively acknowledged.

REFERENCES

[1] M. A. Ng *et al.*, "Has the COVID-19 Pandemic Accelerated the Future of Work or Changed Its Course? Implications for Research and Practice.," *Int. J. Environ. Res. Public Health*, vol. 18, no. 19, Sep. 2021, doi: 10.3390/ijerph181910199.

[2] N. Base, *Cooling of Electronic Systems NATO ASI Series*. .

[3] S. A. Nada, R. M. El-Zoheiry, M. Elsharnoby, and O. Osman, "Enhancing the thermal performance of different flow configuration minichannel heat sink using Al2O3 and CuO-water nanofluids for electronic cooling: An experimental assessment," *Int. J. Therm. Sci.*, vol. 181, p. 107767, Nov. 2022, doi: 10.1016/j.ijthermalsci.2022.107767.

[4] M. Akbarzadeh *et al.*, "A comparative study between air cooling and liquid cooling thermal management systems for a high-energy lithium-ion battery module," *Appl. Therm. Eng.*, vol. 198, p. 117503, 2021, doi: https://doi.org/10.1016/j.applthermaleng.2021.117503.

[5] E. Santi, S. Eskandari, B. Tian, and K. Peng, "6 - Power Electronic Modules," M. H. B. T.-P. E. H. (Fourth E. Rashid, Ed. Butterworth-Heinemann, 2018, pp. 157–173.

[6] C. T. Nguyen, G. Roy, C. Gauthier, and N. Galanis, "Heat transfer enhancement using Al2O3–water nanofluid for an electronic liquid cooling system," *Appl. Therm. Eng.*, vol. 27, no. 8, pp. 1501–1506, 2007, doi: https://doi.org/10.1016/j.applthermaleng.2006.09.028.

[7] M. Asim and F. R. Siddiqui, "Hybrid Nanofluids—Next-Generation Fluids for Spray-Cooling-Based Thermal Management of High-Heat-Flux Devices," *Nanomaterials*, vol. 12, no. 3, pp. 1–29, 2022, doi: 10.3390/nano12030507.

[8] Z. Said and M. A. Sohail, "1 - Introduction to hybrid nanofluids," in *Micro and Nano Technologies*, Z. B. T.-H. N. Said, Ed. Elsevier, 2022, pp. 1–32.

[9] H. Babar, H. Wu, H. M. Ali, T. R. Shah, and W. Zhang, "Staggered oriented airfoil shaped pin-fin heat sink: Investigating the efficacy of novel water based ferric oxide-silica hybrid nanofluid," *Int. J. Heat Mass Transf.*, vol. 194, p. 123085, 2022, doi: https://doi.org/10.1016/j.ijheatmasstransfer.2022.123085.

[10] H. A. Tariq, M. Anwar, A. Malik, and H. M. Ali, "Hydro-thermal performance of normal-channel facile heat sink using TiO2-H2O mixture (Rutile–Anatase) nanofluids for microprocessor cooling," *J. Therm. Anal. Calorim.*, vol. 145, no. 5, pp. 2487–2502, 2021, doi: 10.1007/s10973-020-09838-x.

A Data Mining Perspective on Polio Eradication in Pakistan

Uzair Tariq[1,] *, Hafiz Muhammad Khurram Ali[1] and Muzumil Anwar[1]
[1]*Industrial Engineering Department, University of Engineering and Technology Taxila, Taxila*
*Correspondence: uzairtariq1@gmail.com

***Abstract*—The eradication of polio in Pakistan has proved to be the toughest nut to crack for Global Polio Eradication Initiative (GPEI) and the Government of Pakistan. As rest of the world has been declared polio free by the WHO, Pakistan and Afghanistan are miserably losing their battle against polio. The eradication of polio in Pakistan is affected by many factors such as low literacy rates, poverty, rurality, vaccine refusal, counter insurgencies, poor management of immunization activities, misconceptions, poor health infrastructure and security issues. This work presents the data mining perspective on polio eradication in Pakistan. The aim of this study is to find the relationship between the number of polio cases with literacy, poverty, rurality, vaccine refusal and the number of children vaccinated using Data Visualization and Correlation Analysis and to find the high risk and high priority areas, age and gender groups for targeted vaccination using Naïve Bayes Classification and Density Based Clustering. 89% of the total number of cases occurred in the areas with literacy rates less than 50%. 75% of all the infected districts have literacy rates less than 40%. 82.8% of the cases occurred in the areas with poverty percentages more than 40%. 81.25% of the total infected districts have poverty percentages greater than 40%. 28.46% of the cases occurred only in Khyber Agency and North Waziristan, having poverty percentages 82.8% and 96.9% and rurality percentages 90.12% and 99.2% respectively. 93.13% of the total number of cases occurred in the districts having rurality percentage greater than 50% and 82.34% of the cases occurred in the districts with rurality percentage greater than 60%. 96.875% of all the infected districts have rurality percentage more than 50%. Khyber Agency has reported the greatest number of polio cases i.e., 15.34% with a future likelihood of 13.22%. North Waziristan has reported the second the greatest number of polio cases i.e., 13.12% with a future likelihood of 10.19%. Khyber Agency, North Waziristan, Peshawar, Killa Abdullah, Lakki Marwat, Karachi, Bannu, South Waziristan, Quetta and Tank have been identified as the polio hotspots with 65.7% of the polio cases. 65.19% of the polio cases are reported from KP and FATA alone.**

Keywords—GPEI; polio; vaccination; Data Visualization and Data Mining; Naïve Bayes Classification; Density Based Clustering.

I. INTRODUCTION

Pakistan is consistently proving to be the toughest nut to crack when it comes to eradication of polio. Global Polio Eradication Initiative was taken in 1988 when polio virus was causing devastation, paralyzing thousands of children in the world on daily basis. Since 1988 more than 99% reduction in polio cases in the world is achieved. Approximately, 350,000 number of polio cases were recorded in the world in 1988 which was reduced to only 650 in 2011. As a result of this global battle against polio, Europe, Americas, Western Pacific and South-East Asia are now certified polio-free. More than 200 countries in the world are now certified polio-free countries.

Epidemics scared people more than polio did in the early part of the 20th century. Polio raged during the summer months, sweeping through populations every year. Most of the people suffering from polio recovered quickly, some of them suffered temporary or permanent paralysis and some of them lost their lives as well. Many people suffering from polio were

disabled for life. They were a painful and agonizing reminder to the world of how much damage this disease can cause. Most of the survivors were incapacitated for life leaving behind frightening reminders in the form of crutches, wheelchairs and distorted limbs [1].

Polio is the short form for poliomyelitis. It is a Greek word. “Polio” means grey, “myelos” means marrow and “itis” means inflammation. Grey marrow refers to spinal cord. So “poliomyelitis” means the inflammation of the spinal cord. Polio is mostly used instead of poliomyelitis. Polio was previously, also called infantile paralysis though it did not affect only the infants. Polio is a highly contagious disease and is caused by three types of polio virus. These are the members of the Enterovirus genus. Polio spreads through fecal-oral route and affects mostly the children [2]. It is an intestinal infection and spreads through contact with faeces, dirty hands, contaminated water and food. The virus cannot survive on its own. It must need a living cell to invade for its reproduction. It enters the body through mouth and travel down the digestive tract and is secreted with the stools. It also multiplies in the tonsils and in the lymph nodes of throat, but its main breeding ground is small intestine. More often the infection is not severe or apparent with minor symptoms such as nausea and headache or no symptoms at all. These are called asymptomatic cases [3]. In about 1% of the cases, the virus takes over the central nervous system and the brainstem through blood stream, destroying the motor neurons, that triggers the contraction of muscle fibres. It is extremely difficult to predict the extent of paralysis. Some of the infected nerve cells will overcome the virus while others will die [4].

After conducting a comprehensive literature review, it was identified that the prevalence of polio in Pakistan is just theoretically linked with poverty, rurality and low literacy rates. There is no statistical analysis and evidence to back up the argument. The extensive Literature Review about the prevalence of polio reveals that the prevalence of polio depends upon many factors which includes refusal to the polio vaccines due to lack of awareness and education, poor delivery of health services and poor health infrastructure in rural areas, malnutrition, and poor sanitation system due to poverty and non-seriousness and poor performance of the health workers. But there is hardly any statistical analysis and data evidence available to support the study. The aim of this research is to find the relationship between the number of cases in each district in recent years with literacy rate, percentage rurality, percentage poverty and multidimensional poverty index of those districts.

This research also aims to identify the hotspots of polio cases by using clustering. It will help us in the identification of High Risk/High Priority areas, age and gender groups to target for vaccination using. For example, for a given area, which gender or age group is most likely to be affected by polio. If only these high-risk groups, regions and time of polio spread can be identified, effective health programs can be targeted at these sections for adequate control and prevention of spread of this disease. Something which is done by the world a long ago and we are still lagging.

II. RESEARCH METHODOLOGY

Research problem was to find out whether the prevalence of polio depends upon literacy rate, poverty percentage, multi-dimensional poverty index, rurality, vaccine acceptance

percentage and vaccination coverage and to identify high priority/high risk areas, age and gender groups for targeted vaccination. The data for total number of polio cases in each district in the last ten years was collected from the Expanded Program on Immunization (EPI) Islamabad. The data for total annual cases for the last 20 years, vaccine acceptance percentage and children vaccinated per month was also collected from the EPI Islamabad. The data for literacy rates and rural population percentage of each district was obtained from Pakistan Bureau of Statistics Islamabad. The data for poverty percentage and multidimensional poverty index for each district of Pakistan was obtained from the website of United Nations Development Programme (UNDP). The techniques used in this study are Naïve Bayes Classification, Density Based Clustering, Data Visualization and Regression and Correlation Analysis. The software used for Naïve Bayes Classification and Density Based Clustering is WEKA 3.8. The software used for Regression and Correlation Analysis is ORANGE 3.23.

Naïve Bayes Classifier is based on Bayesian Theorem which is shown in equation (1). It is a probabilistic machine learning algorithm used for classification task [5]. It is based on conditional probabilities.

$$P(A|B) = \frac{P(B|A)x\,P(A)}{P(B)} \qquad (1)$$

Where:

P(A|B) = the probability of event A occurring, given event B has occurred

P(B|A) = the probability of event B occurring, given event A has occurred

P(A) = the probability of event A

P(B) = the probability of event B

A linear regression analysis generates estimates for the slope and intercept of the linear equation predicting an outcome variable Y, based on values of a predictor variable X [6]. A general form of this equation is shown below:

$$Y = a + bX \qquad (2)$$

Where:

Y = Dependent Variable

a = intercept and it is the predicted value of Y, when X = 0

b = Slope

X = independent variable

The dependent variable Y will be taken as the number of polio cases and will be analyzed against different factors by taking them as independent variable X. The intercept a and the slope b is calculated as:

$$\boldsymbol{b} = \frac{\sum_{i=1}^{n}(\boldsymbol{x_i} - \overline{\boldsymbol{x}})(\boldsymbol{y_i} - \overline{\boldsymbol{y}})}{\sum_{i=1}^{n}(\boldsymbol{x_i} - \overline{\boldsymbol{x}})^2} \qquad (3)$$

$$\boldsymbol{a = \bar{y} \cdot b\bar{x}} \qquad (4)$$

Where:

x_i = Value of X variable

y_i = Value of Y variable

$\bar{x}$ = Mean of the values of X

$\bar{y}$ = Mean of the values of Y

Pearson's product moment correlation coefficient (r) is given as a measure of linear association between the two variables.

$$\boldsymbol{r = \frac{\sum_{i=1}^{n}(x_i - \bar{x})(y_i - \bar{y})}{\sqrt{\sum_{i=1}^{n}(x_i - \bar{x})^2 \sum_{i=1}^{n}(y_i - \bar{y})^2}}} \qquad (5)$$

It can also be calculated by the following equation:

$$\boldsymbol{r = \frac{n(\sum xy) - (\sum x)(\sum y)}{\sqrt{[n\sum x^2 - (\sum x)^2][n\sum y^2 - (\sum y)^2]}}} \qquad (6)$$

Density Based Clustering is an unsupervised machine learning technique that recognizes distinctive clusters/groups in the dataset, based on the concept that a contagious region of high point density in the data space is called a cluster, which is separated from a contagious region of low point density, which are called outliers or noise [7].

There are two parameters in Density Based Clustering algorithm.

• Min Pts: The minimum number of points (a threshold) grouped or clustered together for a region to be considered dense.

• Epsilon (ε): The distance that will be used to locate the points in the neighborhood of any point.

These parameters can only be understood by explaining the concepts of Density Connectivity and Density Reachability. Reachability in terms of density establishes a point to be reachable from another point if it lies within a particular distance (ε) from it. Density Connectivity involves a transitivity-based chaining-approach to determine whether points are in a particular cluster. For example, p and q points could be connected if p->r->s->t->q, where a->b means b is in the neighborhood of a.

There are three types of points after the Density Based Clustering is complete:

Core — This is a point that has at least m points within distance n from itself.

Border — This is a point that has at least one Core point at a distance n.

Noise — This is a point that is neither a Core nor a Border. And it has less than m points within distance n from itself.

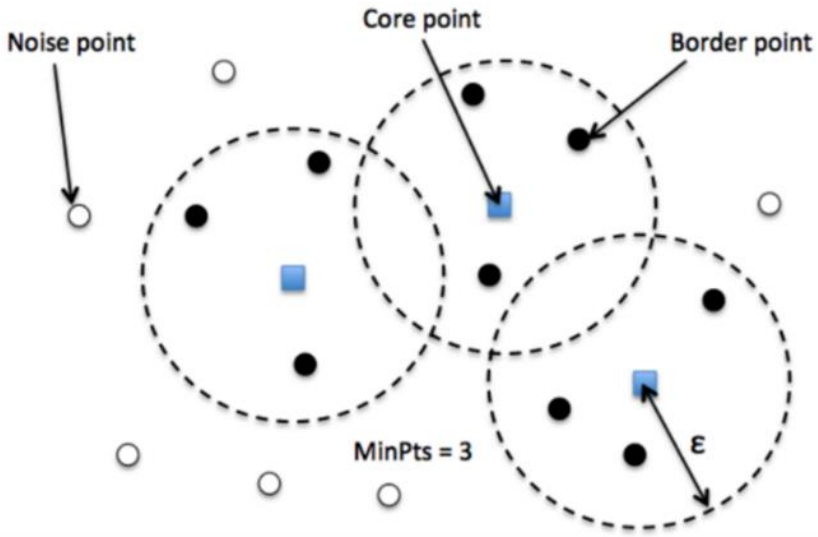

Fig. 3 : Density Based Clustering Algorithm [7]

III. RESULTS AND DISCUSSION

The total number of cases in each district was compared with different factors such as literacy rates, poverty percentage, multidimensional poverty index and rurality percentage of each district to find their impact on the number of polio cases. The number of polio cases was also compared with the vaccine acceptance percentage per month and children vaccinated per month. Scatter plots, normal distribution curves and box and whiskers plot were drawn for data visualization to find the impact of these factors on the prevalence of polio in Pakistan. The data for total number of polio cases in each district in the last ten years was collected from the Expanded Program on Immunization (EPI) Islamabad. The data for total annual cases for the last 20 years, vaccine acceptance percentage and children vaccinated per month was also collected from the EPI Islamabad. The data for literacy rates and rural population percentage of each district was obtained from Pakistan Bureau of Statistics Islamabad. The data for poverty percentage and multidimensional poverty index for each district of Pakistan was obtained from the website of United Nations Development Programme (UNDP).

Multidimensional poverty index is a new and improved measure to calculate the extent of poverty. It is developed by United Nations Development Programme (UNDP) and Oxford Poverty and Human Development Initiation (OPHI). Multidimensional poverty index is measured in terms of deprivation in three aspects i.e., health, education, and standard of living. The Multidimensional Poverty Index measures the extreme deprivations faced by the people in terms of healthcare, education and living standards. It is the product of two elements, the percentage of people who are considered multidimensional poor (incidence of poverty) and the percentage of dimensions in which the people are deprived (intensity of poverty) [8]. The data collected was then arranged and pre-processed to make it compatible to be processed in the

software. The excel sheets of the data were created and were converted to Comma Separated Values (.CSV) format.

The software used in this study for data visualization and analysis is ORANGE 3.23. Orange is a machine learning and data visualization toolkit. The pre-processed data was then processed, visualized, and analyzed in Orange. The relationships between the prevalence of polio in Pakistan and the various factors responsible for its prevalence were found, visualized, and analyzed [9].

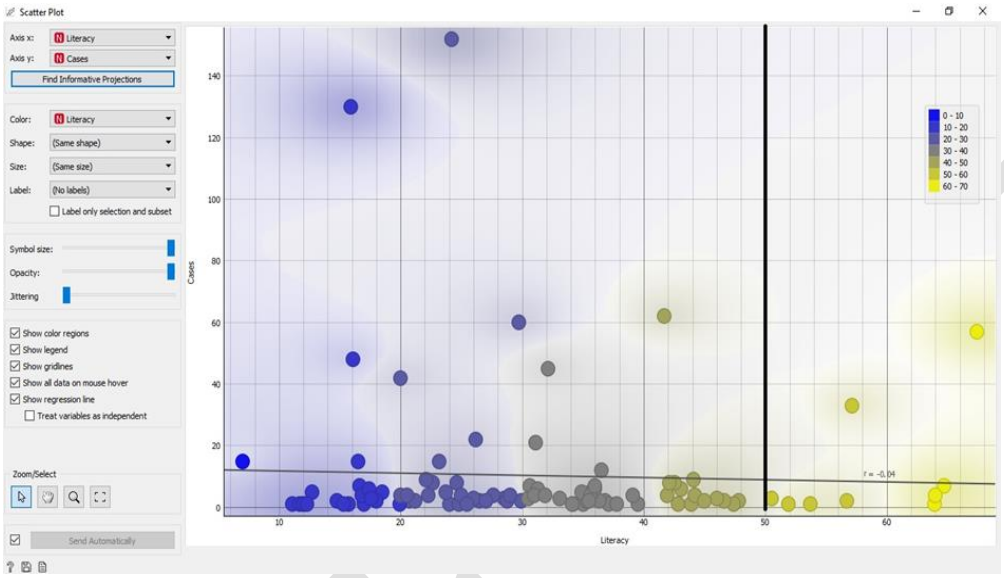

Fig. 2 : Relationship between literacy rates and the no. of cases in each district.

The relationship between literacy rates and the number of cases in each district are shown in Figure 2. It can be observed that 89% of the total number of cases (882 out of 991) occurred in the areas with literacy rates less than 50%. The value of the correlation coefficient is -0.04 which indicates that there is a negative relationship between the number of cases and the literacy rates.

From Figure 3, normal distribution of infected districts with literacy rates can be observed. It is to be noted that 75% of all the infected districts (72 out of 96) have literacy rates less than 40%. The visualization and analysis of data indicates that low literacy rate is a major hurdle in eradication of polio.

Relationship between poverty rates and the number of cases in each district is illustrated in Figure 4. It is shown that 82.8% of the cases (821 out of 991) occurred in the areas with poverty percentages more than 40%. The value of the correlation coefficient is +0.11 which indicates that there is a positive relationship between the number of polio cases and the poverty percentage.

In Figure 5, normal distribution of infected districts with poverty rates with bin width 20 is observed. It can be observed that 81.25% of the total infected districts (78 out of 96) have poverty percentages greater than 40%. Khyber Agency with 82.8% poverty rate, has the highest number of polio cases i.e., 152 in last ten years. North Waziristan with 130 polio cases in the

last ten years has the highest poverty percentage with 96.9%. The visualization and analysis of data indicates that poverty is a major hurdle in eradication of polio.

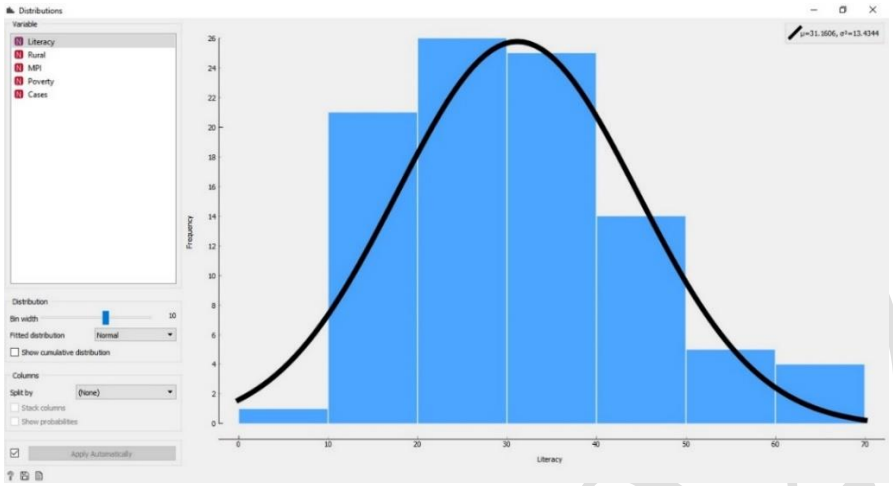

Fig. 3: Normal Distribution of infected districts with literacy rates.

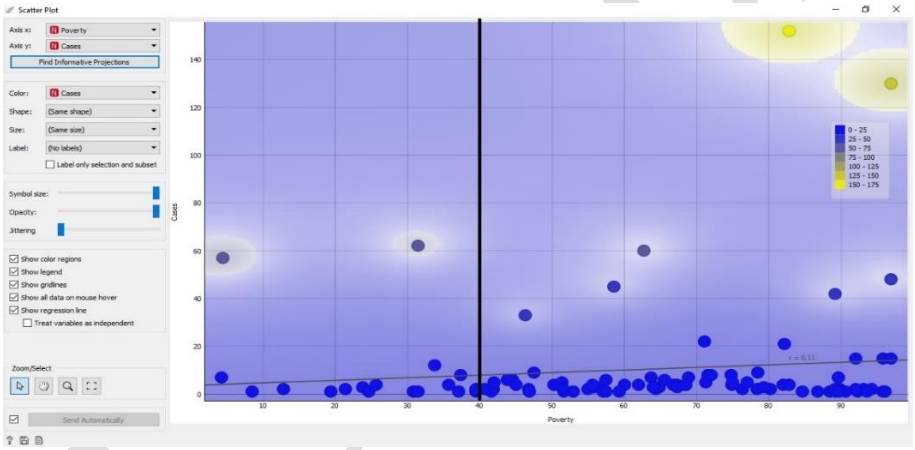

Fig 4: Relationship between poverty rates and the no. of cases in each district

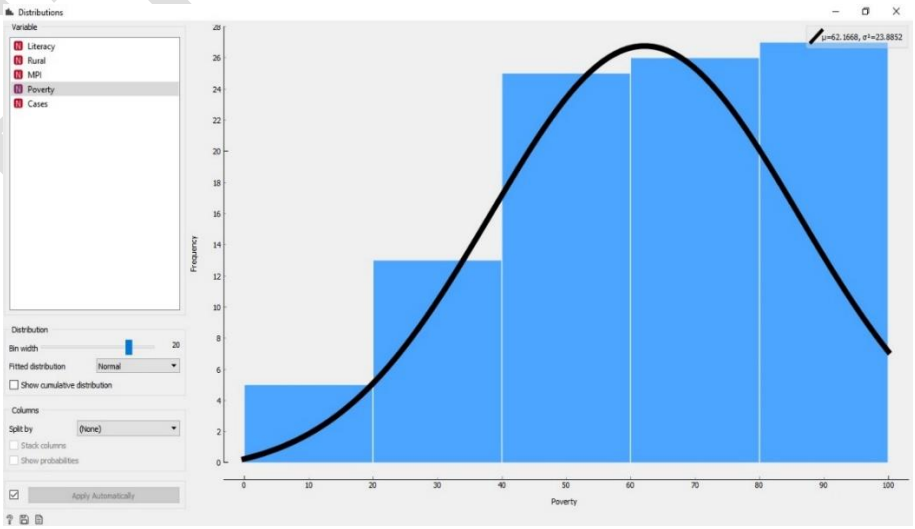

Fig 5: Normal Distribution of infected districts with poverty rates with bin width 20

The relation between rurality percentage and the number of cases is shown in Figure 6. It represents that 82.34% of the cases (816 out of 991) occurred in the districts with rurality percentage greater than 60%. 93.13% of the cases (923 out of 991) occurred in the districts with rurality percentage greater than 50%. The positive value of the correlation coefficient also indicates the positive relationship between the number of cases and the rurality percentage.

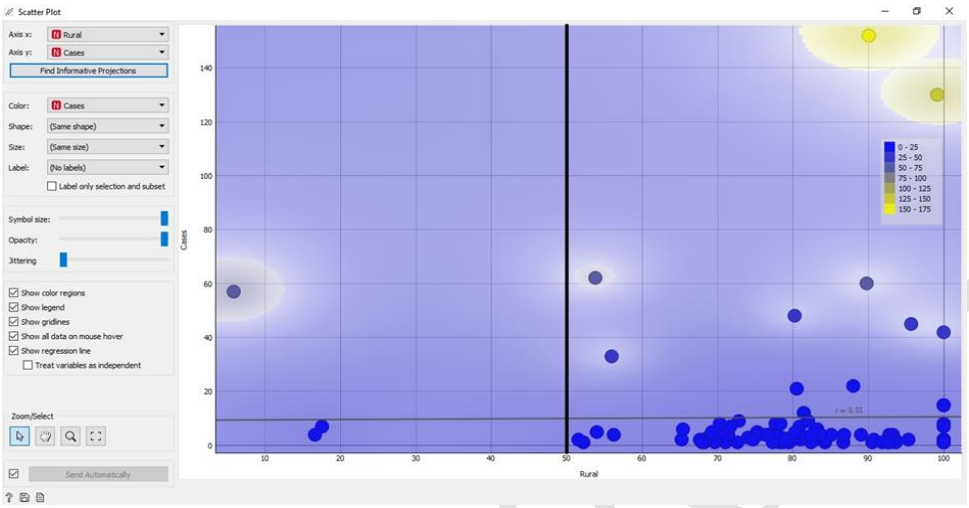

Fig 6: Relationship between rurality percentage and the no. of cases in each district.

The normal distribution of infected districts with rural percentage with bin width 50 is shown in Figure 7. It shows that 96.875% of all the infected districts (93 out of 96) have rurality percentage more than 50%. Khyber Agency with 90.12% rurality rate, has the highest number of polio cases i.e., 152. North Waziristan with 99.2% rurality rate, has the second highest number of polio cases i.e. 130. The visualization and analysis of data indicates that high percentage of rural population is a major hurdle in eradication of polio.

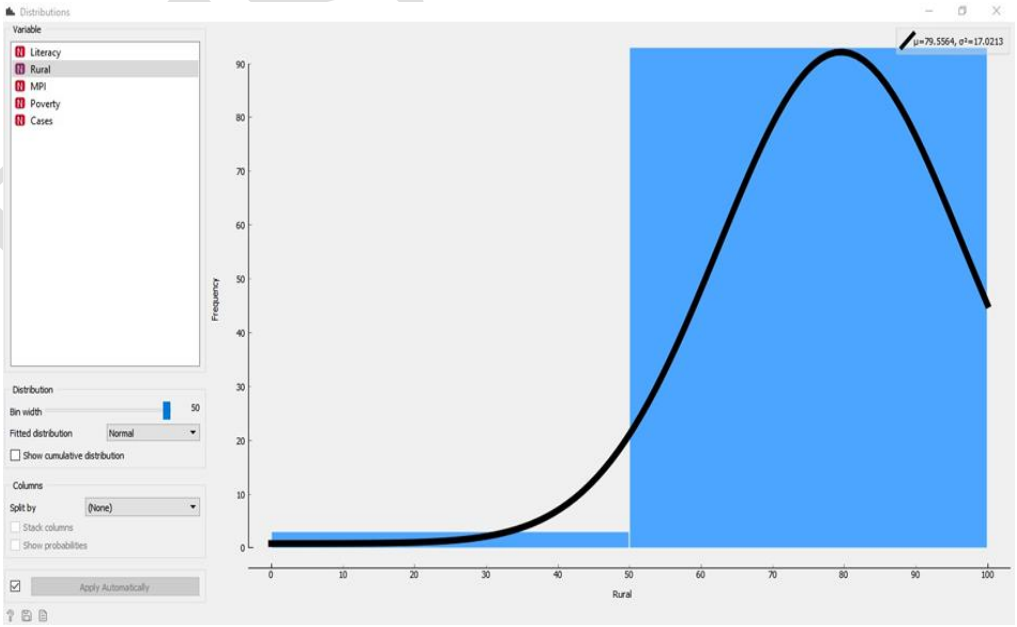

Fig 7: Normal distribution of infected districts with rural percentage with bin width 50

Naïve Bayes Classification and Density Based Clustering techniques in Figure 8 and Figure 9 shows that 28.46% of the cases occurred only in Khyber Agency and North Waziristan. Khyber Agency has reported the greatest number of polio cases i.e., 15.34% with a future likelihood of 13.22%. North Waziristan has reported the second the greatest number of polio cases i.e., 13.12% with a future likelihood of 10.19%. Khyber Agency, North Waziristan, Peshawar, Killa Abdullah, Lakki Marwat, Karachi, Bannu, South Waziristan, Quetta and Tank have been identified as the polio hotspots with 65.7% of the polio cases. 65.19% of the polio cases are reported from KP and FATA alone.

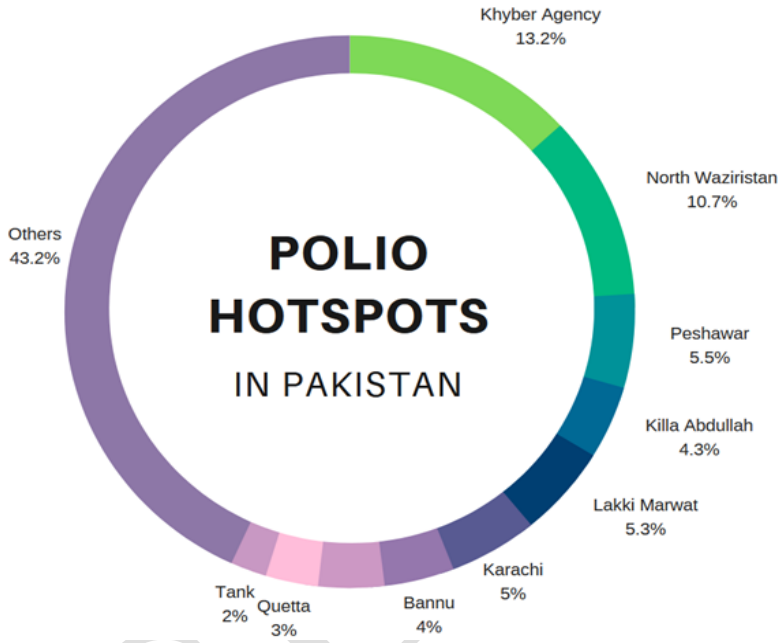

Fig 8: Polio Hotspots in the country

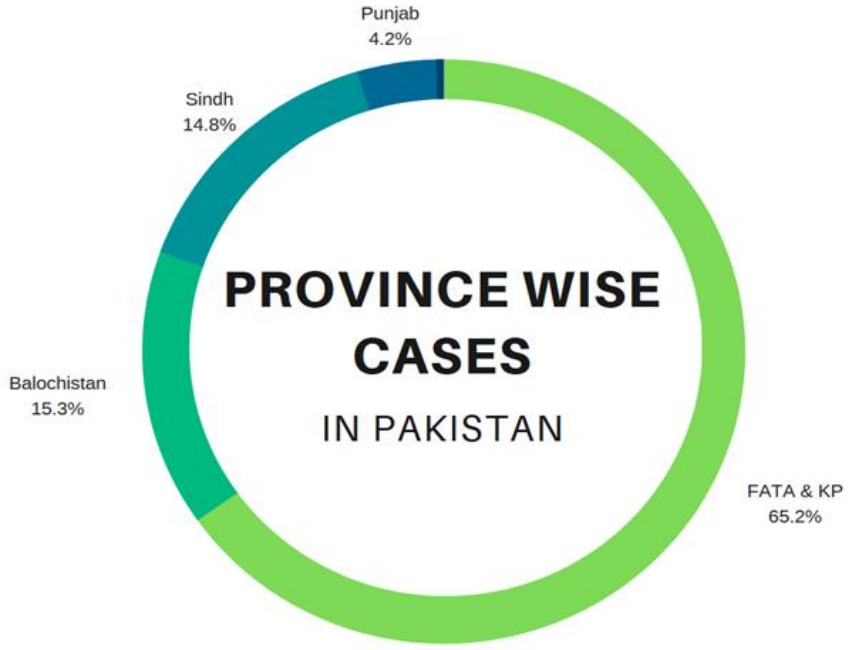

Fig 9: Province wise polio hotspots

IV. CONCLUSION

Lack of awareness and temptation to believe false propaganda related to vaccines due to low literacy rates, lead to refusal of vaccine by the patients and has been identified as the major factor affecting eradication of polio in Pakistan. Poverty leads to unhygienic living standards without proper system of human waste disposal and insufficient food for the households which causes vitamin deficiency and consequently low immunity levels. All these circumstances lead to the transmission of polio. Poverty is one of the biggest causes of the transmission of polio. The high percentage of rural population is a major hurdle in polio eradication due to lack of proper healthcare infrastructure in rural areas of Pakistan and lack of management of immunization campaigns in far flung areas of the country. The immunization emergency must be enforced in these polio hotspots and immunization activities must be held seven days a week. These activities must be supervised by Deputy Commissioners and Assistant Commissioners. The eradication efforts must be decentralized, and immunization cards of children must be made compulsory for inter district travel. The government must focus on poverty alleviation and improvement in literacy rates. Islamic scholars, celebrities and influential figures must be engaged in immunization awareness campaigns because refusal to the vaccination can be extremely dangerous as Covid-19 is also **causing** devastation in the world and sooner or later, its only solution is immunization.

REFERENCES

[1] Axelsson, P., 'Do not eat those apples; they've been on the ground!': polio epidemics and preventive measures, Sweden 1880s-1940s. Asclepio, 2009. 61(1): p. 23-37.

[2] Hovern, D., The Trials and Triumphs of the American Polio Vaccine. 2018, Cooper Medical School of Rowan University

[3] Rogers, N., Dirt and disease: polio before FDR. 1992: Rutgers University Press.

[4] Alomari, S.O., Z. Abou-Mrad, and A. Bydon, COVID-19 and the central nervous system. Clinical Neurology and Neurosurgery, 2020. 198: p. 106116.

[5] Patel, B.A. and A. Parikh. Impact Analysis of the complete blood count parameter using Naive Bayes. IEEE.

[6] Yuan, M., et al., A systematic review of aberration detection algorithms used in public health surveillance. Journal of biomedical informatics, 2019. 94: p. 103181.

[7] Yan, H., Hybrid Hierarchical Spatio-Temporal Methodologies: Model Reduction and Filtering. 2018.

[8] UNDP, P., Multidimensional Poverty in Pakistan. 2016.

[9] Noor, S., et al., Analysis of public reactions to the novel Coronavirus (COVID-19) outbreak on Twitter. 2020.

Finite Element Modeling of Residual Stress and Distortion in Dissimilar TIG Welded Joints of Aluminum 2024 and Stainless Steel 304

Asad Ali [1, a], Mirza Jahanzaib [1, b], Muhammad Jawad [1, c] and Amar ul Hassan [2, d]
[1]*Industrial Engineering Department, University of Engineering and Technology Taxila, 47080, Pakistan*
[2]*Mechanical Engineering Department, University of Wah, 47040, Pakistan*

Email address: [a)] asadiqbal1900@gmail.com, b) jahan.zaib@uettaxila.edu.pk, [c)] engr.jawad@uettaxila.edu.pk, [d)] ammar.hassan@wecuw.edu.pk

***Abstract*—In automobiles, hybrid structures of aluminum and stainless steel have the potential to reduce fuel consumption and air pollution. Stainless steel and aluminum have different thermal conductance and expansion, resulting in uneven distortion and residual stress. These residual stresses and distortions adversely affect the weld joint service life. This study aims to predict residual stresses and distortions in aluminum 2024 and stainless steel 304 joints. Finite element modeling of tungsten inert gas welding has been carried out using the ABAQUS software through the Distributed Flux (DFLUX) user subroutine. Effects of welding speed and welding current on distortions and residual stresses are investigated. The results revealed that an increase in welding current resulted in high stresses and distortions, while an increase in welding speed caused low residual stress and distortion. The minimum values of tensile residual stresses found are 175 MPa and 127 MPa for the aluminum and stainless-steel sides respectively.**

Keywords—Thermal conductance, Expansion, Tungsten inert gas welding, Finite element modeling, Distributed flux

I. INTRODUCTION

During manufacturing processes, residual stresses accumulate in the structures or materials regardless of external or thermal influence. These stresses cause brittle fractures and shorten the fatigue life of the structures [1]. The fabrication of lightweight parts achieved by welding of dissimilar aluminum and stainless steel is gaining attention in automobile and chemical industries. However, the differences in thermal and mechanical properties result in uneven expansion and contraction of materials, which leads to residual stresses and distortions that causes weld failure [2]. Therefore, assessment of residual stress in aluminum and stainless-steel dissimilar welds is crucial for structural safety. The finite element modeling (FEM) is a novel engineering approach that finds approximate solutions without undergoing actual experiments. Moreover, the FEM has proven its reliability over the decades for finding temperature fields, residual stresses, and distortions in welding applications [3]. Numerous studies used the FEM to predict residual stress and distortion for aluminum and stainless-steel welding. Using the FEM, Li [4] compared and validate the temperature field, residual stress, and distortion in aluminum and steel joints welded with single laser welding and arc-assisted

laser welding. The results showed that arc assisted laser welding the reduced residual stress and distortion by creating high-temperature zones. Ogawa [5] made a friction stir weld of aluminum 6061 and stainless steel 304 by offsetting the tool on the aluminum side and rotating the tool at 700 rev/min. This study includes the measurement of residual stresses and the examination of the effect of post-aging treatment on residual stresses. According to the results, tensile residual stress occurred parallel to the weld line with an average value of 36 MPa, and compressive residual stress occurred perpendicularly with an average value of -29 MPa. Further study found that post-ageing treatment had little or no significant effect on residual stress distribution. Huang [6] conducted a finite element analysis of aluminum and galvanized steel laser welding for predicting residual stresses and temperature field. This was at a welding power of 1200 W and a welding speed of 600 mm/min. According to the temperature field and longitudinal residual stresses graphs, the aluminum side had a higher temperature (363 °C) and lower residual stresses (293 MPa), while the galvanized steel side had a lower temperature (200 °C) and a higher longitudinal residual stress (329 MPa). A close match was found between experimental and FEM results, confirming the capability of FEM. The microstructure formation and residual stresses of cold metal transfer (CMT) weld joints of aluminum and steel were studied by Agudo [7]. With AlSi3Mn1 filler, the CMT weld was made by 70 A welding current and 60 cm/min welding speed. Compressive residual stress was observed on the steel side, and tensile residual stress was detected on both the steel and aluminum sides, but aluminum had a higher tensile residual stress (100 MPa) due to its high thermal conductivity. The above literature review revealed that the evaluation of residual stress and distortion of TIG welded Al2024 and SS304 joints need further exploration. This study examines the influence of welding speed and welding current on the distortion and residual stresses during TIG welding of Al2024 and SS304 using FEM. The prediction of residual stresses and distortion will aid manufacturer to join dissimilar welds before conducting extensive experiments.

II. MATERIALS AND MODELLING

Base metals aluminum (Al) 2024, stainless steel (SS) 304, and filler metal of copper-nickel alloy (ER CuNi30) are chosen for finite element modeling. The dimensions of 100 mm × 50 mm × 3 mm are selected for each base metal. Based on the literature review, FEM has been conducted at the two levels of welding speed (100 mm/min, 120 mm/min) and two levels of welding current (80 A, 90 A).

III. TIG WELDING FINITE ELEMENT MODELING

Many industries are using the FEM because of its low cost and ease of analysis. In this study, the Distributed flux (DFLUX) user subroutine with Abaqus software is used to carry out the FEM. The first step involves modeling geometry and materials based on their dimensions and temperature-dependent mechanical properties. Table I shows the temperature-dependent properties of base and filler metals.

In the geometry modeling process, the filler metal has been taken as part of geometry as suggested by previous study. Secondly, DFLUX written in FORTRAN language has been used to model Goldak's double ellipsoidal heat source. The C3D8T elements of global size 0.0012 are used for meshing, resulting in 18288 nodes and 13938 elements. Fig. 1 depicts a mesh model.

TABLE I. TEMPERATURE DEPENDENT PROPERTIES

304 stainless steel (Base Metal)							
Temperature °C	**Density kg/m^3**	**Yield Strength MPa**	**Elastic Modulus GPa**	**Thermal Conductivity W/m°C**	**Specific Heat J/kg°C**	**Poisson's ratio**	**Expansion coefficient 1/°C × 10^{-6}**
20	8010	206	199	15.26	500	0.28	16.0
200	7931	153	180	17.6	544.3	0.28	17.2
400	7840	108	166	20.2	582	0.28	18.2
600	7755	82	150	22.8	643	0.28	18.6
800	7667	69	125	25.4	686	0.28	19.5
2024 Aluminum (Base Metal)							
Temperature °C	**Density kg/m^3**	**Yield Strength MPa**	**Elastic Modulus GPa**	**Thermal Conductivity W/m°C**	**Specific Heat J/kg°C**	**Poisson's ratio**	**Expansion coefficient 1/°C × 10^{-6}**
20	2780	473	72.4	164	881	0.33	14
100	2780	416.5	66.5	182	927	0.33	23
200	2780	293.5	63.5	194	1047	0.33	24.5
300	2780	239.8	60.4	202	1130	0.33	25.1
400	2780	150	56.1	210	1210	0.33	25.5
500	2780	100	50	220	1300	0.33	26.6
ER CuNi30 (Filler Metal)							
Temperature °C	**Density kg/m^3**	**Yield Strength MPa**	**Elastic Modulus GPa**	**Thermal Conductivity W/m°C**	**Specific Heat J/kg°C**	**Poisson's ratio**	**Expansion coefficient 1/°C × 10^{-6}**
20	8950	483	150	29	377	0.34	16

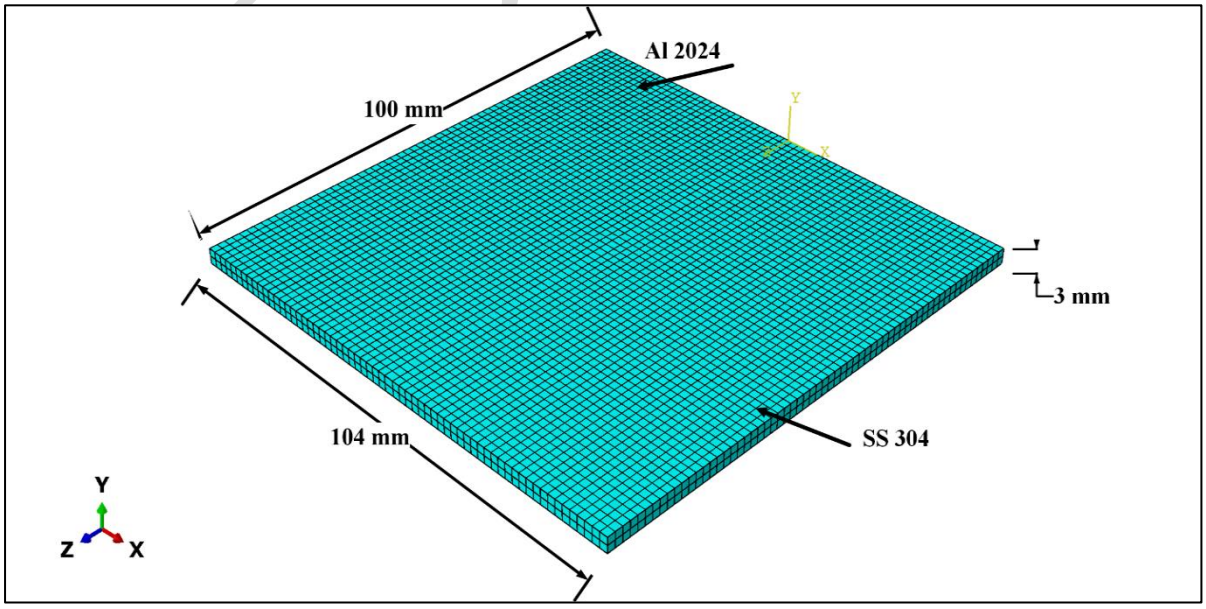

Fig. 1 Finite Element Mesh Model

The heat source model, initial and boundary conditions are discussed below.

A. Heat Source Model

The double ellipsoidal model of Goldak is used in this study because of the deep heat input in Tig welding. In Goldak's heat source, a front ellipsoidal produces a high heat rate, while a rear ellipsoidal produces a low heat rate [8]. The front and rear ellipsoids equations are shown in 1 and 2 respectively.

$$q_{front}(x,y,z,t) = \frac{6\sqrt{3}f_f Q}{a_f bc\pi\sqrt{\pi}} e^{\left(\frac{-3x^2}{a^2{}_f}-\frac{3y^2}{b^2}-\frac{3z^2}{c^2}\right)} \quad (1)$$

$$q_{rear}(x,y,z,t) = \frac{6\sqrt{3}f_r Q}{a_r bc\pi\sqrt{\pi}} e^{\left(\frac{-3x^2}{a^2{}_r}-\frac{3y^2}{b^2}-\frac{3z^2}{c^2}\right)} \quad (2)$$

In these equations, f_f and f_r indicate the fractions of heat deposit at the front and rear part of the heat source. Their values are 1.33 and 0.67, respectively. Semiaxes of the ellipsoidal shape a_f, a_r, b and c have values of 4 mm, 12 mm, 5.9 mm, and 1.5 mm, respectively [8]. Q represents the input power that is equal to the product of the welding plant's efficiency, current, and voltage. The value of voltage and efficiency in this study were 0.7 and 17 V respectively.

B. Initial and Boundary conditions

To avoid rigid motion, the degree of freedom is restricted at the corners of the geometry during simulation and heat has been transferred from welding to the surrounding area by convection and radiation. The equations 3 and 4 are used for convective heat flux and radiation heat flux respectively.

$$q_{convection} = h(T - T_{ambient}) \quad (3)$$

$$q_{radiation} = \varepsilon\sigma\left(T^4 - T_{ambient}{}^4\right) \quad (4)$$

Simulation have been conducted using the convection coefficient of $h = 15\ Wm^{-2}K^{-1}$, Boltzmann constant of $\sigma = 5.67 \times 10^{-8}\ Wm^{-2}K^{-4}$ and emissivity of $\varepsilon = 0.7$.

IV. RESULTS AND DISCUSSION

This section discusses the effects of welding current and welding speed on residual stress and distortion in aluminum and stainless-steel welding.

A. Effects of Welding Current

The distortion and residual stresses of the welded parts have been investigated at a welding current having two levels (80 A and 90 A) at a constant speed of 100 mm/min. Fig. 2 illustrates the residual stress distribution and distortion contours in aluminum and stainless-steel sides. The red zone in residual stresses contours shows the maximum tensile stresses and blue zone in the distortion contours shows the maximum distortion. As a result of the steep thermal

gradient, joint interfaces experienced higher tensile residual stresses and it became compressive away from the weld [9].

As aluminum has higher thermal conductivity and thermal expansion than stainless steel, heat flows more toward the aluminum side, resulting in a significant expansion of the aluminum side. After welding, the shrinkage of this expansion is constrained by the stainless-steel side. This causes compressive stresses on the stainless steel side, tensile stresses and large distortion on the aluminum side [7]. Longitudinal residual stress and distortion analysis have been performed in the transverse direction of the weld. Fig 3 depicts the graphical representation of residual stresses and distortion. At current of 80 A, the maximum tensile stresses and distortion are of 194 MPa and 0.19 mm respectively for Al side, whereas 153 MPa and 0.1 mm on SS side. At 90 A current, the maximum tensile stress and distortion on aluminum plate are 300 MPa and 0.23 mm respectively whereas 180 MPa and 0.12 mm on SS side. This is because increase in heat input at high current cause higher thermal expansion of Al [10].

B. Effects of Welding Speed

The finite element experiment has been performed at welding speed of two levels (100 mm/min and 120 mm/min) at constant current of 80 A. Fig. 4 shows the residual stress distributions and distortion contours on Al and SS sides. The higher tensile residual stresses occurred at the weld zone on both two levels of welding speed as depicted by red zones in Fig 4 a and b. The high distortion occurred on the Al side than SS due to high thermal expansion of Al as shown in blue zone (Fig 4 c and d).

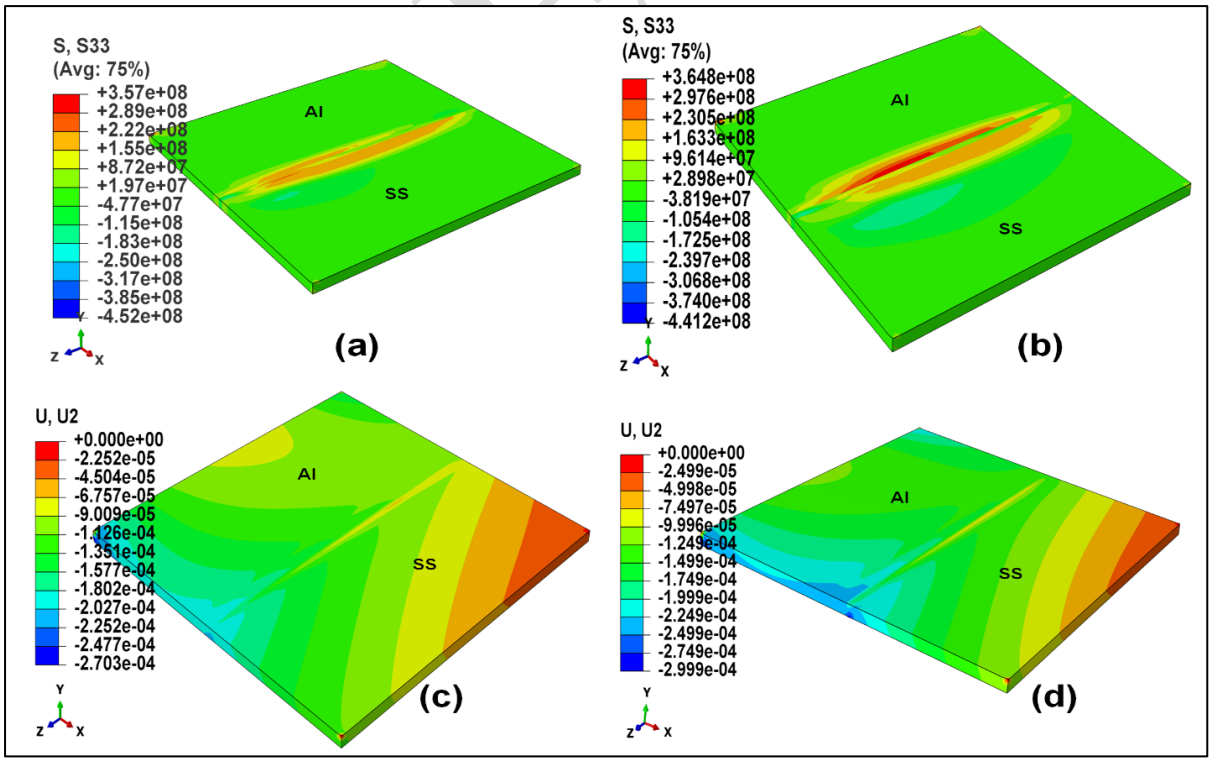

Fig. 2 Residual Stress and Distortion Contours (a) Residual Stress at 80 A (b) Residual Stress at 90 A (c) Distortion at 80 A (d) Distortion at 90 A

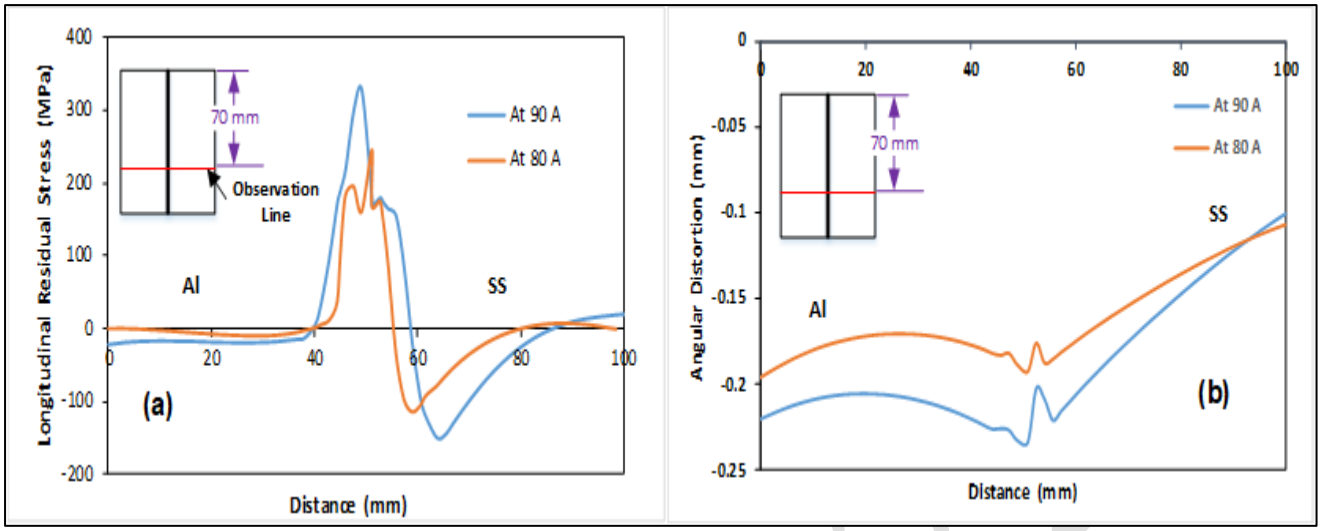

Fig. 3 Comparison Graphs (a) Residual Stress at 80 A, 90 A (b) Angular Distortion at 80 A, 90 A

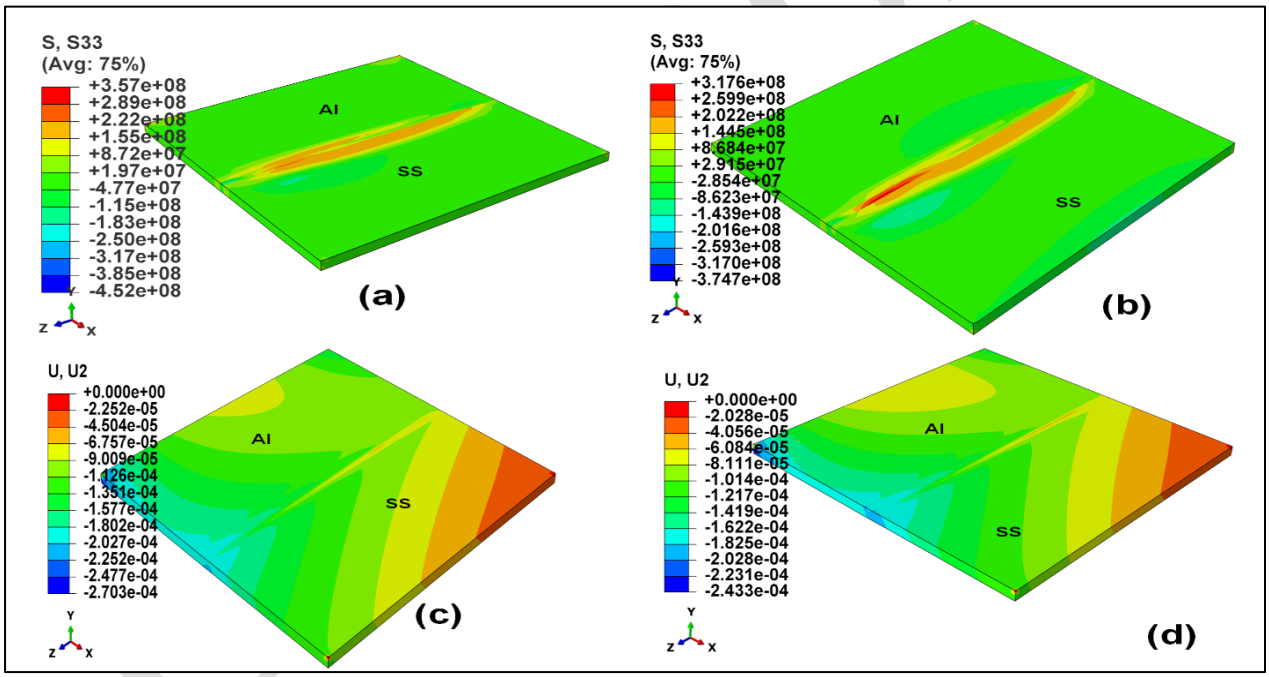

Fig. 4 Residual Stress and Distortion Contours (a) Residual Stress at 100 mm/min (b) Residual Stress at 120 mm/min (c) Distortion at 100 mm/min (d) Distortion at 120 mm/min

Fig 5 shows the graphical tendency of residual stress and distortion. At welding speed of 100 mm/min, Al and SS sides show maximum tensile residual stresses of 194 MPa and 153 MPa, with distortions of 0.19 mm and 0.1 mm respectively. The maximum tensile residual stresses of 175 MPa and 127 MPa and distortion of 0.166 mm and 0.09 mm are at Al and SS sides respectively at welding speed of 120 mm/min. Heat input is reduced at high welding speed, which reduces heat transfer to adjacent materials. Due to the reduced heat in the material,

there is low expansion and shrinkage of material during the heating and cooling cycles of welding, resulting in minimal distortion and residual stresses[11].

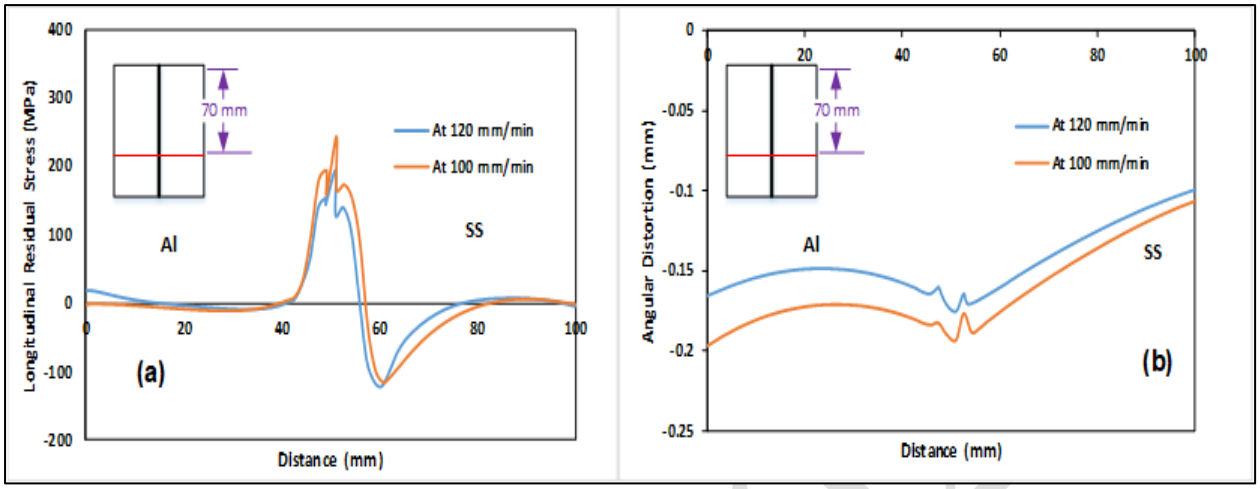

Fig. 5 Comparison Graphs (a) Residual Stress at 100 mm/min, 120 mm /min (b) Angular Distortion at 100 mm/min, 120 mm/min

V. CONCLUSION

In this study the effect of welding current and welding speed on residual stress have been investigated during the joining of Al 2024 and SS 304 through TIG welding. The FEM is carried out to find out the critical levels of parameters. Abaqus with DFLUX subroutine code is employed to simulate the welding process at different conditions (Current of 80 A and 90 A, Welding speed of 100 mm/min and 120 mm/min). The following conclusion are drawn.

- In the weld zone and Al side, the tensile residual stresses were observed whereas both tensile and compressive residual stresses are observed on SS side.
- The minimum residual stresses of 194 MPa on Al side and 153 MPa on SS side were achieved at current of 80 A and welding speed of 100 mm/min. As the welding speed increased from 100 mm/min to 120 mm/min, the residual stresses were decreased as 175 MPa (Al side) and 127 MPa (SS side).
- The minimum distortion of 0.19 mm on Al side and 0.10 mm on SS side were achieved at current of 80 A and welding speed of 100 mm/min. The distortion was decreased further 0.166 mm (Al side) and 0.09 mm (SS side) with increase in welding speed (120 mm/min).

REFERENCES

[1] Rossini, N., et al., *Methods of measuring residual stresses in components.* 2012. **35**: p. 572-588.

[2] Watanabe, T., H. Takayama, and A.J.J.o.M.P.T. Yanagisawa, *Joining of aluminum alloy to steel by friction stir welding.* 2006. **178**(1-3): p. 342-349.

[3] Ghafouri, M., et al., *Finite element simulation of welding distortions in ultra-high strength steel S960 MC including comprehensive thermal and solid-state phase transformation models.* 2020. **219**: p. 110804.
[4] Li, C.-l., et al., *Residual stress and welding distortion of Al/steel butt joint by arc-assisted laser welding-brazing.* 2019. **29**(4): p. 692-700.
[5] Ogawa, D., et al., *Residual stress measurement of Al/steel dissimilar friction stir weld.* 2019.
[6] Huang, J., et al., *Residual stress field analysis of Al/steel butt joint using laser welding–brazing.* 2017. **33**(17): p. 2053-2063.
[7] Agudo, L., et al. *Study of microstructure and residual stresses in dissimilar Al/steels welds produced by cold metal transfer*. in *Materials science forum*. 2008. Trans Tech Publ.
[8] Sriram, R.G., et al., *Finite element simulation of temperature distribution and residual stress in single bead on plate weld trial using double ellipsoidal heat source model.* 2019. **8**(1S2): p. 133-138.
[9] Kwabena Adomako, N., et al., *Finite element modeling of residual stress at joint interface of titanium alloy and 17-4PH stainless steel.* 2021. **11**(4): p. 629.
[10] Khoshroyan, A. and A.R.J.T.o.N.M.S.o.C. Darvazi, *Effects of welding parameters and welding sequence on residual stress and distortion in Al6061-T6 aluminum alloy for T-shaped welded joint.* 2020. **30**(1): p. 76-89.
[11] Teng, T.-L., C.-C.J.I.J.o.P.v. Lin, and piping, *Effect of welding conditions on residual stresses due to butt welds.* 1998. **75**(12): p. 857-864.

Tribological Analysis of Ionic Liquid as an Additive to the Bio Based Oils

Hira Nawaz[1, *] and M. Gulzar[1]
[1]Department of Mechanical Engineering, University of Engineering and Technology Taxila, Punjab, Pakistan
*Correspondence: hiranawaz08@gmail.com

***Abstract*—As a result of ongoing environmental codification, the lubrication industry has been working to develop environmentally sound and efficient lubricants that may be utilized as metal cutting fluids. A lubricant that complies with environmental regulations and still provides great lubrication performance must be developed due to environmental concerns. In this research, the tribological workability of bio-based oils that have been combined with ionic liquid for metal cutting or machining applications is examined. Ionic liquid was used as an addition to bio-based oils to create tribologically enhanced bio-based lubricants. The specific bio-based oils examined in this research were coconut oil and cottonseed oil. In both bio-based oils, choline chloride was added as a lubricant additive. The research started with an examination of the behavior of pure coconut in terms of wear prevention and friction reduction. The examination of the lubricating behavior of various concentrations of ionic liquid added to bio-based oils has been done using a pin on disc tribotester. The outcomes have demonstrated that the addition of 1.5 weight percent of choline chloride to coconut oil reduces friction coefficient by 56% accompanying a 80% decrease in wear volume. Similarly, at a concentration of 1 wt.% ionic liquid, cotton seed oil demonstrated a 40% decrease in average wear. The results of the surface analysis demonstrated that the ionic liquid enhanced the interacting surfaces ability to create tribo-films and hydrogen bonds, therefore improving lubrication performance. The measurement of the viscosity of formulated oil samples also revealed that an increase in ionic liquid concentration causes the viscosity of bio-based oils to increase as a result of the creation of hydrogen bonds. The results of the overall investigation showed that ionic liquids have the potentiality to amend the tribological behavior of bio-based lubricants used as metal cutting fluids.**

Keywords—Ionic Liquid, Material Removal Rate, Lubrication, Metal Cutting Fluid, Bio-Based Oils

I. INTRODUCTION

The achievement of sustainability in the machining process is pivotal in the production industry. The risks associated with traditional flood cooling or lubrication methods using mineral oils have adverse effect on the climate and the vigor of the operator. Around 85% of metal cutting lubricants used worldwide are mineral-based cutting lubricants which are hazardous to store and dispose of. As these fluids are not perishable and require costly treatment prior to disposal as a result the disposal cost of these oils is two to four times more than the entire cost of product's machining. Mineral based oils are hazardous for the machine operator as the skin contact with cutting fluids caused 80% of all intermittent contagions in operators. [1]

Mineral oils can be replaced with bio-based oils to overcome these limitations. Contrasted with mineral-based oils, bio-based oils have remarkable attributes such as less toxicity, better lubrication, renewability, biodegradability and better resilience to shear. Due to the bio-based oil's high polarity and increased attraction for metallic surfaces, they offer good boundary

lubrication properties. About 90% of the mineral based oils can be replaced by bio-based oils. [2]

Cutting oils made from renewable resources offer excellent reliability and favorable economic circumstances. These oils produce less mist in air and have a clean output which minimizes health risks.

Vegetable oils have a desirable characteristic because of the formation of fatty acids and their polar nature. Polar fatty acids when bound to metal parts produce a high strength adhesive film that reduces wear and friction. Use of vegetable-based oil such as commercial vegetable oil and rapeseed oil increase the tool life of AISI 316L stainless steel by 177% and reduces force by 7% as compare to industrial mineral oil. [3] For turning operation of AISI 304 coconut bio-based oil offer better surface finish as compared to mineral based oil. [4]

In the absence of suitable additives bio-based lubricants have poor lubrication performance. Ionic liquids can be employed as an additive due to their low vapor pressure, high polarity and great heat stability. Ionic liquids produce incredible outcomes in low quantity machining at ambient temperature and 100°C. [5]

Comparison of tribological properties of imidazolium tetra fluoroborate and per fluoro-polyether synthetic oils using steel-steel contact at a load of 200N shows that 50% friction reduction occurs when using the ionic liquid as lubricant as compare to PFPE. [6]

It is not practical to utilize ionic liquids as a neat lubricant as they are expensive. Therefore, ionic liquids are used as a lubrication additive. Abdul Sani Al presented research on the tribological characteristics of phosphonium-based ionic liquids as an addition to modified palm olein trimethylolpropane ester using four ball tribotester. The tribological characteristics of the MRPO are improved by the addition of a small amount of PIL (1 wt.%). [7]

II. METHODOLOGY

This research comprises of three phases which includes material and oil selection phase, experimental phase and surface characterization phase. The sequential information of primary research activities is provided as a flow chart in Fig. 1 for the overview of this research study.

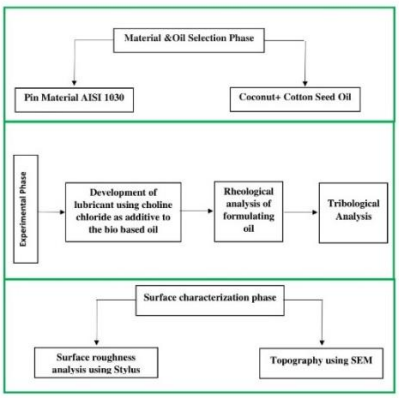

Fig 1. Work Flow Chart Diagram

1. SELECTION PHASE

A. *Selection of Bio Based Oils*

In order to create environmentally friendly bio-based lubricants, the current study Employed coconut oil and cottonseed oil as neat lubricants.

Coconut oil has a high viscosity, high flash point, excellent lubrication and low production of vapors. Due to saturated nature of constituents, coconut oil exhibits significantly superior thermal and oxidative stability.

Similarly, cottonseed oil can withstand high pressure due to its highly dense homogenous strong lubricating film and dipolar nature.

B. *Selection of Ionic Liquid*

For the improvement of the tribological and lubricating ability of bio based oils, choline chloride ionic liquid is used as additive by varying its concentration. The ionic liquid is purchase from the sigma-Aldrich private limited and then dried under vacuum.

C. *Selection of Pin Material*

The pin material is AISI 1030 steel is used. It is a high carbon steel having high percentage of carbon (0.30%). The pin specimen is cylindrical in shape and the dimension of the pin are as follow:

Diameter of pin=8mm

Length of the pin =25mm

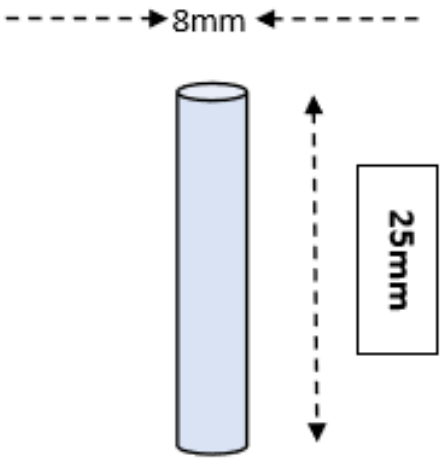

Fig 2. Pin's Dimension

2. EXPERIMENTAL PHASE

A. *Formulation of Lubricant Oil*

For the formulation of lubricating oils, a homogenous solution of the bio-based oils is prepared by adding different concentrations of ionic liquids such as 0.5wt%, 1wt% and 1.5wt%.

For proper mixing of ionic liquid in the bio-based oils stir the mixture for 1.5 hour using the magnetic stirrer at the RPM of 1150 and temperature of 20℃.

B. Rheological Analysis

The kinematic viscosity of the formulating oil at 40℃ is analyzed using Redwood viscometer.

When temperature of oil bath containing 50ml oil samples reaches 40℃, collect oil in a flask and record the falling time of 50ml oil using stop watch. Then kinematic viscosity of formulated oil samples is calculated according to Eq. (1).

Kinematic viscosity=Υ= (A×t) - B/ (t) (1)

A= Viscometer constant

B=Kinetic Energy Coefficient

t= Seconds of Flow

For all formulated samples the values of these constants are A=0.00247 and B=0.5 respectively.

C. Tribological Analysis

Utilizing a pin-on-disc tribometer, the formulated lubricating oil is subjected to a tribological study. Testing parameters used in the study are as follows:

Load: 45N
Speed: 400RPM
Testing Time: 10 minutes
Track Radius: 40mm

Dead weights are used in a loading pan to apply a load to the pin and a load cell is used to record the friction values. For recording the data on PC a Lab view based software of national instrumentation “data acquisition software” is used which convert analog data into digital and processed it in the NI data card.

To examine the effect of a specific load on the wear proportion of steel, the specific wear of the steel pin is measured in millimeter cube per newton meter. To determine the weight change for that purpose, measure the pin's weight before and after the test.

$$\text{Specific wear}=\frac{change\ in\ volume}{load \times displacement}$$

3. SURFACE CHARACTERIZATION PHASE

A. SEM

The topography of surface of pin is examined at a magnification of 500μm using the high vacuum analytical TESCAN SEM VEGA3 microscope to comprehend the lubricating mechanism of formulating ionic liquid-based bio lubricants.

B. Stylus Surface Roughness Machine

For the direct measurement of surface roughness of steel pin stylus apparatus is used. For each pin samples two readings of roughness are noted and their average values are computed. For measuring the surface roughness of steel pins move stylus tip equipped with a detector across the surface of the sample which provide a clear wave profile by digitally translating the electrical signal of the detector.

III. RESULTS AND DISCUSSION

As the experimentation has been completed. The results of each experiment will be discussed in this section.

A. Rheological Analysis of Formulated Oil

The result obtained from redwood viscometer using equation (1) indicate that the addition of choline chloride increases the kinematic viscosity of the both bio-based oils because hydrogen bonds are formed as a result molecular mobility of ions in solution is reduced. These experimental results are supported by the work of Nicolas.

TABLE I: RESULTS OF RHEOLOGICAL ANALYSIS OF FORMULATING OIL SAMPLES

Oils+IL (wt%)	**Redwood Second**	**Kinematic viscosity (10^{-4} m^2/s)**
Pure Coconut oil	103.95	0.2519
Coconut oil+0.5wt% IL	107.252	0.2602
Coconut oil+1wt% IL	111.25	0.2702
Coconut oil+1.5wt% IL	116.33	0.2830
Pure Cottonseed oil	132.40	0.3232
Cottonseed oil+0.5wt% IL	137.43	0.3358
Cottonseed oil+1wt% IL	141.66	0.3463
Cottonseed oil+1.5wt% IL	143.27	0.3503

B. Friction of Steel Disc

Fig. 3 displays the frictional coefficient of coconut oil with choline chloride as an additive. According to the friction profile, pure coconut oil has a coefficient of friction of 0.09, however adding choline chloride as an additive causes the friction coefficient to decrease because it forms a protective film between the contact surfaces, which causes less heat to be produced. The earlier works of Joseph Babu K. provides the confirmation of the results of the coefficient of friction of pure coconut oil (2003). The addition of 0.5wt%, 1wt% and 1.5wt% of choline chloride decrease the coefficient of friction of steel by 11%, 33% and 56% respectively.

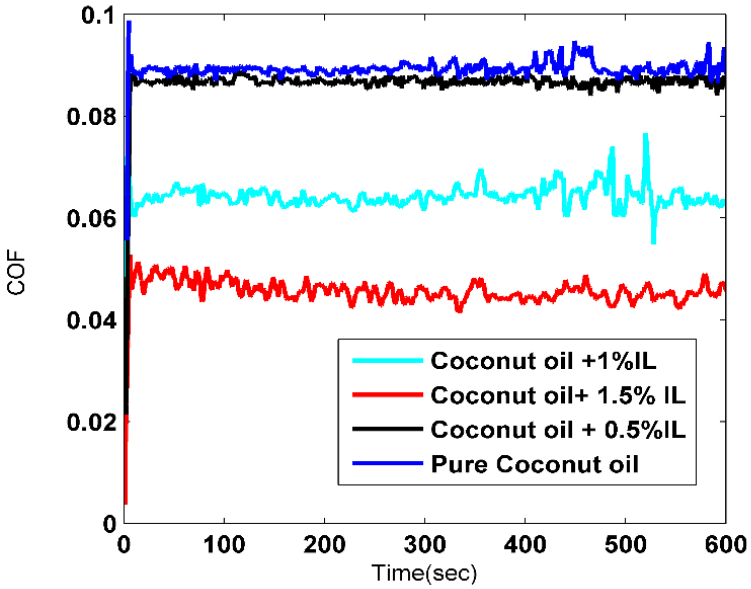

Fig 3. Coefficient of Friction Vs Time (Coconut oil)

Similarly, the addition of choline chloride as an additive to the cottonseed oil reduces the coefficient of friction by 40% when concentration of choline chloride is 1wt%. Further surge in the concentration of choline chloride increases the coefficient of friction due to the development of the residual films of chloride which affects the dipolar nature of cottonseed oil as a result rapid reduction in the strength of the protective film take place.

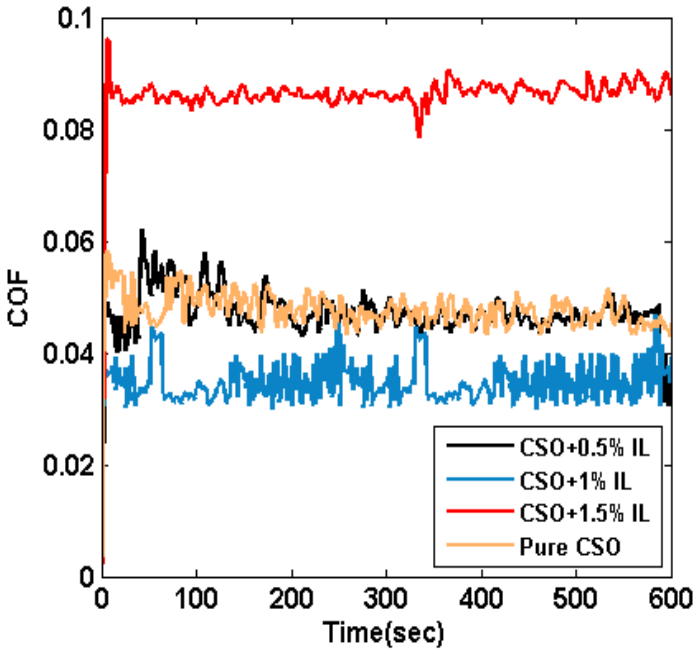

Fig 4. Coefficient of Friction Vs Time (Cottonseed oil)

TABLE II: RESULTS OF COEFFICIENT OF FRICTION OF FORMULATING OIL SAMPLES

Oils+I (wt%)	COF
Pure coconut oil	0.09
coconut oil+0.5wt% IL	0.08
coconut oil+1wt% IL	0.06
coconut oil+1.5wt% IL	0.04
Pure cottonseed oil	0.05
Cottonseed oil+0.5wt% IL	0.04
cottonseed oil+1wt% IL	0.03
Cottonseed oil+1.5wt% IL	0.08

C. Specific Wear of steel pin

The specific wear rate of steel using coconut oil containing choline chloride as an additive reduces as choline chloride concentration increases. These wear results of steel using pure coconut oil are supported by earlier research of Manu Varghese and Chacko Preno Koshy (2014). The specific wear rate of steel reduced by 80% when using 1.5wt% of ionic liquid-based coconut oil.

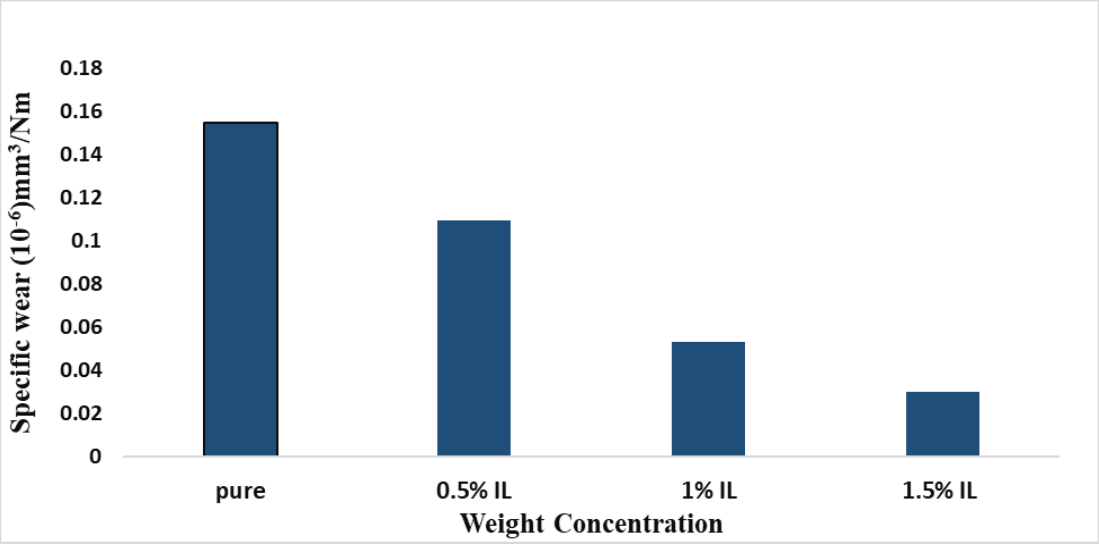

Fig 5. Specific Wear Vs Weight concentration of IL (Coconut oil)

Similarly, the specific wear rate of steel employing ionic liquid-based cottonseed oil has reduced to 44.4% when concentration of ionic liquid is 1wt%. However, when the concentration of ionic liquid will increase further the wear rate of steel increase due to the development of the residual films of chlorine which will act as resistive barrier for the lubricating oil.

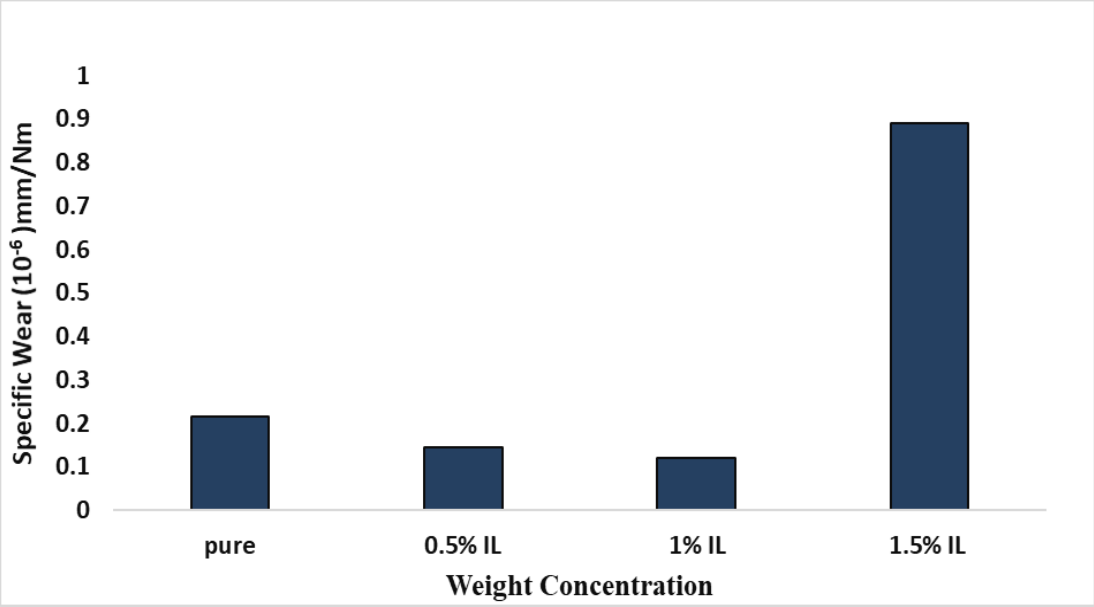

Fig 6. Specific Wear Vs Weight concentration of IL (Cottonseed oil)

TABLE III: RESULTS OF SPECIFIC WEAR OF STEEL PIN

Oils+IL (wt%)	**Wear Volume**	**Specific Wear 10^{-6} mm^3/Nm**
Pure coconut oil	0.006988	0.1544
coconut oil+0.5wt% IL	0.004955	0.1090
coconut oil+1wt% IL	0.002414	0.0533
coconut oil+1.5wt% IL	0.001397	0.030
Pure cottonseed oil	0.009814	0.21695
Cottonseed oil+0.5wt% IL	0.006543	0.1442
cottonseed oil+1wt% IL	0.005452	0.12043
Cottonseed oil+1.5wt% IL	0.040348	0.89120

D. *SEM Micrographs*

SEM micrographs of steels pin tested with ionic liquid enriched bio-based oils are shown in Fig 7 and Fig 8. It can be seen that the highly magnified images of steel pins at a magnifying power of 500**µ**m shows less tendency of the shallow grooves and pits at high concentration of ionic liquid but for a cottonseed oil having 1.5% IL the micrograph show high roughness of surfaces which results in the formation of more grooves and pits.

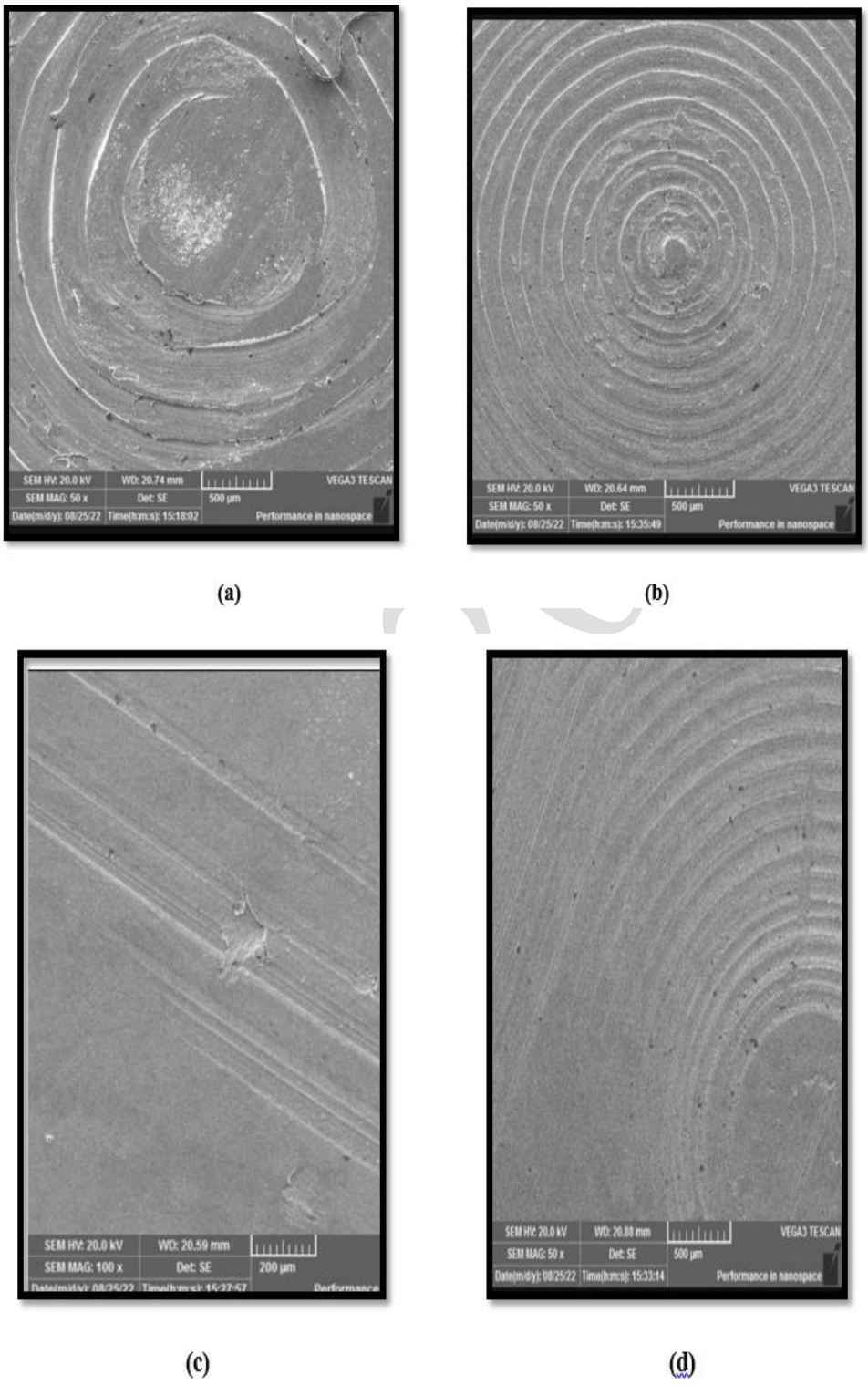

Fig. 7 SEM Micrograph of Steel Pin Using Ionic Liquid Based Coconut Oil

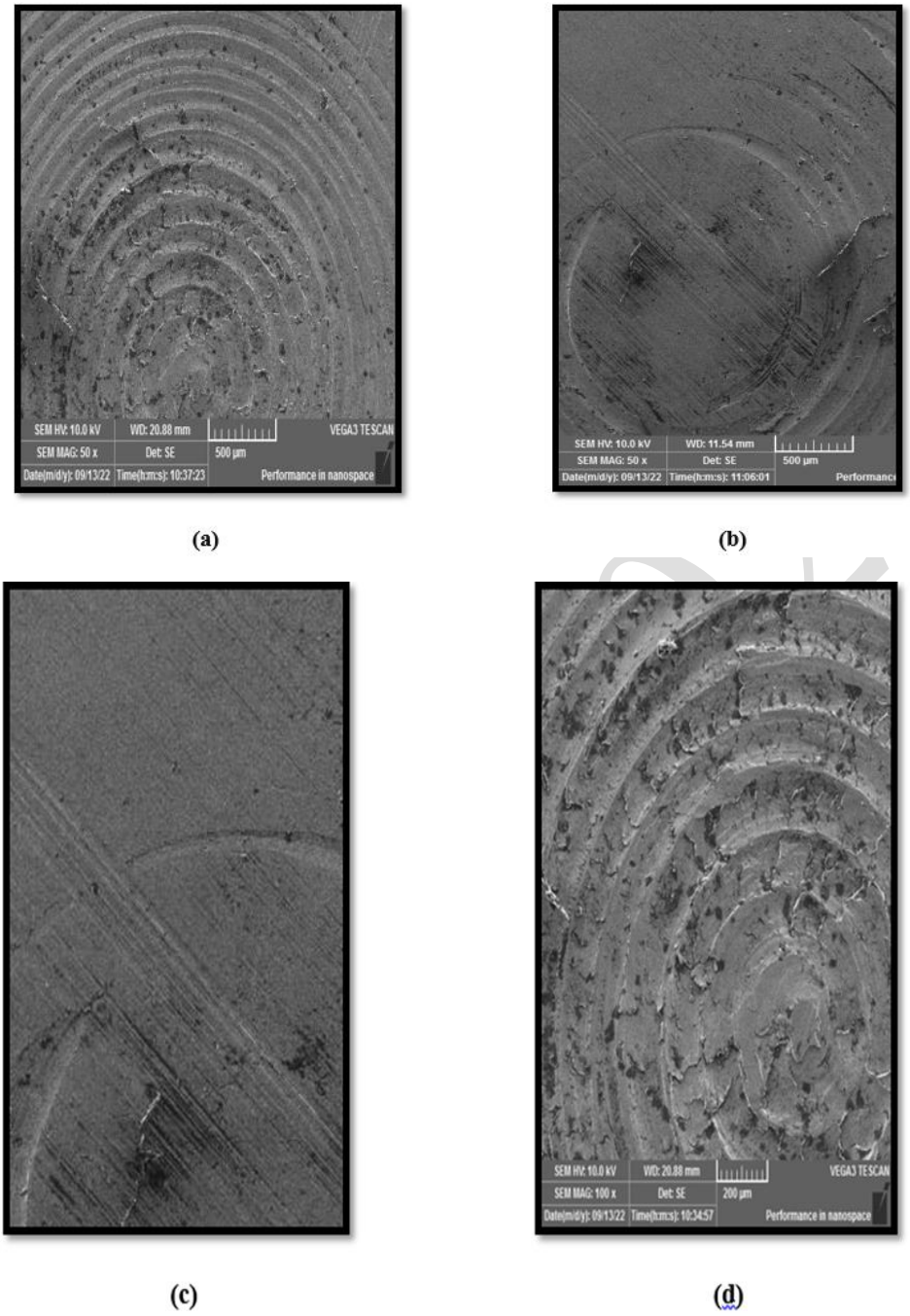

Fig. 8 SEM Micrograph of Steel Pin Using Ionic. Liquid Based Cottonseed Oil

E. Surface Roughness Measurement Using Stylus

The average value of all steel pin lubricated by the formulated oil samples and pure bio based oil are shown in table IV.

TABLE III: RESULTS OF AVERAGE SURFACE ROUGHNESS OF STEEL

Oils+IL (wt%)	Avg. Surface Roughness (µm)
Pure coconut oil	0.893
coconut oil+0.5wt% IL	0.613
coconut oil+1wt% IL	0.436
coconut oil+1.5wt% IL	0.266
Pure cottonseed oil	0.861
Cottonseed oil+0.5wt% IL	0.845
cottonseed oil+1wt% IL	0.562
Cottonseed oil+1.5wt% IL	1.612

IV. CONCLUSION

Tribological analysis of choline chloride as additive to bio-based oils showed that choline chloride is an efficient eco-friendly lubricant additive which can be used for steel machining operations. The use of choline chloride as additive reduces the friction of coconut and cottonseed oil by 56% and 40% respectively. Similarly, the surface finish of steel pins improved by using the ionic liquid based formulated oil due to less wear loss. It is envisaged that in the near future there will be clean and safe lubricating solutions that will aid in the development of industrial and economic competence by creating an environment friendly bio-based ionic liquid lubricant.

REFERENCES

[1] Shashidhara YM, Jayaram SR. Vegetable oils as a potential cutting fluid-an evolution. Tribol Int 2010;43:1073–81.

[2] Reeves, C. J. "An experimental investigation characterizing the tribological performance of natural and synthetic bio-lubricants composed of carboxylic acids for energy conservation and sustainability" (2013) The University of Wisconsin-Milwaukee.

[3] Belluco W, Chiffre LD. Performance evaluation of vegetable oil-based cutting fluids in drilling austenitic stainless steel. J Mater Process Technol 2004;148:171-6.

[4] Xavior MA, Adithan M. Determining the influence of cutting fluids on tool wear and surface roughness during turning of AISI 304 austenitic stainless steel. J MaterProcess Technol 2009:209:900-9

[5] Mehta, P. “Tribological Study of Textured Surfaces Created Using Modulation Assisted Machining for Steel- Aluminum Contact.” (2016)

[6] Zhou, F., Liang, Y., and Liu, W.,, “Ionic Liquid Lubricants: Designed Chemistry for Engineering Applications,” 2016 Chem. Soc. Rev., 38(9), p. 2590.

[7] Sani, Abdul, et al. "Performance Evaluation of Palm-Olein TMP Ester Containing Hexagonal Boron Nitride and an Oil Miscible Ionic Liquid as Bio-Based Metalworking Fluids/Amiril Sahab Abdul Sani...[et al.]." Journal of Mechanical Engineering (JMechE) 1 (2017): 223-234.

A Statistical Framework for Optimization of Cylindrical Grinding Parameters on AISI-D6 Steel

Iftikhar Ali Waleedy[1, a], Waqar Ahmed Qureshi[1, b] and Muhammad Mahboob[1, c]
[1]Mechanical Engineering Department, University of Engineering and Technology, Taxila

Email address: [a)] aliiftikhar53@hotmail.com, [b)] waqar.ahmed@uettaxila.edu.pk, [c)] Muhammad.mahboob14140@gmail.com

***Abstract*—Surface finish and dimensional perfection of AISI D6 steel is costly but core constraint of many machining industries. An excellent wear resistance and high strength AISI D6 steel is used in blanking and forming tools due to its high strength and great wear resistance. In this research, main focus is to achieve viable production during cylindrical grinding of AISI D6 on CNC machine by the Aluminium Oxide grinding wheel. Thus, optimization of surface finish and material removal rate (MRR) with respect to cutting parameters is key part of this research. It is achieved through enhancing productivity (increasing material removal rate), improving surface roughness and ultimately, integrity of finished product. The effect of three major influencing factors i.e. Work speed (rpm), machine bed feed rate (mm/min) and depth of cut (mm) have been investigated for production performance measures. Taguchi L9-orthogonal array is used to get best combination of input parameters against each machining run. Optimum levels of process parameters are identified through S/N ratio response analysis. Contribution of process parameters over response parameters is analyzed through ANOVA. Empirical models have been developed for response parameters by regression analysis. Confirmation experiments are performed and results are compared with predicted values to check validity of developed models. According to the parameters used in this study, it is concluded that the impact of work speed on the surface roughness is 78.25% of total influence, while the contribution of feed rate and depth of cut on MRR is 49.80% and 43.12% respectively. Optimum surface roughness achieved at 200rpm work spindle speed, 200mm/min machine table feed rate and 0.007mm depth of cut.**

Keywords—AISI D6 Steel, Grinding, Surface Roughness, Material removal rate, S/N ratio, ANOVA.

I. INTRODUCTION

In production industries, Machining is mostly used production technique to convert material from raw form into final product with desired quality and dimensional accuracy. Different Machining techniques like turning, drilling, milling, shaping, grinding etc. are being used for this purpose. Lot of study is available in academic as well as in industrial regime to understand these processes to improve quality, efficiency also by minimizing process/product cost [1]. In machining operations, grinding plays an important role by giving ultimate finish to material surfaces. It is a material removal process of abrasive machining in which abrasive grains act like cutting tool individually. Grinding is also a costly process that accounts for 20%-25% of total cost of machining operations in industrial sector but widely considered and used under finest conditions [2]. Due to several effects like mechanical, tribological and thermal loading, tool making industries face complex and aggressive conditions because materials with poor machinability are very difficult to process [4]. High carbon/ high chromium materials

with hardness around 60 HRC (as in case of AISI D6 steel) need appropriate combination and range of input/process parameters to predict of surface roughness [5]. B. Sato, R. Rodriguez [6] investigated grinding wheels for better performance of abrasives with high hardness, chemical stability and appropriate thermal conduction. During experimental analysis of EN8 steel, D. Goyal, and B. Pabla [7] in their study proved that abrasive type and wheel grade have great effect on surface roughness. Ran and W. Wang [3] proved in their study that parameters are correlated linearly to the grinding indicators. Experiments have been performed on universal cylindrical grinder to optimize cylindrical grinding parameters [8]. Patel, D. and B. Pabla [9] selected work spindle speed, machine table feed and infeed of grinding wheel (depth of cut) as main parameters for cylindrical grinding of EN8 steel using Al2O3 grinding wheel. Several researches have been made to analyze these parameters through Taguchi design and ANOVA. Taguchi Design of experiment (provided by Dr. Genichi Taguchi) is an engineering solution that offers systematic and very simple approach for optimization. It is an important tool that helps to discover key parameters those affect the quality of process and product. ANOVA(Analysis of variance) is the best statistical tool to determine significance and influence of process/input parameter on response/output parameter [10].

In this study, cylindrical grinding parameters are optimized to achieve better surface finish and increased material removal rate on AISI-D6 steel by considering work spindle speed, machine bed feed rate and depth of cut as process parameters. It has been achieved through Taguchi method and ANOVA.

II. EXPERIMENTAL SETUP

A. Material Selection and Sample Preparation

AISI D6 is air hardened tool steel (63 HRC) with high dimensional stability and edge holding quality. With good cold hardness, it is mainly used in tool making industries for manufacturing of shearing, blanking and forming tools due to its excellent wear resistance and high strength. Chemicalcomposition is shown in Table-I. To perform experiments, samples are prepared with 20 mm diameterand 120 mm length. Diameter of samples is maintained by grinding to obtain precise results.

TABLE I. CHEMICAL COMPOSITION OF AISI-D6 STEEL

Element	**C**	**Cr**	**Ni**	**Mn**	**P**	**S**	**Si**	**T**
Percentage	2.1	11.85	0.15	0.26	0.016	0.015	0.23	0.64

B. Process Parameters Selection

Based on previous research studies, speed of work, rate of feed and infeed of grinding wheel (depthof cut) are taken as cutting parameters with 3 levels. Aluminium oxide wheel is used for grinding to investigate its behavior on response. Input parameters are shown below along with their levels in Table-II.

TABLE II. CUTTING PARAMETERS WITH CORRESPONDING LEVELS

Sr. No.	Parameter	Level		
		1	*2*	*3*
1	Work speed (S)	100	150	200
2	Feed rate (F)	200	400	600
3	Depth of cut (DOC)	0.007	0.014	0.02

Except from above input parameters, some parameters are also considered and kept same foreach machining run to get precise results.

- Grinding wheel diameter: 350 mm
- Grinding wheel speed: 1400 rpm
- Number of passes: 05
- Coolant: Water miscible with 5% concentration
- Coolant flow rate: 27 liter/min
- Dressing tool Diamond point dresser
- Dressing feed: 100mm/min
- Dressing depth: 0.01mm
- Machining environment temperature: 25^{o} -30^{o} C
- Humidity 50-70%

C. Taguchi Design of Experiment

Taguchi DOE is very important tool that offers systematic and very simple approach to optimize design data**.** It provides a matrix of process variables designed through a suitable orthogonal array byexplaining combinational arrangement to conduct experiments to get response parameters for furtheranalysis. With three input parameters and 3 levels, Taguchi L9 orthogonal array is followed and combination matrix is generated accordingly in Table-III.

TABLE III. TAGUCHI L9 ORTHOGONAL ARRAY

Exp. No.	Work speed	Table speed	Depth of cut
1	100	200	0.007
2	100	400	0.014
3	100	600	0.02
4	150	200	0.014
5	150	400	0.02
6	150	600	0.007
7	200	200	0.02
8	200	400	0.007
9	200	600	0.014

D. Machining Setup, Procedure and Response Measurement

ROBBI CNC cylindrical grinder is selected for experimental work. Work piece is placed betweenheadstock and tail stock of machine and rotational energy is provided by head stock work spindle. Grinding wheel is mounted in wheel head assembly.

CNC programs are generated followed by input parameters and total 9 experiments are conducted on the basis of orthogonal array design. After experimentation, roughness (µm) is measured with Mitutoyo SJ-410 surface roughness tester following post process technique. Average surface roughness is calculated on the basis of three readings taken for each sample. Weight of each specimen is recorded before and after experiment to measure MRR. Volumetric MRR (mm3/sec) is calculated by weight difference of work material before and after grinding by dividing it with machining time and density of material. Density of AISI D6 steel is 7.67 g/cm3 which is constant for all machining runs. Machining time is measured by digital stop watch and weight is measured by a precise electronic weighing scale after proper calibrations.

Fig. 1. Experimental setup

III. RESULTS AND DISCUSSION

A. Signal to Noise Ratio

Response values are measured against each machining run and tabulated for further analysis. Obtained results have been analyzed through Taguchi analysis by MINITAB statistical software. It is a significant and useful parameter that describes how response parameter differs from target values under noise conditions. S/N ratio is calculated in different ways (Larger is better/nominal is best/ smaller is better). Response values and corresponding S/N ratios against each machining run are given below in Table-IV.

TABLE IV. RESPONSE PARAMETERS AND S/N RATIOS

Exp. No.	S	F	DOC	Ra (µm)	MRR (mm^3/s)	S/N Ratio against Ra	S/N Ratio against MRR
1	100	200	0.007	0.293	1.266	10.6626	2.0487
2	100	400	0.014	0.332	5.577	9.5772	14.9280
3	100	600	0.02	0.405	11.917	7.8509	21.5233
4	150	200	0.014	0.261	2.497	11.6672	7.9484
5	150	400	0.02	0.302	7.804	10.3999	17.8463
6	150	600	0.007	0.290	4.175	10.7520	12.4131
7	200	200	0.02	0.195	3.865	14.1993	11.7430
8	200	400	0.007	0.205	2.492	13.7649	7.9310
9	200	600	0.014	0.219	8.381	13.1911	18.4659

This table shows that experiment-7 yields minimum surface roughness and larger S/N ratio from Taguchi design matrix. As for material removal rate, experiment-3 results in maximum MRR and larger S/N ratio hence it is best available combination of input parameters.

B. Analysis of Signal to noise Ratio for Roughness of Surface

Values for S/N ratio i.e. Signal to noise Ratio are achieved by considering smaller is better approach to get minimum values for surface roughness. Surface roughness S/N response is given in table-V.

TABLE V. RESPONSE TABLE OF SIGNAL TO NOISE RATIOS FOR ROUGHNESS OF SURFACE

Level	S	F	DOC
1	9.364	12.176	11.727
2	10.940	11.247	11.479
3	13.718	10.598	10.817
Delta	4.355	1.578	0.910
Rank	1	2	3

S/N ratios response table 5 gives clear picture for optimization. Regardless used combination of input parameters for experimentation, response table refers to the best combination by giving S/N ratios of individual parameter with its levels. It is also can be analyzed that how S/N ratio changes when level of parameter is changed. Delta is obtained from difference of higher and lower values. More value of delta shows more influence of process parameters over response.

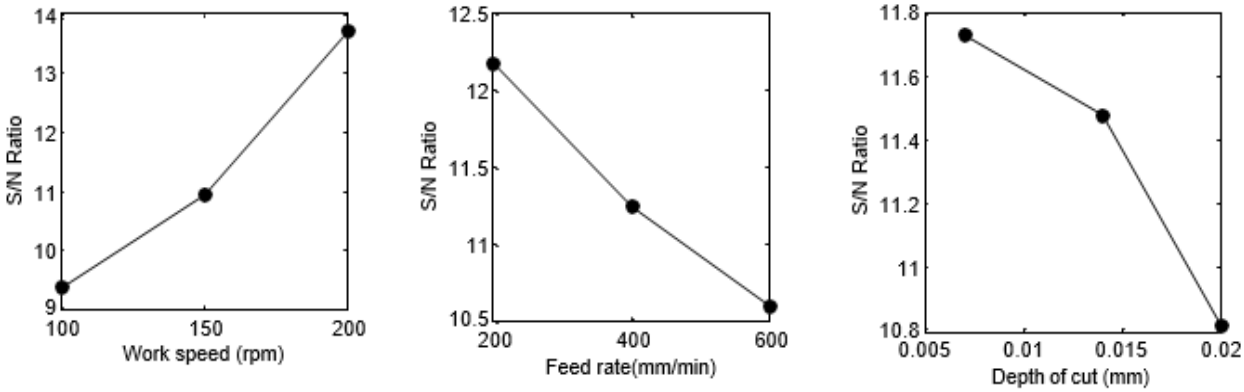

Fig. 2. Mean Effect of S/N Ratios for Surface Roughness

From graphs in Fig. 2, it can be observed that work speed has strong effect over surface roughness. Feed has less effect than speed and depth of cut has smaller effect among all process parameters. These graphs also yield that surface roughness is decreased by increasing work speed but increases by increasing feed rate and cut depth.

C. Analysis of Signal to Noise ratio for MRR

Values of S/N ratio against MRR are obtained by considering larger is better approach to maximize the values for MRR. Data is shown in table-VI.

TABLE VI. RESPONSE TABLE OF S/N RATIOS FOR MRR

Level	S	F	DOC
1	12.833	7.247	7.464
2	12.736	13.568	13.781
3	12.713	17.467	17.038
Delta	0.120	10.221	9.573
Rank	3	1	2

Effect plots for MRR are shown in the following figure.

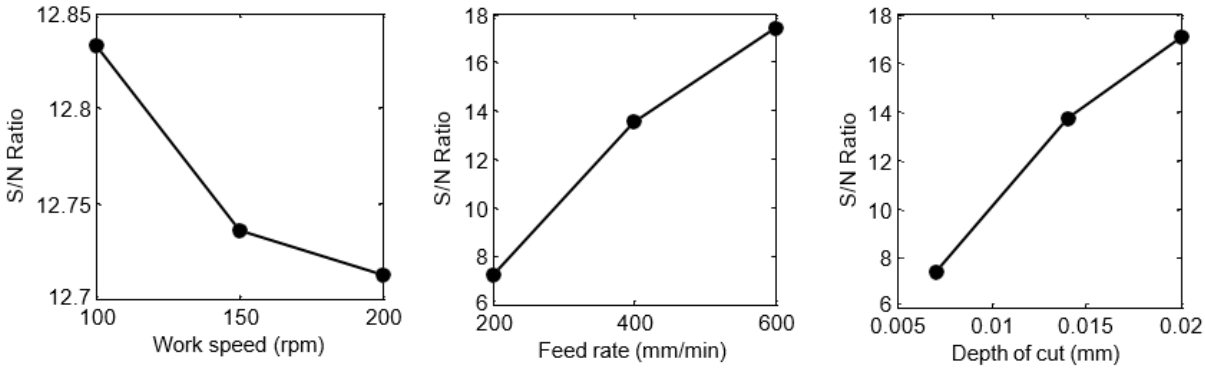

Fig. 3. Mean Effect Plot for S/N Ratios for MRR

It can be analyzed from fig.3 that feed rate then depth of cut have great influence to affect material removal rate whereas work speed has a negligible effect. Graphs have also proven that MRR is increased by increasing values of machine bed feed rate and depth of cut.

ANOVA is applied to identify significant factors and their impact on performance characteristics with 95% confidence level. P-value less than 0.05 yields that corresponding parameter is the significant parameter. Following are the results of ANOVA for the roughness of surface are showed in table-VII.

TABLE VII. ANOVA FOR SURFACE ROUGHNESS

Source	DF	Adj SS	Adj MS	F-Value	P-Value	Contribution
Regression	3	0.034789	0.011596	48.77	0.000	96.70%
S	1	0.028154	0.0281454	118.39	0.000	78.25%
F	1	0.004538	0.004538	19.08	0.007	12.61%
DOC	1	0.002098	0.002098	8.82	0.031	5.83%
Error	5	0.01189	0.000238	-	-	3.30%
Total	8	0.035978	-	-	-	-

By analyzing above data, it is concluded that work speed is significant parameter having major contribution to influence surface roughness that is 78.25%. Feed rate is also a significant parameter with less contribution than speed that is 12.61% while depth of depth has negligibly affected the roughness.

TABLE VIII. ANOVA FOR RATE OF REMOVAL FOR MATERIAL

Source	DF	Adj SS	Adj MS	F-Value	P-Value	Contribution
Regression	3	90.930	30.310	37.65	0.001	95.76%
S	1	2.696	2.6961	3.35	0.127	2.84%
F	1	47.292	47.2923	58.74	0.001	49.80%
DOC	1	40.942	40.9416	50.86	0.001	43.12%
Error	5	4.025	0.8051	-	-	4.24%
Total	8	94.955	-	-	-	-

Table-VIII shows ANOVA results for material removal. It shows that feed rate and depth of cut are statistically significant and have major contribution for MRR that is 49.80% and 43.12% respectively. Work speed is statistically insignificant and has negligible effect.

Empirical models have been developed on the basis of ANOVA. Regression is implemented by using statistical software MINITAB.

Ra (µm) = 0.3892 - 0.001370 S+ 0.000137 F + 2.847 DOC

MRR (mm3/s) = -3.76 - 0.01341 S + 0.01404 F + 401.5 DOC

IV. VALIDATION

Experiments are performed and results are compared with predicted values to check adequacy ofdeveloped empirical models. Results are shown in table-IX and table-X.

TABLE IX. VALIDATION OF DEVELOPED MODELS FOR SURFACE ROUGHNESS

Sr. No.	S(rpm)	F(mm/min)	DOC (mm)	Exp. Value in µm	Pred. value in µm	Difference
1	160	450	0.018	0.291	0.2836	0.00737
2	190	350	0.012	0.197	0.2115	0.0145

TABLE X. VALIDATION OF DEVELOPED MODELS FOR MATERIAL REMOVAL RATE

Sr. No.	S(rpm)	F(mm/min)	DOC (mm)	Exp. Value in mm^3/s	Pred. value in mm^3/s	Difference
1	160	450	0.018	7.913	7.6379	0.275
2	190	350	0.012	3.683	3.4232	0.260

It is found that there is very small difference between experimental and predicted values that confirms the reliability of developed empirical models.

After experimentation, Optimized values are calculated for minimum surface roughness at 200rpm work speed, 200 mm/min feed rate and 0.007 mm depth of cut that is 0.172µm. optimized value for MRR at 100rpm work speed, 600 mm/min feed rate and 0.02mm depth of cut is 11.917 mm3/sec.

V. CONCLUSION

Cylindrical grinding is the best option to furnish components by maintaining good surface integrity with dimensional accuracy. This research study applies Taguchi optimization technique to optimize cylindrical grinding of AISI D6 steel. Research findings are given below.

- Work speed is the major factor to influence surface roughness. It has contribution of 78.25% with Aluminum oxide wheel but it has negligible contribution to effect material removal rate.
- Contribution of feed rate and depth of cut on MRR is 49.80% and 43.12% respectively.
- Feed rate has less effect over roughness of surface as compared to work speed. Depth of cut has smaller effect on surface roughness among all selected parameters.
- Surface roughness is decreased by increasing work speed but increases by increasing feed rate and depth of cut.

- MRR has direct relation with feed rate and depth of cut. It gradually increases when these parameters are increased.
- Optimum value for better surface finish are 200rpm work speed, 200 mm/min feed rate and 0.007 mm depth of cut. Hence the optimized surface finish is 0.172 µm.
- Optimum combination of parameters for MRR are 100rpm work speed, 600 mm/min feed rate and 0.02mm depth of cut. Optimized value of MRR is 11.917 mm3/sec.

REFERENCES

[1] T. H. TRAN, X. T. HOANG, H. K. LE, Q. T. NGUYEN, T. T. NGUYEN, T. T. N. NGUYEN, ET AL., "A STUDY ON COST OPTIMIZATION OF EXTERNAL CYLINDRICAL GRINDING," IN MATERIALS SCIENCE FORUM, 2020, P. 18.

[2] S. Talapatra and I. Islam, "Optimization of grinding parameters for minimum surface roughness using Taguchi method," in International Conference on Mechanical, Industrial and Energy Engineering, 2014, pp. 25-26.

[3] S. Kumar and O. Bhatia, "Experimental Analysis & Optimization of Cylindirical Grinding Process Parameters on Surface Roughness of En15AM Steel," Journal of Mechanical Engineering, vol. Volume 12, 07/01 2015.

[4] S. Zhang, G. Zhang, Y. Ran, Z. Wang, and W. Wang, "Multi-Objective Optimization for Grinding Parameters of 20CrMnTiH Gear with Ceramic Microcrystalline Corundum," Materials, vol. 12, p. 1352, 04/25 2019.

[5] M. Nayak, R. Sehgal, and R. Sharma, "Mechanical Characterization and Machinability Behavior of Annealed AISI D6 Cold Working Steel," Indian Journal of Material Science, vol. 2015, 08/01 2015.

[6] P. V. Vinay and C. S. Rao, "Experimental Analysis and Modelling of Grinding AISI D3 Steel," International Journal of Recent advances in Mechanical Engineering, vol. 4, pp. 47-60, 02/28 2015.

[7] B. Sato, R. Rodriguez, A. Talon, J. C. Lopes, H. Mello, P. Aguiar, et al., "Grinding performance of AISI D6 steel using CBN wheel vitrified and resinoid bonded," The International Journal of Advanced Manufacturing Technology, vol. 105, pp. 1-16, 12/01 2019.

[8] D. Patel, D. Goyal, and B. Pabla, "Optimization of parameters in cylindrical and surface grinding for improved surface finish," Royal Society Open Science, vol. 5, p. 171906, 05/01 2018.

[9] L. A. Tung, V. N. Pi, L. X. Hung, and T. L. Banh, "A study on optimization of surface roughness in surface grinding 9CrSi tool steel by using Taguchi method," in International Conference on Engineering Research and Applications, 2018, pp. 100-108.

[10] D. Tien and N.-T. Nguyen, "Multi-objective optimization of the cylindrical grinding process of SCM440 steel using Preference Selection Index Method," Journal of Machine Engineering, 08/28 2021.

Design and Development of Speed Bumps System for Energy Scavenging

Shahzaib Tariq [1, a], Shahzad Arshad [1, b], Zubair Butt [1, c], Ahsan Zafar [1, d] and Riffat Asim Pasha[2, e]
[1]Department of Mechatronics Engineering, University of Engineering and Technology Taxila, Pakistan [2]Department of Mechanical Engineering, University of Engineering and Technology Taxila, Pakistan

Email address: [a)] 18-MCT-20@students.uettaxila.edu.pk, [b)] 18-MCT-11@students.uettaxila.edu.pk
[c)] zubair.butt@uettaxila.edu.pk, [d)] (18-MCT-36@students.uettaxila.edu.pk, [e)] asim.pasha@uettaxila.edu.pk

Abstract*—Due to daily rise in inhabitants and lack of resources, many countries facing energy calamities problems. In order to cope with this, it is necessary to use other sources of producing electricity. The automobile industry is growing massively and manufactured a vast number of automobiles every year. In this paper, the energy scavenging from the motion of vehicles was considered. For this, Eco-Friendly Energy Generation (EFEG) bumps system was developed. Energy is produced when a vehicle passes onto the bumps via mechanical and electrical assembly. Many researchers have used crankshaft and roller mechanisms for power generation, but we have used the rack and pinion mechanism because of its good strength and efficiency. When a vehicle moves on a bump it presses rack and pinion, which transmits linear motion into rotational motion to the gear system. The gears are used to increase the rotations. The permanent magnet direct current (PMDC) motor scavenges the power, which is then stored in a battery. The generated power is to be used by traffic signals and lighting up the roads via streetlights. Two analog sensors i.e., voltage and current sensor are connected with the PMDC motor for data acquisition purposes. Both the sensors are interfaced with a microcontroller (ESP 32) and the results are examined on a serial monitor. The experiments were performed to check the voltage and current values gained by the bump in a sing push. By using a digital millimeter (DMM), the voltage and current values of 29 volts and 0.7 amperes were recorded. Also, current and voltage sensors were used as data loggers to check the exact amount of current and voltages via ESP 32 and Arduino. It was found that the speed bump generates 15 Watts of power on the application of 140 Kg only. Moreover, the voltage and current values were measured from the sensor as 18 volt and 0.6 ampere. A capacitor was also charged from 0 volts to 10 volts by pushes of a bump. The calculated power of 15.4 Watts is obtained by using equations whereas actual power is measured in real-time with a speed bump. If we choose the vehicle with a heavy load, the output power was also increasing. This mechanism of generating electricity is valuable because there are no harmful effects on the environment, and are also economical.

Keywords—Energy Generation, Speed Bumps, Rack and Pinion mechanism, Eco-friendly System, Clean Energy Production

I. INTRODUCTION

A great invention, speed bumps in 1953 was introduced by Arthur Compton, and solved many daily life problems such as road accidents and traffic calming. Speed bumps were one of the most innovative ways to prevent vehicles, drivers, and pedestrians from over-speeding and accidents. As the evolution goes on, the engineers, mathematicians, and physicists are focusing on novelties of sustainable energy sources like hybrid cars, solar panels, wind turbines, etc. [1,2].

The automobile industry is growing enormously and manufacturing a vast number of automobiles every year. According to a report from the national transport research center (NTRC) which is part of the ministry of communication of Pakistan, the number of cars on roads is increasing tremendously; the energy scavenging from the motion of vehicles should be considered [3,4].

An energy crisis is a boundless bottleneck in the supply of energy resources to an existing economy. [5,6]. It is necessary to add conventional and non-renewable energy resources with new, innovative, and renewable resources. To accomplish the idea of the eco-friendly environment factor, the speed bumps are designed to generate energy whenever a vehicle passes over them without even harming the environment. Many countries, such as Japan and UK use speed bumps to generate electricity. It has also been the topic of various scientific types of research [7-10].

Over the years, many researchers have worked in power scavenging from speed bumps using different mechanisms. These mechanisms include piezo-electric disc mechanism, Roller mechanism and hybrid mechanism. All these mechanisms scavenge power whenever a load is applied to them as per their working capacity. Some of the mechanisms enlisted above have disadvantages. For instance, the roller mechanism is less efficient and requires more maintenance than any other mechanism [11-14].

In our project, we have used the rack and pinion mechanism due to its efficiency. Our research is based on EFEG (Eco-Friendly Energy Generation) Bumps. These bumps are convert kinetic and potential energy from vehicles into electrical energy via rack and pinion mechanism. The stored energy in batteries may be used later for any purpose like streetlights, traffic caution signals, etc. The rack and pinion mechanism is used to transmit the translational motion into rotational motion to the gear system [15, 16]. The axis of the pinion is coupled with the spur gear. The spur gear is made up of two gears of different sizes. The power is transmitted from the larger gear to the smaller gear. Compound gears are used with one being the idle gear to restrict the movement to one direction only. At the end, a PMDC motor is used which converts mechanical energy to electrical energy [18]. In our data acquisition phase, we performed a few experiments to check how much power is generated when we apply different weights.

II. METHODOLOGY

Design is essential for every project to show its impact on results and efficiency. For any good project, a successful design selection is required [17]. In this project, we have used rack & pinion mechanisms for energy generation from speed bumps. The proper structure and size matter a lot in speed bumps. So, the bump is designed in such a way that it produces no harmful safety issues. It is placed at the top of the mechanism joined with shocks via long-length bolts. The bump is welded with the rack so that when the bump is pushed downwards the rack also moves accordingly. By implementing this, we have got the power that is safe from any pollution. We have get approximately 95% efficiency by this mechanism. Gear systems are beneficial to increasing the gear ratio and ultimately increase the speed. Fig. 1 assembly gives good mounting convenience. Implementing speed bumps for power generation will satisfy

world doubts regarding its effectiveness. The spring is used to store mechanical energy. When pressure is applied, it remains resilient under the action of load and after removing its load it would regain its original shape. It changes its shape according to the load applied. The mild steal material has been used for this project so that it can endure more vibrations or shocks. The spring model is designed on Solid Works software as shown in Fig. 2.

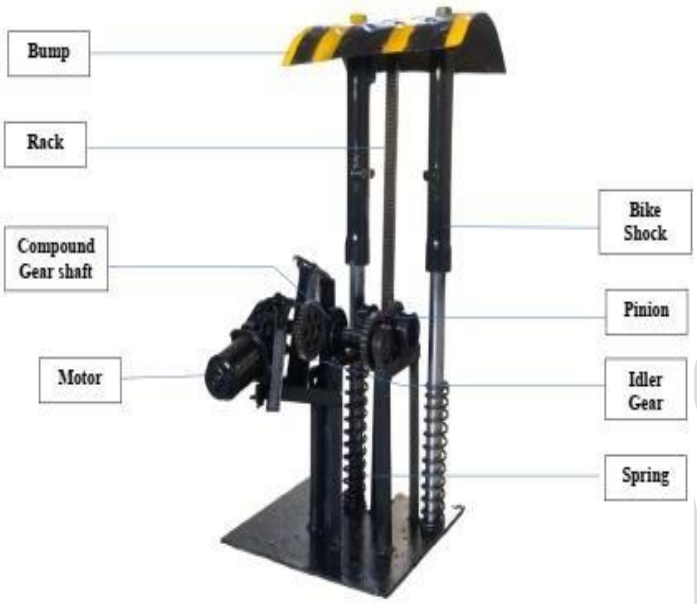

Fig. 1: Speed Bump System

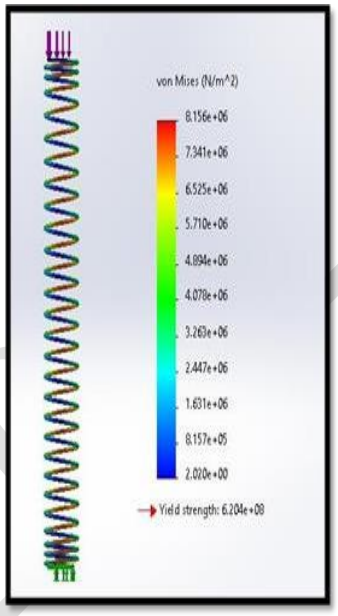

Fig. 2: Stress calculation via Solid works

A PMDC motor is another part that is attached to the shaft. For this project, the high shock absorption and wear resistance was obtained in the gears. The rotational action from the rack and pinion to the motor is continued via gears. We have used a DC motor that transforms mechanical energy into electricity and afterward it goes to the batteries for storage. Finally, we have connected the voltage sensor's VOUT pin to ESP's 36 pins and the current sensor to ESP's 34 pins. The output of the motor goes into sensors as input. VCC and GND pins are connected to ESP's VIN (5V) and GND respectively. The schematic diagram of the complete circuit is shown in Fig. 3 and necessary libraries were extracted into the arduino libraries folder after being installed through the library manager. To measure the current, sensor (ACS712) is used which works on the Hall Effect principle. The ESP32's analog pin D34 is connected to the pin output of current measuring (ACS712) sensor. This sensor produces an analog voltage output proportional to the measured current [18].

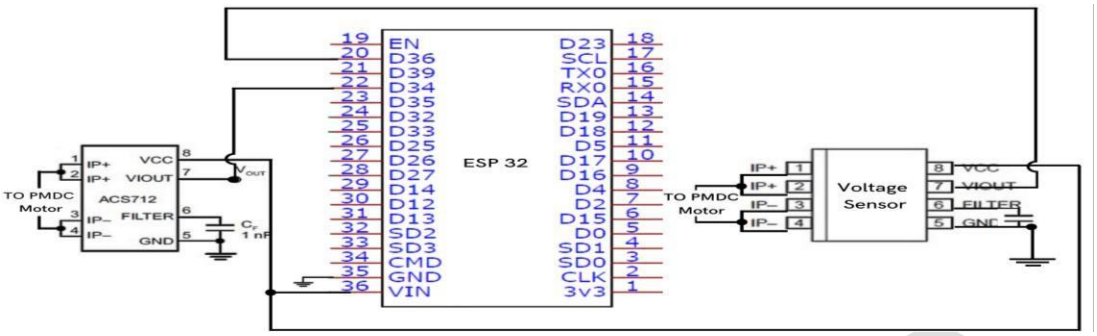

Figure 3: Schematic diagram showing connections of ESP with sensors.

III. RESULTS AND DISCUSSION

In this section calculated and measured values of voltage, current and power are deliberated and interpreted.

First, we have calculated the output power by using formula W=F.D under variable loading conditions. Fig. 4a and 4b clearly shows that when a heavy load is applied to the bump, more power is produced, more than enough to illuminate the street lights all of the day. Batteries have been utilized to store the additional energy for usage in the case of an emergency. The actual power was obtained by applying different weights to generate voltages and current, which were then measured by DMM. It is observed that, the calculated values of average current and voltage are 0.7 Amperes and 22V. The relationship between different parameters (current, and voltage) is shown in the Fig. 5.

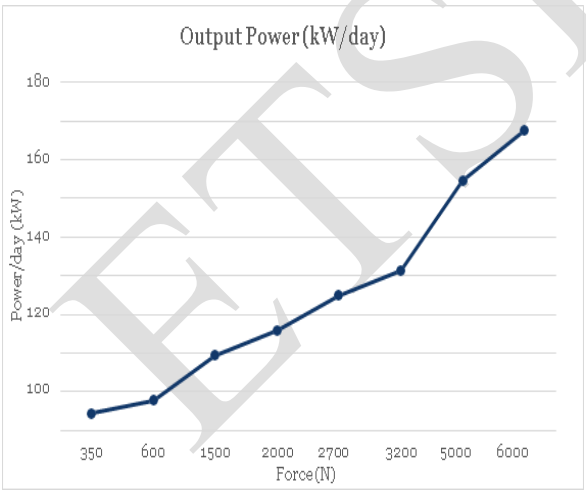

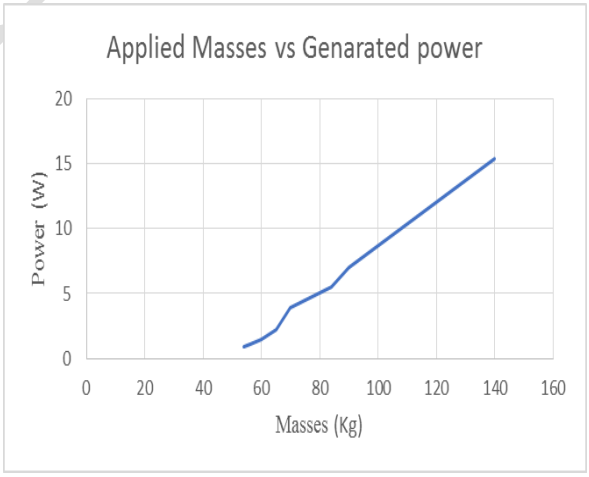

Fig. 4a: calculated power under different loads Fig. 4(b): Measured power under different loads

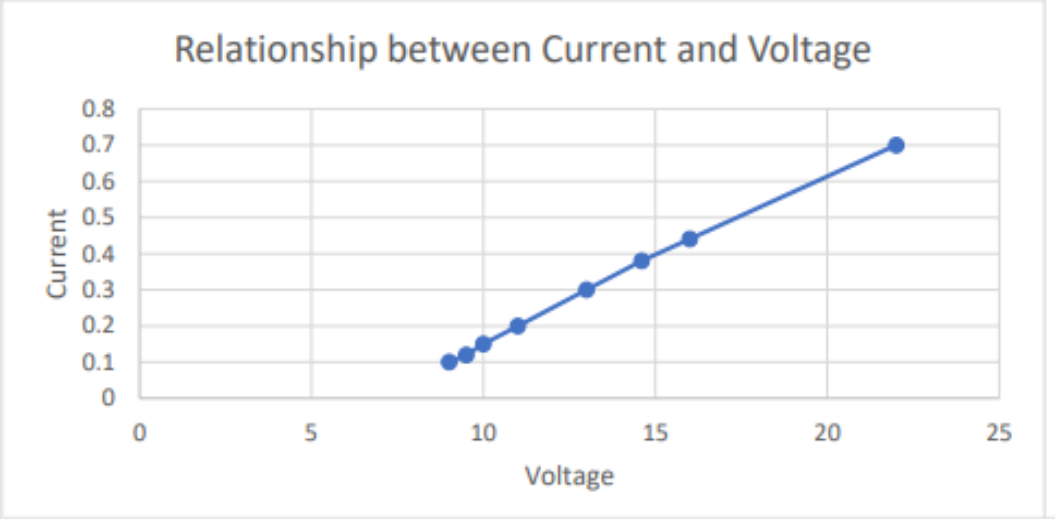

Fig. 5: Output voltage and current under constant load of 350Kg

Fig. 5 shows that as mass/load increases, current and voltages climb noticeably, which in turn causes power to rise. The voltages and currents were also taken by applying different weights using sensors interfacing with ESP 32 as shown in Fig. 6. The average value of voltage and current are found to be 12 Volts and 0.4 Amperes.

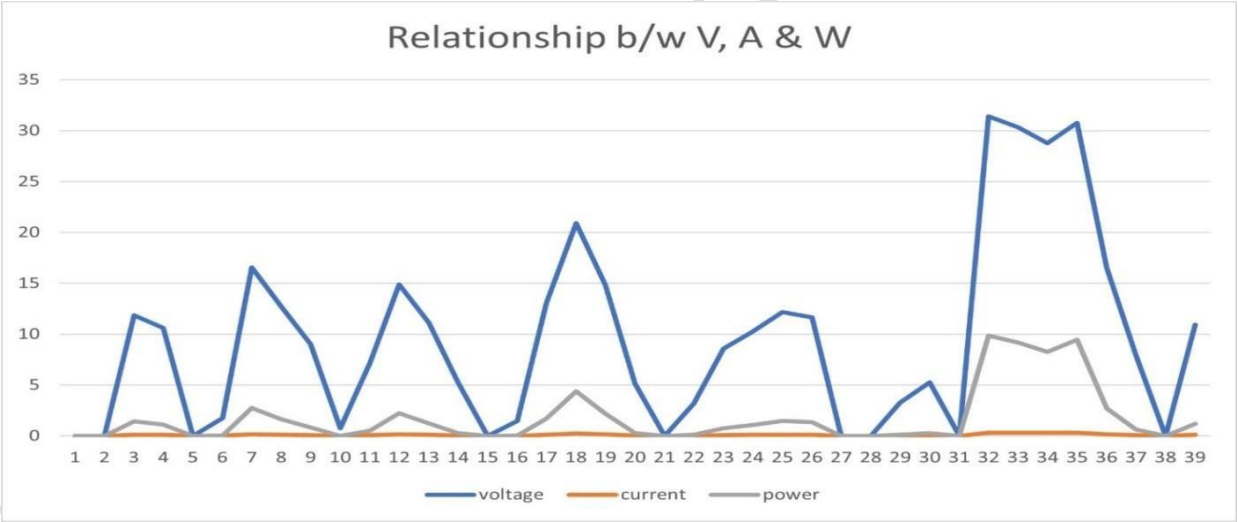

Fig. 6: Serial monitor showing current and voltage values respectively

IV. CONCLUSION

Because of worse energy crisis and inflation in energy prices, traditional methods of generating power are not much sustainable. In addition, a shortage of resources and a rise in the population have cause calamities in many developing nations, particularly in Pakistan. To cope with this, there is a dire need to develop more inventive and unconventional methods of generating power. Furthermore, the automotive business is rapidly expanding and producing a large number of vehicles each year. In light of this, we have developed Energy Generation Eco-friendly (EFEG) Bumps, which employ a rack and pinion system to scavenge energy. When a

vehicle drives over a bump, the rack turns the pinion, converting the vehicle's linear motion into circular motion. This rotary motion then drives compound gear shafts to increase the gear speed. Many experiments were also conducted to determine how much current and voltage it produces when pushed against the bump. A capacitor was charged from 0 to 10 Volts by several pushes. The current & voltage sensors were attached, and it was found that the speed-bump generates 29 volts and 0.7 Amperes. On increasing load on the bump, the output currents & voltages are also increased. A 12-Volt battery was also charged. It was found that by 10 pushes, the battery charges up to 0.01 to 0.03 volts. According to our research, socially, economically, and environmentally, the bump is advantageous as it is a Clean-Green, Eco- friendly, Tax- free, and innovative design that can work 24 hours in a week.

AKNOWLEDGEMENT

This research project was carried out at Department of Mechatronics Engineering, University of Engineering and Technology Taxila, Pakistan which is gratefully acknowledged.

REFERENCES

[1] A. Laksimi, "SPEED BUMP GENERATING ELECTRICAL POWER," SCHOOL OF SCIENCE & ENGINEERING – AL AKHAWAYN UNIVERSITY, 2019.

[2] H. Khawar, "Lahore ring road and toll rates," The Express Tribune, Lahore, January 30, 2018.

[3] Masoud Bakht, Omair , "Traffic Counts on M-9, And National Highway N-05," July, 2012.

[4] D. J. J, "Power Generation from Speed Breakers by Air Compression Method," International Journal of Engineering Development and Research, vol. 3, no. 2, 2015.

[5] Haneea Isaad, Sam Reynolds, "Finding the Right Way Forward in Pakistan's Energy Crisis," The Debate, 2022.

[6] D. mitriev, "Electric Power Generating Speed Bump," Google Patents, 2012.

[7] J. N. (Twitter), "Speed Bumps installed on NorthSouth Highway," JIS NEWS, 2019.

[8] AbdelGawad, A. F., " Power Generation Using Compressed Air from Artificial Road Bumps.," Thirteenth International Conference of Fluid Dynamics, pp. 21-22, December 2018.

[9] A. Symeoni, "A review on energy harvesting from," M.Sc. Thesis, Environmental Engineering and Sustainable Infrastructure., 2018.

[10] Mrs. S.S Pitre , Mr. Rahul Raj , Mr. Sachin Raina , Mr. Akash Bhoria , Mr. Alok Kumar , "Electricity Generation Using Speed Breaker," International Research Journal of Engineering and Technology (IRJET), 2018.

[11] Aniket Mishra, Pratik Kale, Atul Kamble, " Electricity Generation from Speed Breakers," The International Journal Of Engineering And Science (IJES), vol. 2, no. 11, pp. 25-27, 2013.

[12] ANUPAM TRIPATHI, ANURAG MISHRA, AMOD KUMAR,, "POWER GENERATION USING SPEED BUMPS," JSS Academy of technical education.

[13] R. Raman, "Sustainable Design of Speed Breaker for Production of Materials," IEEE Conference on Sustainable Utilization and Development in Engineering and Technologies (CSUDET), pp. 200-204, 2019.

[14] S. M. R. S. K. B, "Energy Harvesting using Speed Breaker," international Conference on Electrical, Electronics, Communication, Computer and Optimization Techniques, pp. 201- 204, 2017.

[15] A. Mishra, "Electricity Generation from Speed Breakers," The International Journal Of Engineering And Science (IJES), vol. 02, pp. 25-27, 2013.

[16] M. H.-E.-H. M. Rokonuzzaman, "Analysis of Speed Breaker Mechanism for More Effective Electricity," International Conference on Mechanical, Industrial and Materials Engineering (ICMIME), pp. 11-13, 2015.

[17] C. G. J. A. Abraham, "Eco-Friendly Power Generation from Speed," IJIRST – International Journal for Innovative Research in Science & Technology, vol. 03, pp. 227-230, 2017.

[18] N. M. Abhishek Gupta, "Electricity Generation from Speed Breakers," International Journal of Electrical and Electronics Research, vol. 04, pp. 135-139, 2016.

Thermal analysis and the optimum pin fin configuration for a heat sink design for a central processor unit (CPU)

Abu Summama Sadavi Bilal[1*], Abid Hussain[1], Muhammad Umar Munir[1], Muhammad Arslan Liaqat[1], Inaam Ullah Mesum[1] and Zartasha Shafqat[1]
[1]Department of Mechanical Engineering, University of Engineering and Technology, Taxila 47050, Pakistan
*Correspondence: summamabilal12@gmail.com

***Abstract*—For electronic cooling the most remarkable gadget used is heatsink. Continuing to expand the thickness of the execution in the computer chip processor, acquiring the size of electronic things, fulfilled the importance of the issue of Heat connection in business. This issue will improve the presence of the hardware group while decreasing the responsiveness of the central processor. A drop-in intensity with a strong development force is necessary to prevent these outcomes. Choosing a sensible cooler consideration requires splitting the difference between space openness, weight, and cost as well as performance qualities when developing the surface of the cooler model. it gives an ideal heatsink configuration utilizing an unpredictable system that haphazardly creates the pin position by envisioning a Heat profile utilizing Ansys programming. The discoveries of this study suggest a new (great) pin balance plan that can give better Heat execution, which is 2.84 percent and 0.63 percent, independently, as opposed to the typical straight-line and staggered plans. Empowering a direct and proficient strategy with a sporadic methodology can be an imperative obligation to the movement of game plans and tackling present day issues.**

Keywords—heat sink, CPU, heat transfer, Ansys, thermal

I. INTRODUCTION

In a similar way, there are several rules to consider when choosing the best attenuator, such as deciding on the power drop edge, material used, wind current, and more. As shown by Chen et, shown by Confined Part Framework and inheritance calculation improvement procedure, can be used to find the ideal force drop value plot for better energy dissipation. A directly adaptable control framework for the microprocessor cooler process is then created. A fan was employed to regulate the presentation of the intensity power in an ideal show in order to provide a fantastic performance. Another conclusion raised by Khan et al. is that altering the types of intensity slows down the process of refining the system for choosing the best levelling board. To lessen the Heat hindrance, the approach to improve the procedure involves finding the ideal inspiration for the five perspectives, the essential part of the strength drop, and the distance between the plates. Then, at this point, at this point, tests were additionally conducted between the two power damper materials, which are aluminum and copper.

When working continuously, the transparency of the power sink is based on the region on the computer. S. Manivannan presented an older procedure for registering the improvement of a chip study of declining performance by reducing the entropy clock. Trial and error was aimed at finding CPU performance using the Intel Pentium Center 2 Gathering processor. Another revolved around the typical standard power point model convection. The two evaluations were

investigated by playing the mathematical recovery of the performance drop and reintroducing the limited model on the current and the Heat obstacle on the heatsink. Another improvement technique introduced a three-layer pin-equilibrium and plate cooler plan using Ansys programming. A legacy computational methodology was used to investigate the capability between inline pin balance plans; edge sharp edge then again the system and plate balancing the cooler. By extension, this shows that a state-of-the-art heatsink can encourage specific intensity dissipation after a plate change. This then shows that different ways of dealing with rationalization can be used to create an ideal arrangement. For now, specialists suggest further study with other different improvement procedures.

II. THEORY OF HEAT SINKING MODELING

Heat is portrayed as an energy or as a respectable degree of heat. Temperature can be evaluated in degrees Celsius or Kelvin while power can be quantified as energy in watts (W). In thermodynamics, intensity enhancement is a cycle that involves an increase in energy beginning in one location and moving to the next region as a result of temperature contrasts. The cold zone will be heated by the nuclear energy being transferred from a hot to a cold region, directly, or possibly from a hot region. The intermittent transfer of Heat energy between a substance and a sink, such as a central processor (microchip), is known as heat conduction. Convection is the process of transferring energy between the climate inside the air chamber channel and the intensity drop.

An item that enables replacement away from the power source is a cooler. Similar to the CPU, random access memory, and chipset, the majority of power sensors are frequently employed as heat-lead components. It is mostly used as a gadget since it is economical, simple to operate, and has a practical design that sets it apart from other cooling systems. There are two extensively utilised forms of power sinks in the industry, with the top heatsink and the Level Harmony heatsink serving as clear examples. In this work, a 3D model is suggested to mimic a different pin balance heat sink layout model. The model given by typical pin weight cooler layout plans is implanted and dampened, then the accompanying base motion is fleeting as shown in Figure 1 below. Power sink models are made of aluminum material. Perhaps it could be isolated into two segments, which are the heatsink base and the square faces. The edges of the square pegs are joined by various plans on the bases of the conventional sides.

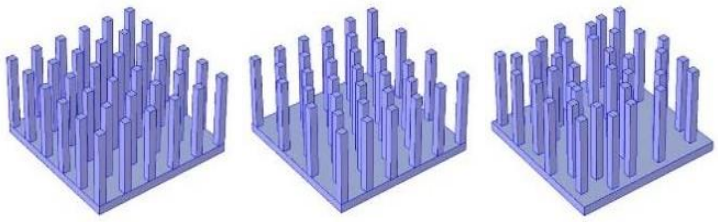

Fig. 1: Heat sink's models: (1) Inline: (2) Staggered: (3) Random

The ordered intensity drop model is impaled on the Processor N450 computer chip. Manufactured by Intel Affiliation, this processor chip is a supposed basic PC character,

significantly more explicitly a insignificant cost, restricted PC client for the web and web access. Total energy usage or the absurdest This chip only disperses 5.5 watts of nuclear energy. Table I displays the pin balance cooler model's development status and model parameters. With regard to the Ansys programming group under the Heat development module, the redirection is completed, including the required component technique. This lesson offers the fundamental instruments needed to test the heat sink model in flow and conduction heat transfer. Exploratory run-in with the fan acting as a delta for the wind flow and the intensity dip inside the airbox duct. Rating of the pin balance cooler model in general. The evaluation revealed four steps for building a pin fin cooler model. The creation of a mathematical model of power reduction is the initial stage. Several boundaries are laid out in this document, such as the power base view, pin front line, and channel air box. Then at this point 36 square stakes proportion join the energy sink, either typical (inline/dead) or inconsistent technique.

After completing the mathematical drawing on the power drop model, an example of selecting material properties and representing boundary conditions in the Heat development module follows. Choosing aluminum as a material for a serious sink. A square-shaped region was selected as a bay current with a delta temperature setting of 20 °C and a channel velocity of 10 cm/s. Currently, the resulting stage is to create a limited cross-section of parts on the performance drop model. This collaboration aims to isolate the science into a small model-shaped unit. In Ansys programming, the client can choose a material science management cross-section or a client management association. The actual control network is a modified procedure that selects a section size that is not completely fixed in the programming nuances. For the client inspection organization, the scope of the inspection part size should be chosen, for example, the most incredible part size, the smallest part size, the tight target of the locale and so on.

TABLE I. DIMENSION OF PIN FIN

Name Parameter		Values	Descriptions
Airbox (channel)	L (channel)	6.0 cm	Length (channel)
	W (channel)	5.0 cm	Width (channel)
	H (channel)	2.0 cm	Height (channel)
Chip processor unit	L (chip)	2.20 cm	Chip size
	H (chip)	0.10 cm	Chip height
	P (Total)	5.55 W	Total power dissipated
Pin fin	L1	1.70 cm	Pin height
	L2	0.20 cm	Square pin thickness (in the heat sink)
	Number of pin	36.0	Inline, staggered or random arrangement
Heat sink base	H-size	0.20 cm	Base thickness
	L-size	4.0 cm	Square

Air flow inlet	Uo	10.0 cm/s	Mean inlet velocity
	To	20.0°C	Inlet Temperature
Material		Aluminium	

III. RESULTS AND DISCUSION

The redesign was carried out on a PC with a 12GB Mallet 3.30 GHz processor using Ansys' Design Power Move Affiliation Point module. For the power well and the wind flow in the channel box, the models have a heat profile. Everywhere in the electronic component, different types of heatsinks with jagged edges are used as power dissipators. Nuclear energy is transmitted from the chip processor, which operates at a high temperature, to the power sensor's aluminium pin, which operates at a low temperature. The convection connection is another source of energy that is transferred between the power well's outer layer and the moving liquid at various temperatures.

A. Pin fin heat sink with inline alignment

Qualifications during the event are the length and circumstance of the division between the sharp edges of the pin. Deferred result of a Heat execution with a different inline methodology plan and a different Heat execution. All things considered, for a full inline curve, the pin balance is 36. As the W and L ratings become more modest, the Heat consequence of the performance drop is reduced. The best thermal response for the sink model's inline pin balance plan is 90.78°C. It's surprisingly simple to notice that all versions of inline pin balance coolers have smooth airflow created inside the channel box.

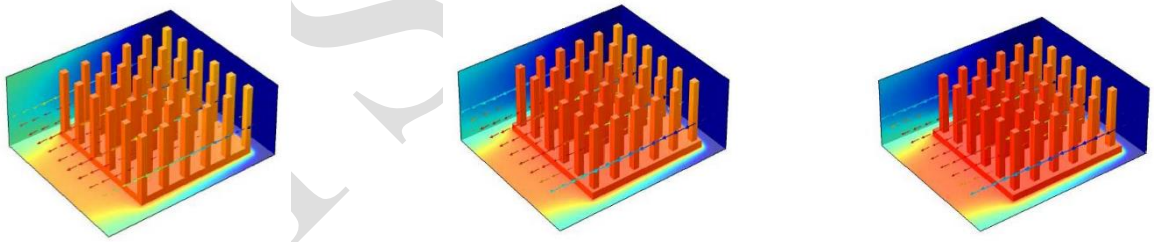

(a) 91°C (b) 92°C (c) 94.5 °C

Fig. 2: Inline alignment of heat sink models

B. Pin heat sink with a staggered design

A remarkable development is yet another common component of the model of the cooler with sharp edges. In this study, various variants of the sharp-edged heatsink type with various layouts were tested. He settled on a three-spread type with pin balance sink strength. The best heat component this model can produce is 88.83°C. Overall, it will be clear that obstacle currents are created for the majority of intensity sink models using a stun pin.

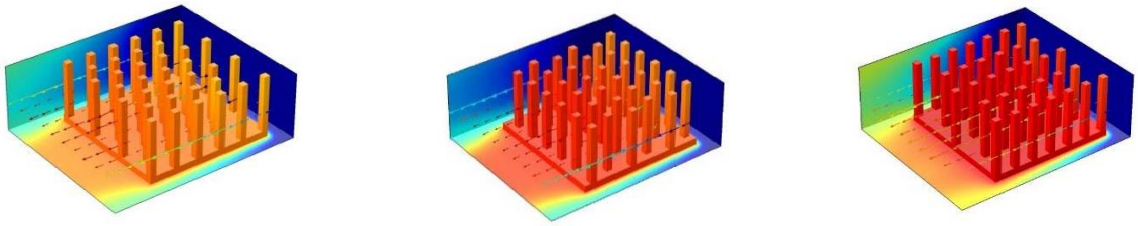

(a) 93.21°C (2) 89°C (3)98°C

Fig. 3: Staggered alignment of heat sink models

C. Thermal model analysis

Given the results of the renovation, this study shows that a replacement drawing of the sharp edge of the pin mounted on the power well support will provide a Heat profile. Regarding the three kinds of diagrams, organized as irregular improvement, the affirmation plan with the greatest temperature is simply 88.27°C, which are not exactly different frameworks. These findings demonstrate how the calculation and placement of the pin face, which ensures a smooth wind flow on the outer layer of the pin modifies the heatsink, determine the decent strength of the heat scheme.

IV. CONCLUSION

This report introduced a Heat execution of different pin balance heat sink model strategies, for the PC (CPU) regulator model, N450 focal processor. The reenactment results showed that the ideal pin cutting edge strategy would give a more worthwhile force spread over the customary methodology. The outcome communicates that it is vital to pick a reasonable course of activity of the pin cutting edge since it gives a superior Heat presentation to electronic cooling, particularly the CPU processor. Another coherence and significant thing in arranging the game-plan of offsetting the cone with blended stream around the pin cutting edge in with laminar and tempestuous stream will give better power of the Heat plan. From the best rule of the approach made from this archive, it can before long work with the straightforwardness of the review, particularly in the execution of the populace advancement procedure while following the best course of action of the Heat profile.

The consequences of the diversion recommended an alternate blueprint (ideal) with pin balance that is prepared to give 2.84% and 0.63% better hot execution rather than the standard arrangement that is inline and staggering game-plan. Further exploration ought to be finished involving the system of working on formative calculations on people looking for the best strategy of the turn edge. Moreover, the concentrate ought to also be conceivable at various material power sink, wind speed and channel airbox for future work. Furthermore, there is a need to make a model on the ground side concerning the consequence of generation.

REFERENCES

[1] L. C. Jenkins and A. Bennett, "21st century challenge: thermal management design requirements," in Digital Avionics Systems Conference, 2004, pp. 9.D.1-9.1-7 Vol.2.

[2] A. Bar-Cohen, "Thermal management of microelectronics in the 21st century," in Electronic Packaging Technology Conference, 1997, pp. 29-33.

[3] P. Ravibabu, K. Rajshekar, and K. Rohit Kumar Gupta, "Heat pipes - integrated circuit heat sinks," in Nanoelectronics Conference (INEC), 2010 3rd International, 2010, pp. 260-264.

[4] F. Yongling, Z. Meng, Q. Haitao, and A. Gaocheng, "Application of heat pipe technology in the design of hydraulic motor pump," in Electronic and Mechanical Engineering and Information Technology (EMEIT), 2011, pp. 1033-1036.

[5] M. C. Zaghdoudi and A. Teytu, "Use of heat pipes for avionics cooling," in Electronics Packaging Technology Conference, 2000. (EPTC 2000). Proceedings of 3rd, 2000, pp. 425-430.

[6] C. Anbin, X. Fengyu, L. Xiaokun, H. Yubao, W. Zonglin, Z. Yingshun, et al., "Sub-Cooled Liquid Nitrogen Test System for Cooling HTS Synchronous Motor," Applied Superconductivity, IEEE Transactions on, vol. 22, pp. 4701304-4701304, 2012.

[7] Chen, C.-T., Wu, C.-K. & Hwang, C., "Optimal Design and Control of CPU Heat Sink Processes," IEEE Transaction on Component and Packaging Technologies, 2008, pp. 184-195.

[8] W. A. Khan, J. R. Culham, And M. M. Yovanovich, "Modeling Of Cylindrical Pin-Fin Heat Sinks For Electronic Packaging," IEEE Transactions On Components And Packaging Technologies, 2008, Vol. 31, pp. 536-545.

[9] S.Manivannan, R.Arumugam & Sudharsan, N. M., "Design Optimization of Microprocessor Heatsink and Its Impact on Processor Performance," International Journal on Information Sciences and Computing, 2009, vol. 3, pp. 8-14.

Mechanical and durability properties of 3D printing concrete A-Review

Haseeb Murtaza[1, a]* and Nouman Mustafa[2, b]
[1]Department of Civil Engineering, University of Engineering and Technology, Taxila 47080, Pakistan.
[2]Department of Civil Engineering, University of Engineering and Technology, Lahore, Pakistan.
*Correspondence: haseebmurtazasansi@gmail.com

Email address: [a)] haseebmurtazasansi@gmail.com, [b)] nouman135799@gmail.com

***Abstract*—Due to control of digitization, mechanization, and a high degree of intelligence 3D-printing concrete has influenced extra and further recognition for bold construction. This article initiates fundamental basics, linked operations of 3D-printing concrete, and analysis its evolution through the subsequent four departments: the printing criterion, preparation technology, material properties, and assessment principles of 3D-printing concrete automation. Afterwards, actual awkwardness, evolution supervision, and crucial mechanization of 3D-printing concrete are defined. Lastly, we review the onward evolution anticipation of 3D-printed concrete via the appearance of printing mediums, hardware cooperation and software printing technology, etc.**

Keywords—Durability properties, mechanical properties; material properties: 3D-printing; concrete.

I. INTRODUCTION

For concrete construction, 3D-printing automation is the advanced automation enlarged based on 3D printing technology. Its operating principle is to pass the composed sludge via ejection mechanism, by the command of the 3D software, such that under preplanned settings a good printing sludge is ejected by the nozzle. As an advanced type of concrete mold less casting technology [1]. 3D-printing automation can utilize computer-aided design appliances in the construction work. 3D printing concrete automation drains little effort when applied to complicated projects as compared to traditional construction types, and 3D-printing concrete automation can develop the structures of desired quality. By greater utilization and advancement of 3D-printing concrete automation, we can successfully decrease the requirement of materials, labor, and equipment in the construction activity and enhance the progress of computer-aided construction [2]. Rensselaer Polytechnic Institute in New York, USA, developed the technique for 3D printing concrete. Pegna published the first study on 3D printing in building in 1997, demonstrating the usefulness of the technology for construction work [3]. Contour crafting was developed by Khoshnevis et al. in 1998 at the University of California (CC), the method utilizes computerized design to pour concrete and gives a smooth contour surface and composite structure by commanding the nozzle [4], [5]. Dini introduced D-shape technology in 2007. D-shape technology uses fine sand that is sprinkled on the binders and contains magnesia powder to gradually stiffen to produce a solid stone. The process is executed with the help of multiple nozzles available at the base of the printing machine. The sand layers are linked together to configure a stone structure [6].

Figure 1 (a) Mixture B is being sprayed by a 3D printing machine.; Figure 1 (b) depicts a fine-grained, lightweight aggregate concrete that was 3D printed without fibers. (b) for

contrast. The comparison shows that with the increase in the number of fibers. It becomes challenging to obtain an even plane on the casted fibers.

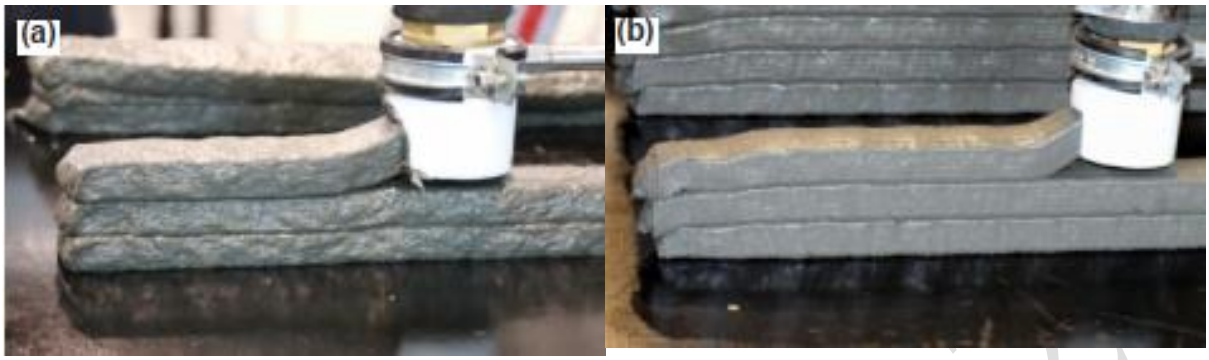

Fig 1. 3D-concrete-printing machine spraying concrete (a) Mixture B and, for contrast purpose, (b) lightweight fine-grained concrete [7].

This dissertation put in place the research repute over 3D-printing figured technology, sums up the effect of embodied fabric properties, answers composting technologies, 3D-printing control framework and mean elements over 3D-printed concrete. Established on concerning the modern reputation then difficulties appear foregoing following the lookup path on 3D-printing embodied technology then evolution trends.

II. Fresh Properties of 3D Printing Concrete

The main thing that affects the workability is water content. If less quantity of water is present, workability will decrease; the mixture will harden. Hence mixture cannot flow through the pipe efficiently. If we increase the amount of water content, bleeding of concrete will occur and significant number of damaging apertures in the printed concrete will influence the load carrying ability of concrete. Moisture ratio can be better managed by the addition of water-reducing superplasticizers to enhance the workability without causing bleeding of cement mixture. Perrot et al. attained a mixture containing a moisture-binder ratio of 0.41 and polycarboxylate polymer powder of 0.3% binder mass, ensuring successful 3D printing. The best results appeared at the construction pace of 1.1m/h [8]. Le et al. attained a mixture that could evenly eject through a nozzle and achieve construction up to 61 layers. The slurry has a moisture-binder ratio of 0.26 and a 1% moisture-reducing admixture. Workability is increased by the addition of mineral admixtures that optimize the particle distribution. The better well-graded the particle distribution, the more helpful in the development of the compact mixture resulting in good fluidity [9]. Güneyisi et al. approach was to create a mixture by replacing ordinary cement with 50% fly ash. The initial setting time was reduced by 43.2% due to the change [10].

III. Mechanical Properties of 3D Printing Concrete

To increase mechanical properties of printed sample like compressive and flexural strength the amount of fiber reinforcement needs to be increased. But it will reduce the workability of the slurry: causing the choking of the nozzle and a decrease in the bonding strength. Christ et

al. investigated the effects of types of fibers on mechanical properties. Results demonstrated flexural ability was increased by 180% [11]. Le and Paul, in turn, chose 0.5% alkali-resistant glass fiber (6 mm) and 12 mm/8 mm (length/diameter) polypropylene fiber to improve the sample's surface qualities. [12], [13]. Hambach et al. concluded if glass fiber and basalt fiber samples with a volume of 1% are used then compressive strength is only 13 MPa, while in the case of carbon fiber with the same percentage the strength can reach 30 MPa [14]. Interlayer print interval is the basic element influencing bond strength [12]. Panda et al. discovered the method to increase printing speed, printing head height and interval can decrease the bonding strength of printed concrete structure [15]. Nerella et al. concluded bond strength is related to time. When we take the time interval of 1 min, there is a 50% decrease in bond strength and bond strength decreases by 90% in a 1-day interval. The interlayer bond strength can be strengthened by the presence of mortar between the interlayers [16]. In their experiment, Hosseini et al. added resin mortar to the interlayer, which was made up of sand, black charcoal particles, and Sulphur. Results demonstrated presence of kelfa fibers and epoxy resins increased interlayer bond strength by 20% [17]. Ma et al. proposed that by adding cellulose fiber mortar, the interlayer bonding performance is increased: when interlude is 60 min, bond strength is greater than 1.91 MPa [18].

The cubic specimen of 40 × 40 × 40 mm was tested at intervals of 10h, 1 day, 3 days, 7 days and 28 days, and the compressive strength of the specimens was noted down. The mean values of compressive strength are in figure 2. The highest values were obtained by B840/SF/FA and B840/SF/FA/LP mixtures, while the least were B640 and B640/LP. After proper curing at 20◦C, it was concluded that an increase in binder amount increases the mechanical properties of the mixture. But these increases in mechanical properties can also happen when the quantity of additives is increased [19].

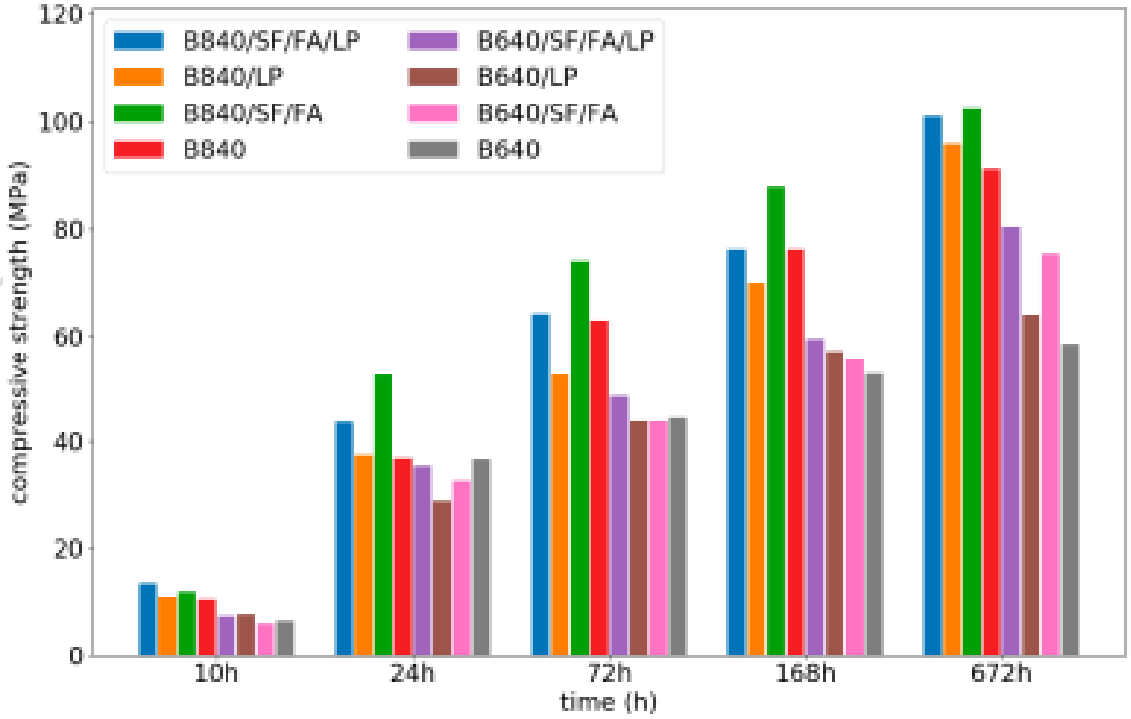

Fig 2. Compressive strength results [19]

Fig 3. Column printed out of B840/SF/FA/LP: a) before test; (b) after compressive strength test [19]

The compressive strength of the columns was calculated using specimens having dimensions D=160 mm and H=205 ± 10 mm. Due to the adequate compressive strength of the B640/SF/FA sample; the pace of its printing lessened. The tests were conducted 10 h after printing. Samples at the start and completion of the test are in Figure 3. For each mix design, three samples were taken [19].

IV. 3D Printing Concrete Durability Properties

Regarding the durability of 3D printing concrete materials, limited reports are available: this is the main parameter that affects the safety parameters of 3D printed buildings and concrete structures. Any problems with the materials will not only result in the loss of material but life may also be endangered. Thus, the study of the durability properties of 3D printing concrete is a must. Durability properties are affected by temperature, chemical effects and external forces. New developing materials can enhance the durability of the printed structure with good seepage and freezing control properties. To determine the fire resistance and high-temperature resistance of concrete composite produced by 3D fiber printing, Weng et al. performed a peeling test, four-point bending test, and compressive strength test. They concluded that flaking and bursting at high temperatures are effectively PVA fibers present in the composite. The flexural and compressive strength of 3DPFRCC at different temperatures was also found to be more than plain 3D printed concrete [20]. Weger et al. assessed the carbonization resistance and freeze-thaw resistance of powder-bonded 3D printed cement-based composites. Outcomes proved that the opposition offered was up to the standard. No, carbonization happened by changing the CO2 concentration [21].

The fracture surfaces were studied to understand the fiber orientations at failure. For this purpose, in Osaka, Japan, the images of the fibers were captured using a VHX-6000 microscope. The results showed that most fibers are oriented at a right angle to the cracks, and the direction of extrusion and fiber distribution appears uniform. While fibers are randomly oriented in the case of mold-cast specimen; see Figure 4 (c) [7].

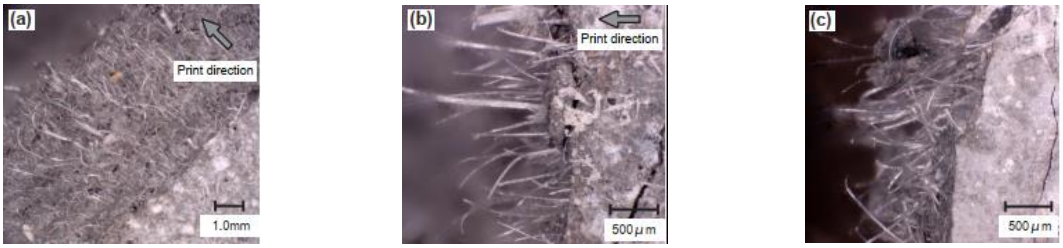

(b) (c)

Figure 4. Microscopic images of fracture surfaces of: (a and b) C-print specimens; and (c) C-cast specimen [7].

V. DISCUSSION AND FUTURE WORK

3D-printing concrete is at the preliminary phase of its evolution. To generalize, application of 3D printing technology, it is essential to utilize modern-day technology to overcome problems related to it. Future research on the 3D printing concrete can follow through the following aspects:

(a) Concrete materials for 3D printing have been studied, and the features those materials must possess have also been proposed. But there is a lack of proper theoretical and systematic processes to get the necessary properties. It is necessary to perform methodical and rigorous research related to the concrete raw materials for better understanding and control. Thus, new raw materials and mixed designs for 3D printing concrete can be developed. Utilization of micro characterization technology. The examination of macroscopic mechanical qualities is the focus of current study, although theoretical underpinnings for macro-performance can be found in studies on the micro-scale at the level of particular materials. The investigation at the microscopic level will promote and increase the comprehension of the mechanical properties.

(b) The durability of printing materials. The focal point is anisotropic mechanical properties, rheology, buildability and interlayer adhesion for 3D printed concrete using the extrusion method. It is mandatory to control a comprehensive investigation of the durability of its material structure considering the environs of the printing structure and the building, and the service time limit. To weigh up the durability of different 3D printed concretes Quantitatively evaluate the durability of 3D printed concrete, and finally improvement of the durability and realize the prediction of 3D printed concrete.

(c) Stiffening ability is a principal measures of 3D printing concrete materials. Due to frail interlayer bonding, 3D printed concrete has evident anisotropy. Although research has been carried out; the current methods lack the flexibility and universality to be applied in all conditions. It is mandatory to further understand the flexibility and interlayer behavior improvement techniques; optimize the design of printing structures.

Being a modern way of construction, concrete 3D printing has a mold-less construction, high precision, and shows good potential. Still some difficulties in the development of construction technology, materials, and equipment concepts such as coordinated and simultaneous printing from many printers, rapid in situ printing of massive building structures, fine printing of manufacturing components, and construction fabrication will progressively

become a reality. This technology would become an important part of the construction industry: and bring a new revolution to it.

VI. CONCLUSION

Following conclusions can be drawn from the conducted study:

As we know that there are numerous troubles and complicated challenges have appeared repeatedly in the application of 3D printing technology, although a lot of research has been conducted. A brief list is given below

(1) Complex structure printing feasibility. The 3D printed concrete mechanical properties are still at the junction of evolution. Monolithic 3D printing cannot be utilized to construct typical high-rise buildings, but it can be used to construct low-rise and large-area buildings. Thus, the workable method is pre-casting and printing prefabricated ones first, like prefabricated buildings. Thus, the edge of fast prototyping is lost. It is demanding to construct high-rise buildings of tens or hundreds of meters with 3D printing. First, it needs a printer well matched with the elevation of the structure. Secondly, to solve the issue of the reinforcement in the building structure and the structural strength of the high-rise building: a rational method is needed.

(2) The building materials requirement is also an issue. High-strength unique concrete materials are used in the construction of many 3D-printed buildings. Portland cement cannot fulfill the standards of the printing process and building performance. The requirements of 3D printing for material potential need to be examined. The 3D-printing utilize printer nozzles to deposit materials to construct walls. The depositing sludge not only requires coarse aggregates of a good standard but particular stress and mechanical characteristics. Very high-quality; aggregates are needed, and even a new process to crush aggregates is also required. The presence of admixtures with ordinary concrete increases variables in the concrete and a significant change in its procedure of action and properties. Materials are therefore the challenge that must be overcome in order to ensure the printing of three-dimensional structures. The height of the molding issue. The current state of 3D printing technology is being developed. It can only be utilized for the construction of low-rise and large-area buildings. However, it cannot print generally used high-rise buildings. It can only be printed by pre-casting and then fabricating the members. If the building consists of dozens of floors, then the 3D printing can be done by using a giant 3D printer which provides structural strength to large buildings, and print steel reinforcement.

The interlayer bonding of 3D printing concrete is evaluated by its tensile and shear strength. Significant research has been done about tensile strength still, uncertainties related to shear strength are present. In addition, changes need to be introduced in safety measures, production processes, etc., which may cause problems. These all require future research.

REFERENCES

[1] H. Nasir, H. Ahmed, C. Haas, and P. M. Goodrum, "An analysis of construction productivity differences between Canada and the United States," *Construction Management and Economics*, vol. 32, pp. 595-607, 2014.

[2] T. Bock, "The future of construction automation: Technological disruption and the upcoming ubiquity of robotics," *Automation in construction*, vol. 59, pp. 113-121, 2015.

[3] J. Pegna, "Exploratory investigation of solid freeform construction," *Automation in construction*, vol. 5, pp. 427-437, 1997.

[4] B. Khoshnevis, S. Bukkapatnam, H. Kwon, and J. Saito, "Experimental investigation of contour crafting using ceramics materials," *Rapid Prototyping Journal*, 2001.

[5] B. Khoshnevis, "Contour crafting-state of development," in *Solid Freeform Fabrication Proceedings*, 1999, pp. 743-750.

[6] S. Lim, T. Le, J. Webster, R. Buswell, A. Austin, A. Gibb, *et al.*, "Fabricating construction components using layered manufacturing technology," in *Global Innovation in Construction Conference*, 2009, pp. 512-520.

[7] H. Ogura, V. N. Nerella, and V. Mechtcherine, "Developing and testing of strain-hardening cement-based composites (SHCC) in the context of 3D-printing," *Materials*, vol. 11, p. 1375, 2018.

[8] A. Perrot, D. Rangeard, and A. Pierre, "Structural built-up of cement-based materials used for 3D-printing extrusion techniques," *Materials and Structures*, vol. 49, pp. 1213-1220, 2016.

[9] T. T. Le, S. A. Austin, S. Lim, R. A. Buswell, A. G. Gibb, and T. Thorpe, "Mix design and fresh properties for high-performance printing concrete," *Materials and structures*, vol. 45, pp. 1221-1232, 2012.

[10] E. Güneyisi, M. Gesoglu, A. Al-Goody, and S. İpek, "Fresh and rheological behavior of nano-silica and fly ash blended self-compacting concrete," *Construction and Building Materials*, vol. 95, pp. 29-44, 2015.

[11] S. Christ, M. Schnabel, E. Vorndran, J. Groll, and U. Gbureck, "Fiber reinforcement during 3D printing," *Materials Letters*, vol. 139, pp. 165-168, 2015.

[12] T. T. Le, S. A. Austin, S. Lim, R. A. Buswell, R. Law, A. G. Gibb, *et al.*, "Hardened properties of high-performance printing concrete," *Cement and Concrete Research*, vol. 42, pp. 558-566, 2012.

[13] S. C. Paul, Y. W. D. Tay, B. Panda, and M. J. Tan, "Fresh and hardened properties of 3D printable cementitious materials for building and construction," *Archives of civil and mechanical engineering*, vol. 18, pp. 311-319, 2018.

[14] M. Hambach, M. Rutzen, and D. Volkmer, "Properties of 3D-printed fiber-reinforced Portland cement paste," in *3D concrete printing technology*, ed: Elsevier, 2019, pp. 73-113.

[15] B. Panda, S. C. Paul, N. A. N. Mohamed, Y. W. D. Tay, and M. J. Tan, "Measurement of tensile bond strength of 3D printed geopolymer mortar," *Measurement*, vol. 113, pp. 108-116, 2018.

[16] V. N. Nerella, S. Hempel, and V. Mechtcherine, "Effects of layer-interface properties on mechanical performance of concrete elements produced by extrusion-based 3D-printing," *Construction and Building Materials*, vol. 205, pp. 586-601, 2019.

[17] E. Hosseini, M. Zakertabrizi, A. H. Korayem, and G. Xu, "A novel method to enhance the interlayer bonding of 3D printing concrete: An experimental and computational investigation," *Cement and Concrete Composites,* vol. 99, pp. 112-119, 2019.

[18] G. Ma, N. M. Salman, L. Wang, and F. Wang, "A novel additive mortar leveraging internal curing for enhancing interlayer bonding of cementitious composite for 3D printing," *Construction and Building Materials,* vol. 244, p. 118305, 2020.

[19] M. Kaszyńska, S. Skibicki, and M. Hoffmann, "3D Concrete Printing for Sustainable Construction," *Energies,* vol. 13, p. 6351, 2020.

[20] Y. Weng, M. Li, Z. Liu, W. Lao, B. Lu, D. Zhang, *et al.*, "Printability and fire performance of a developed 3D printable fibre reinforced cementitious composites under elevated temperatures," *Virtual and Physical Prototyping,* vol. 14, pp. 284-292, 2019.

[21] D. Weger, D. Lowke, C. Gehlen, D. Talke, and K. Henke, "Additive manufacturing of concrete elements using selective cement paste intrusion—Effect of layer orientation on strength and durability," in *Proceedings of the RILEM 1st International Conference on Concrete and Digital Fabricaton, Zürich, Switzerland*, 2018, pp. 10-12.

Comparatively Study Between Monocrystalline and Polycrystalline Photovoltaic Panel Based on PCM

Bushra Nadeem[1,*], Abid Hussain[1], Ammar Akram[2], Tayyab Mohsin[1] and Javeria Qadeer[1]
[1] Department of Mechanical Engineering, University of Engineering and Technology Taxila 47050, Punjab Pakistan
[2] Department of Mechanical Engineering, HITEC University Taxila 47050, Punjab Pakistan
*Correspondence:BushraNadeem176@gmail.com

***Abstract*—As part of this paper, we present a comparative examination of the performance of two commercial photovoltaic modules (monocrystalline and polycrystalline) in Taxila, Pakistan. We investigated the effects of module temperature and solar irradiance on the power output, module efficiency, and performance ratio of each module. The parameters of the module appeared to be strongly dependent upon the solar irradiance and the module temperature. Compared with polycrystalline and monocrystalline modules, monocrystalline modules performed better in high irradiance conditions, while their performance decreased suddenly with a decrease in irradiance. This site exhibited a higher average monthly module efficiency for monocrystalline modules. Increasing irradiance and photovoltaic module back surface temperature decreased module efficiency and performance ratio. The month of September was dedicated to conducting a series of experiments outdoors. The experiment was conducted using phase change materials RT31. The study was conducted in Taxila, Pakistan, during September. RT44HC has shown to reduce maximum temperatures by 11.21 degrees Celsius for PV panels with only PCM compared to the reference panel when used in experiments. Electric conversion efficiency between the hours of 8:00 am and 5:00 pm is characterized as following: efficiency ranges between 7.36% and 7.31%, and electrical conversion power ranges between 9.576% and 9.504%.**

Keywords—Photovoltaic panel, Phase Change Material, Thermal Energy Storage, Latent Heat Storage, Sensible-Heat Storage

I. INTRODUCTION

As renewable energy technology has produced, energy storage has become a progressively important ingredient. An integral part of renewable energy manufacture is the use of solar energy, which is of random nature. Its successful utilization depends on the organization and benefits of store energy systems. The TES "thermal energy storage system "is a method for storing thermal energy by warm or refrigerant a storage standard so that it can be used for both boiler and freezing applications as well as power generation applications later. As a result of current developments in technology, TES has become progressively more common in areas such as area and water boiler, waste temperature deployment, freezing, and atmosphere preparing. There is a critical requirement for power space every time there is a difference between the resource and utilization of energy. The past four years have observed the improvement of a collection of TES procedures [1]

As economic development, improved life cycle requirements, and residents' development increase, energy consumption has moved up in current years. Fossil fuels may be used to join

the energy requirements of the country, although fossil fuels displace 80% of the total strength demand of the country. Fossil fuels cause a risk to the health of people and are restricted in their energy sources [2] Solar photovoltaic panels are a favorable knowledge that can transfer solar energy to electrical energy for the manufacture of energy. However, only 15-20% of solar heat is transformed into electrical energy by PV panels [3]. It is possible that the residue of solar energy will close warming the PV components, rising in various problems. As a result of permanent heating, PV panels can also be broken to the full limit [4].

II. METHODOLOGY

A. . Photovoltaic panel power and efficiency calculation

$$n_e = \frac{P_{mp}}{G.A_{pv}} \times 100$$

Using the following formula, it is possible to calculate electrical efficiency. [5]

B. Electrical Power

$$P_{mp} = V_{mp} I_{mp}$$

In this formula, P is the peak output power (W), G is the solar radiation (W/K), H is the active area of the panels (A_{PV}), and I and V are the current and voltage of the peak output power, respectively.

C. Fill Factor

A short circuit current is determined by the voltage at open circuit and the voltage at short circuit. FF (filled factor) can be calculated as the maximum power conversion efficiency of a PV module by multiplying the maximum power gained from it by the open circuit voltage and the short circuit current at the standard test condition of the PV module to obtain the maximum power gained from it. [6]

$$\text{FF} = \frac{P_m}{V_{oc} \times I_{sc}}$$

An ideal output power could be expressed as the maximum electrical power that can be produced

D. Incident solar Radiation

A calculation is made to determine the incident solar radiation on the cell. [7]

$$\boldsymbol{p_{in} = G_s \times A_{pv}}$$

III. EXPERIMENTAL SETUP

We provide a comprehensive interpretation of the experiment in this section of the investigation. HITEC University in Taxila, Pakistan, performed this experiment under the

conditions of the Taxila town, Pakistan (33.7° N, 72.8° E latitude angle). The purpose of this experiment was to determine the PCM that improves the efficiency of polycrystalline and monocrystalline photovoltaic modules when used at 10 watts. A tilt angle of nearly 34 degrees was maintained for the PV module despite the absence of a tracking mechanism.

A 10W Monocrystalline and a 10W Polycrystalline Panel was selected for the experimentation.

TABLE I. PROPERTIES OF MONOCRYSTALLINE AND POLYCRYSTALLINE PANEL

Property	Monocrystalline PV Panel	Polycrystalline PV Panel
Isc	0.59 A	0.57 A
Voc	21.4 V	21.2 V
Vmax	17.1 V	17.6 V
Imax	0.56 A	0.54 A
Pmax	10 W	10 W

IV. RESULTS AND DISCUSSION

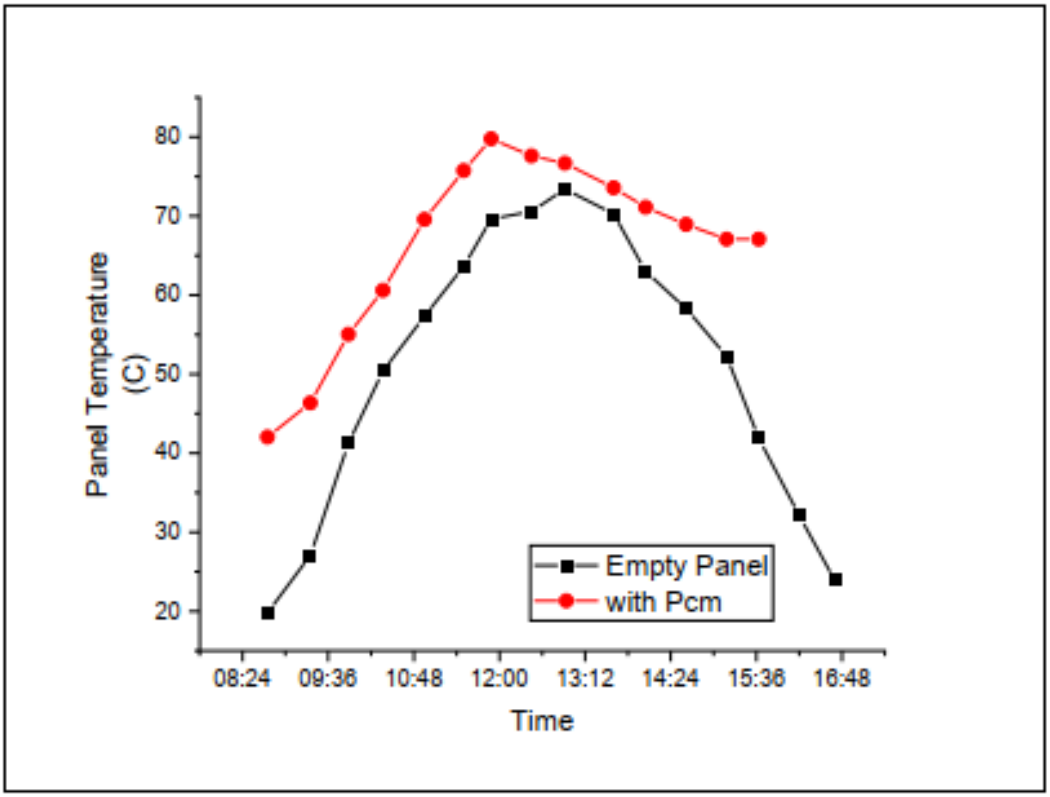

Fig 1: Temperatures in two configurations used in current research

During one week of experiments, the ambient temperature of the radiation was measured on the roof of the Mechanical Engineering Department at HITEC University, Taxila, Pakistan. Figure 2 illustrates the best results are obtained when the average solar radiation is maximum. A maximum atmospheric temperature of 40°C and a power density of 1100 Watts per square meter.

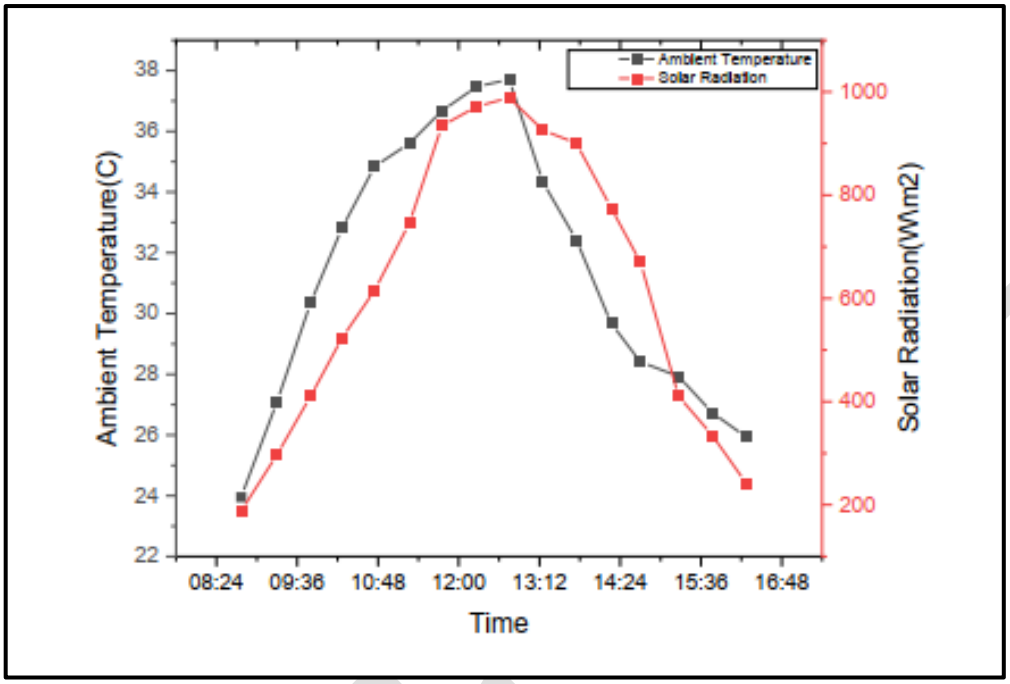

Fig 2: Climate Condition in Taxila

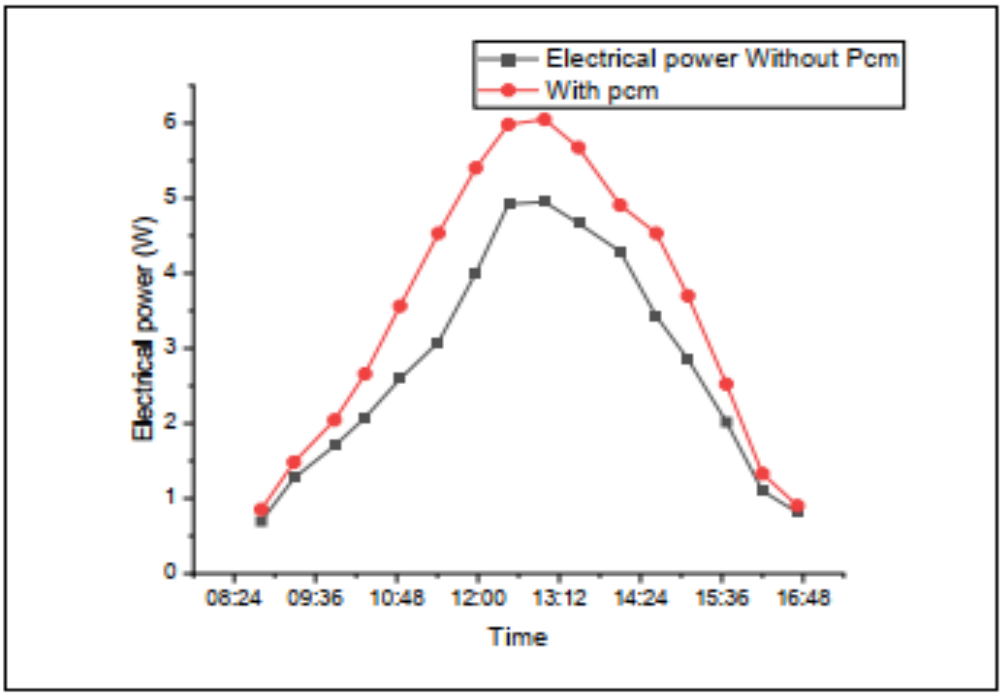

Fig 3: Electrical power between two configurations

Fig 3 presents the electrical power output of a 10-W PV panel for a variety of configurations. This indicates that the electrical power of PCM-based PV panels is greater than that of naturally occurring PV panels. The PV panel should be cooled or used as a reference panel. As a result of configuration, there was a maximum reduction in cell temperature. This configuration also produced the maximum power.

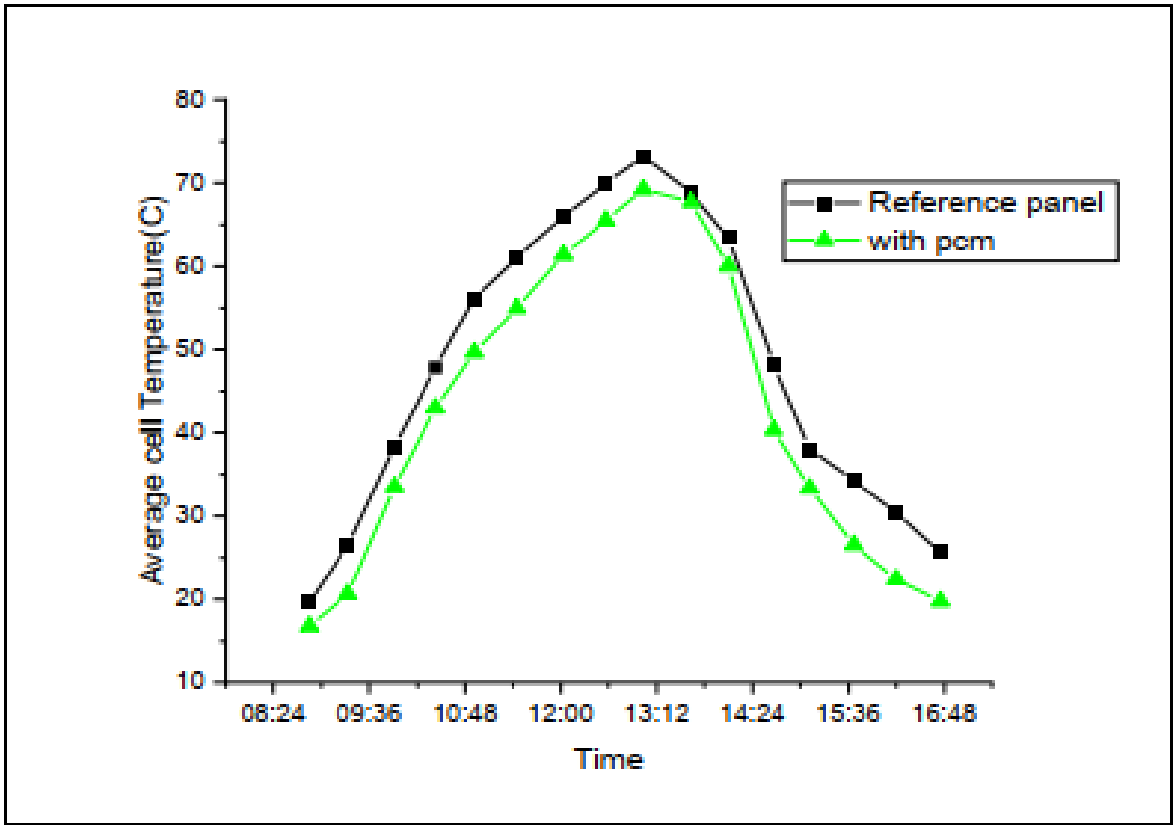

Fig 4: Average cell temperature between two configurations

Among the most important parameters of PV panels is their temperature plays a significant role in managing the thermal performance of PV panels. Estimation of PV modules in terms of performance. A temperature measurement, as shown in Figure 4, the under-regard profile for PV panels. Separately and each PCM that is used in a PV configuration.

A 10-watt PV panel with the following configurations will produce the following electrical output Fig. 5 shows that electrical power is being provided. In terms of power, PV panels based on PCM are more powerful than those based on silicon. The PV panel should be cooled or used as a reference panel. To achieve the maximum decrease. It was observed that the temperature of the cell was elevated during configuration. Therefore, the configuration achieved maximum power as well.

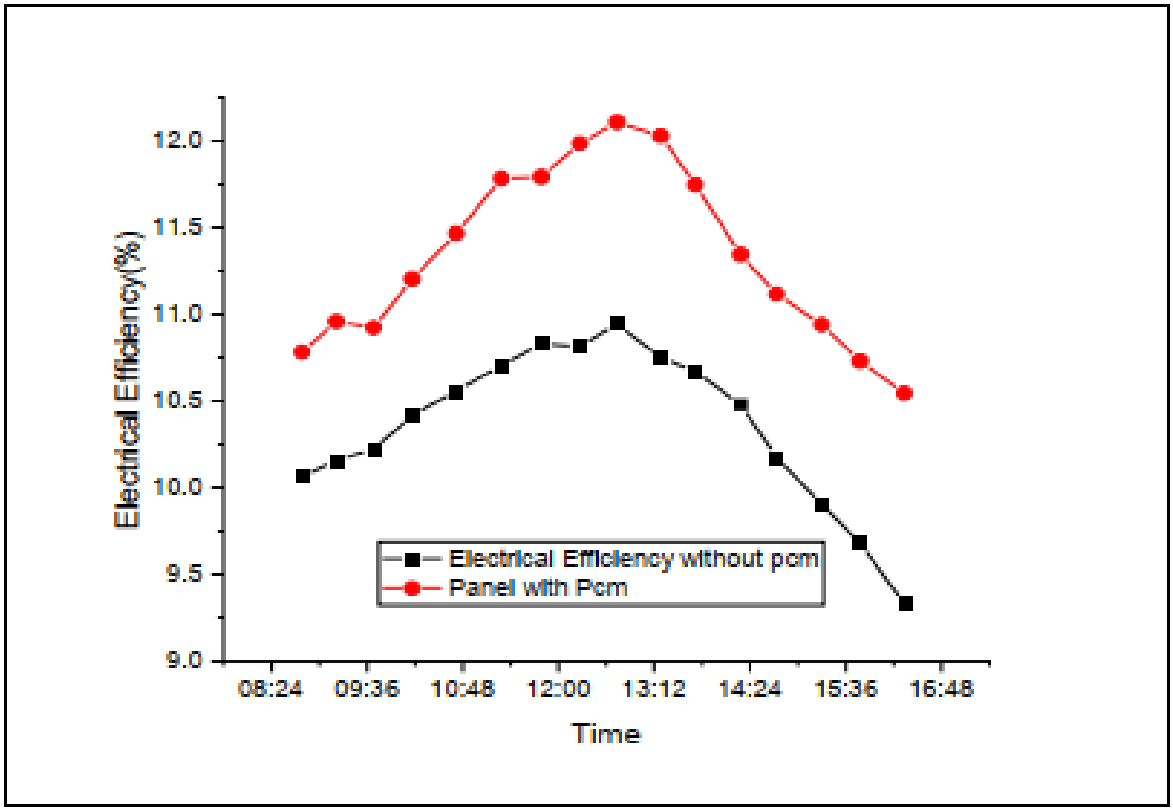

Fig 5: Efficiency of electrical conversion between two configurations.

V. CONCLUSION

Based on an evaluation of the energy available in Taxila, Pakistan, the aim of this study is to investigate the performance of a 10 W Monocrystalline and Polycrystalline photovoltaic solar module. The module's maximum efficiency (2022) was determined based on experimental data collected throughout September. As a result of the PV conversion of heat energy to electricity, we determined the losses associated with the conversion. Based on the results of the study, the following conclusions can be drawn:

It is important to note that the rate of thermal energy supplied by the sun plays a significant role in determining the performance of monocrystalline and polycrystalline photovoltaic solar panels. When the sun's radiation is low, PV modules perform at their maximum efficiency. Solar modules perform at their maximum efficiency when the solar radiation is high.

It is not uncommon for ambient temperatures to increase during high temperature days, as well as solar radiation, resulting in an increase in the temperature of the cells and irreversible losses of power from the module. The output power (electricity) increases because of that condition.

REFERENCES

[1] I. Sarbu and A. Dorca, "Review on heat transfer analysis in thermal energy storage using latent heat storage systems and phase change materials," Int. J. Energy Res., vol. 43, no. 1, pp. 29–64, 2019, doi: 10.1002/er.4196.

[2] M. A. Al-Nimr, B. M. Tashtoush, M. A. Khasawneh, and I. Al-Keyyam, "A hybrid concentrated solar thermal collector/thermo-electric generation system," Energy, vol. 134, pp. 1001–1012, 2017, doi: 10.1016/j.energy.2017.06.093.

[3] M. C. Browne, B. Norton, and S. J. McCormack, "Heat retention of a photovoltaic/thermal collector with PCM,"Sol.Energy, vol.133, pp.533–548, 2016, doi: 10.1016/j.solener.2016.04.024.

[4] S. Odeh and M. Behnia, "Improving photovoltaic module efficiency using water cooling," Heat Transf. Eng., vol. 30, no. 6, pp. 499–505, 2009, doi: 10.1080/01457630802529214.

[5] Choubineh, Negin & Jannesari, Hamid & Kasaeian, Alibakhsh, 2019. "Experimental study ofthe effect of using phase change materials on the performance of an air-cooled photovoltaic system," Renewable and Sustainable Energy Reviews, Elsevier, vol. 101(C), pages 103-111.

[6] Salem, M.R. & Elsayed, M.M. & Abd-Elaziz, A.A. & Elshazly, K.M., 2019. "Performance enhancement of the photovoltaic cells using Al2O3/PCM mixture and/or water cooling-techniques,"Renewable Energy, Elsevier, vol. 138(C), pages 876-890.

[7] Sardarabadi, Mohammad & Passandideh-Fard, Mohammad & Zeinali Heris, Saeed, 2014. "Experimental investigation of the effects of silica/water nanofluid on PV/T (photovoltaic thermal units)," Energy, Elsevier, vol. 66(C), pages 264-272.

Comparative Analysis of Software Development Process Models

Inam Ullah Khan[1, a], Muhammad Bilal Qureshi[1, b], Mir Ahmad Khan [1, c], Abdul Ghafoor [1, d]Sana shaoor kiani[1, e]
[1]*National Center for Cyber Security*
*Correspondence: inam1software@gmail.com

Email address: [a)] inam1software@gmail.com, [b)] muhdbilal.qureshi@gmail.com, [c)] mirkhan346@yahoo.com, [d)] abgafoor469@gmail.com, [e)] sana.raazi90@gmail.com

***Abstract*— The study of several software process models is presented in this work. A review of several publications is conducted in this article, and the software process model is detailed in the reviewed document. The comparison between the various process models and the suggested model is shown in this article. The requirement, planning, design, and implementation are also discussed in this comparative study. Business process models, however, have been heavily utilized to support these components in conventional software engineering approaches. It has not yet been determined to what degree advice to concentrate on coding mean that conceptual modeling should be abandoned.**

Keywords*— *Introduction of Process Model, Phases, Comparative Study of Process, factors affecting to Choose Process Model.

I. INTRODUCTION

There are two main layers to the software engineering process: At the beginning, or first level, actions connected to gathering information, developing software, and maintaining it; at the second level, activities related to the dentition, functioning, measuring, and upgrading the software process itself. Software systems begin and progress via a series of steps that document their beginning, initial development, dynamic operation, maintenance, and switch from one production to the next. This study examines and compares several approaches for describing or modeling the development of software systems. It starts at the very beginning with a backdrop and classification of Models of the software life cycle that are well-known. [1]

Project teams for software development projects are mostly made up of highly competent and trained persons with a technical background. Individuals with high levels of expertise and training will demand considerable monetary compensation for their efforts, which will be expressed in high man-hour or man-day rates. As a result, the project manager is under a lot of pressure to give accurate time estimates in terms of required man-days, because any deviation would result in significant additional costs. Highly competent individuals also have a propensity to be arrogant and self-absorbed, which makes them difficult to incorporate into a team.

Developing a software product organizations follow some software development process. The major purpose of software development process models is to identify the sequence in which the phases of software development and evolution take place, as well as the transition criteria

for moving from one stage to the next. The problem (Software) may be divided into the following activities within the software development process:[2]

A. Development Process

- Recognizing the problem
- Make a solution strategy.
- Programming for the proposed solution
- Putting the final software to the test

For big systems, these activities may be quite complicated. As a result, each action must be subdivided into smaller sub-activities or stages. These stages are then successfully handled in order to create a software project or system. The following are the basic steps in the creation of a software project:

B. Software Project

• Requirement Analysis

• Design

• Implementation/Coding

• Testing

• Deploy

• Maintain

Each operation in a big system might be highly complicated, necessitating the use of methods and processes to do it effectively and accurately. Furthermore, each of the fundamental actions may be so enormous that it cannot be completed in a single step and must be split down into smaller chunks. A big software system, for example, is usually broken down into numerous, different design phases, starting with a very high-Level design that specifies just the system's components and ending with a thorough design that specifies the logic of the components. The common phases of an SDLC are depicted in the diagram below

Fig 1. Image: Phases of the software development

II. MODELS FOR THE USUAL SOFTWARE DEVELOPMENT LIFE CYCLE

A. Waterfall model:

The waterfall model, which is a linear sequential software development life cycle (SDLC) paradigm, was proposed by Royce in 1970. The requirements analysis, design, coding, testing, and implementation stages are followed in such a way that the phase is not repeated and the development does not go on to the next phase until the previous phase is entirely done. As a result, it isn't particularly effective when the project needs are fluid.[3]

Fig 2. Waterfall Model

i. ***Advantages:***

• Before beginning development, make sure the requirements are explicit.
• Before going on to the following phase, each one demands a certain amount of time to accomplish
• Because it's a linear model, it's straightforward to apply, and the resources required to put it into action are minimal.
• Adequate documentation is followed at each phase to ensure the development's quality

ii. ***Disadvantages:***

• Issues with one phase are seldom completely resolved within that phase, and several issues with a single phase arise after it has been signed off, resulting in a disorganized system.
• Any changes to the requirement requested by the client will not be incorporated during the current development phase.

B. V-Model

Testing methodologies are designed early in the life cycle, before any coding is done, at each of the phases preceding implementation. Like the waterfall model, the V-Shaped life cycle is a sequential series of process execution. In comparison to the waterfall paradigm, this strategy places a greater emphasis on testing.

Similar to the waterfall method, the life cycle model starts with requirements.

A system test strategy is developed before development gets started.

The testing strategy makes sure that the functionality specified during requirement gathering is met. System architecture and design are the main topics of the high-level design phase.

At this stage, an integration test strategy is developed to evaluate the software system's interoperability.

In the low-level design stage, unit testing and the actual software components are designed and tested. During the implementation stage, all coding is redone.

After the coding is complete, the execution path proceeds down the right side of the V, where the previously made test plans are now used.

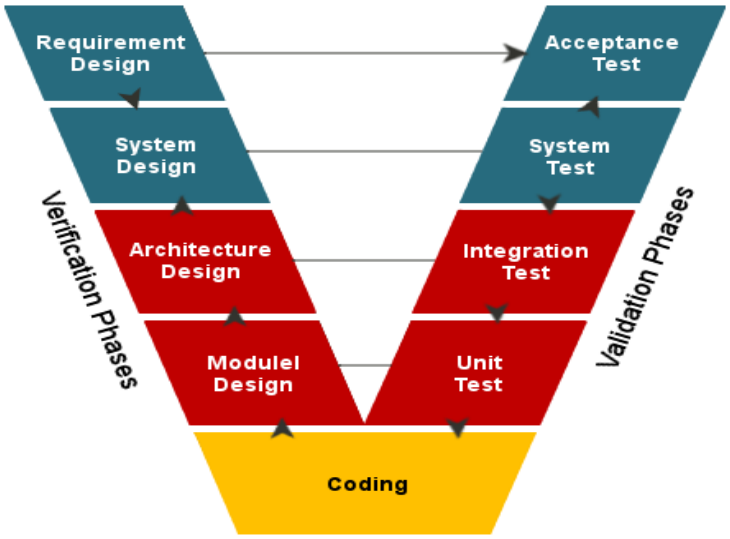

Fig 3. Image: V Model

i. ***Advantages:***

• It's simple and straightforward to u
• There are defined deliverable for each step.
• More likely to succeed than the waterfall model since test plans are created at an initial stage in the life cycle.
• It's ideal for modest tasks with straightforward needs.

i. *Disadvantages:*

• There is minimal room for error, and modifying the scope is difficult and expensive.
• Software is developed during the implementation phase rather than being produced as early software prototypes.
• There is no obvious path for resolving concerns uncovered during testing in this model

C. Prototype Model

The essential idea is to quickly prototype the needs in order to understand them, as opposed to freezing them before beginning design or coding. On currently understood criteria, this prototype is built. In addition to helping the client better comprehend the system's needs, interacting with the prototype can give the consumer a "real feel" for the system.

It allows for the simulation of workflows, workloads, and user interfaces as well as technological comparisons. For complicated and massive systems for which there is currently no manual processing approach to help define requirements, prototyping is a compelling idea.

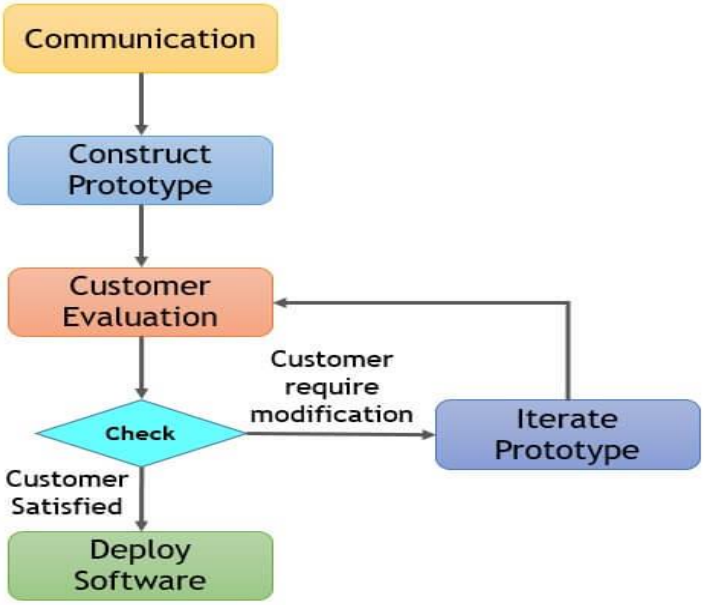

Fig 3. Prototyping Process Model

i. ***Advantages:***

- After each iteration, consumers may see the progress.
- The project's outcome is satisfactory.
- Functionalities that are missing can be discovered, lowering the risk factor. Team members are able to communicate effectively.
- By combining prototype with feedback, a deeper knowledge of the customer's needs may be Achieved
- Prototypes can be modified and abandoned.

ii. Disadvantages:

- It's a time-consuming approach or procedure since several proto types may be required before the customer meets his or her ultimate criteria.
- This approach necessitates an excessive amount of customer engagement and involvement, which can only be accomplished with a dedicated client.

- It's impossible to anticipate the precise amount of time required to complete the final product at first.

D. Incremental Model

When requirements are well specified, there is no uncertainty about the functionality of the end product, and functionality can be supplied in phases according to chosen priorities, incremental process models (such as the Iterative Enhancement model) are successful. The client receives a usable product at the end of each cycle.

Model of iterative enhancement:

The following are the phases of this model:

Requirements analysis and definition

Integration and system testing, operation, and maintenance, as well as design, implementation, and unit testing.

These stages are similar to those in the waterfall model, however in the iterative improvement approach; they can be completed in several cycles. At the conclusion of each cycle, a usable product is delivered, with each release adding more features. At each release, this approach produces a product of operational quality. The entire product is separated into releases, and the developer distributes them one by one. A normal product will have a number of releases. This model allows for a first release in a matter of weeks or months, whereas other models need customers to wait months or years for a product. [2]

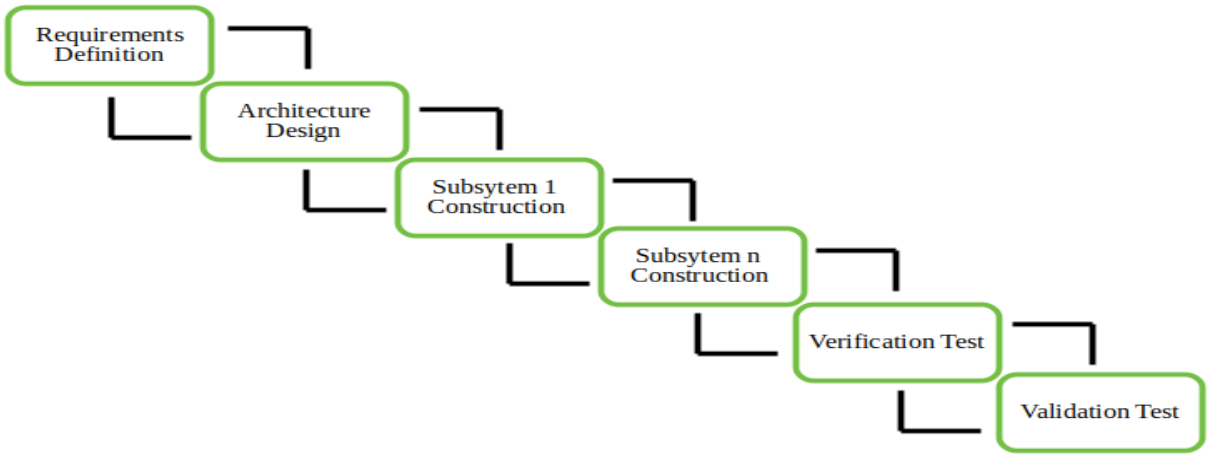

Fig 4. Image: Incremental Model

i. ***Advantages:***

- Breaks down the job into smaller chunks.
- Early on, creates a functioning model and offers useful input.
- The feedback from one step informs the design of the following phase.
- When more manpower is not available, this feature comes in handy.

ii. Disadvantages:

- The project's user community must be actively participating.
- This puts a strain on the staff's time and causes project delays.
- Communication and coordination abilities are put front and center.
- Requests for improvement made informally for each step may cause misunderstanding.

E. Spiral Model

With the exception of a stronger emphasis on risk assessment, the spiral technique is comparable to the incremental model. The planning, risk analysis, engineering, and assessment phases of the model are its four components. In iterations, these stages are frequently traversed by a software project (called Spirals in this model). Planning serves as the foundation of the first spiral, which gathers needs and considers risk. The following spirals build upon the previous ones. When planning is underway, requirements are gathered. The process for identifying risk and potential solutions is in place throughout the risk analysis phase. The risk analysis is conducted before creating a prototype. [3]

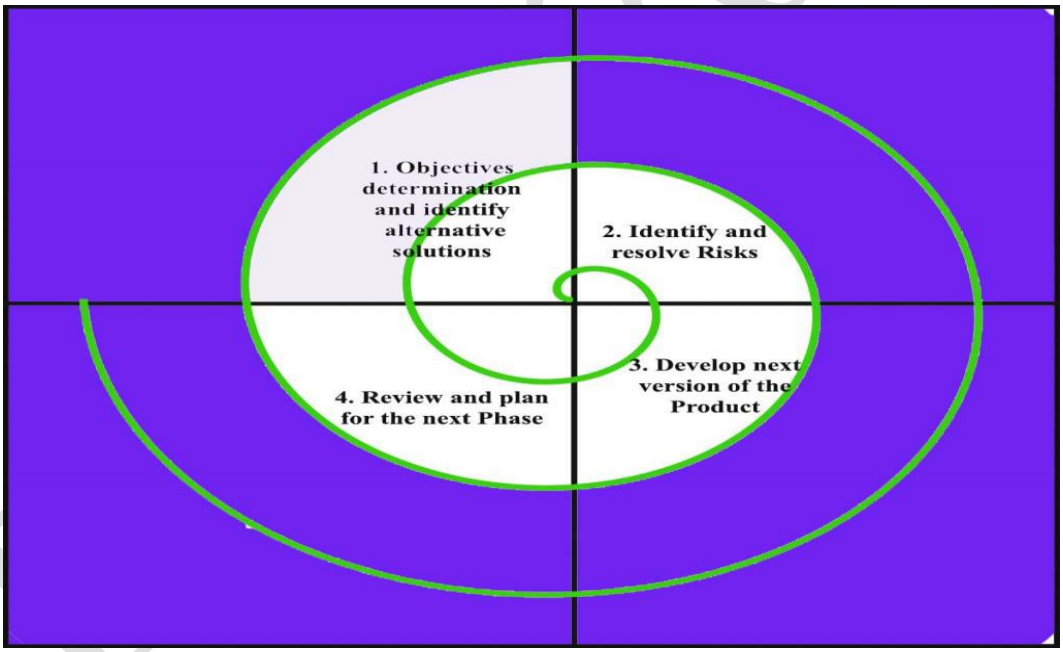

Fig 5. Image: Spiral Model

i. ***Advantages:***

- Later, it is possible to update or add new functionalities.
- Because the prototype is built in small pieces, cost estimating is easy.
- Risk management is made easier by continuous or recurrent development.
- Rapid spiral growth occurs when features are gradually added.
- Client feedback is always welcome

ii. Disadvantages:

- Spiral development is most effective for large projects, although risk assessment skills are required.
- You run the risk of missing deadlines and going over budget.
- For seamless operation, the spiral model protocol must be strictly adhered to.
- Due to the inclusion of intermediary steps, documentation is more extensive.
- Spiral software development can be very time consuming and requires a lot of time and effort

F. Agile Model

In the mid-1990s, an agile system process life cycle model emerged as a result of a reaction. This programmed will address the issue of high weight and project micromanagement. Finally, in 2001, Agile created the lightweight approach. Scrum and crystal cleaner are examples of agile methods. Agile employs a variety of methods for various types of projects, but they all have some basic characteristics. Requirement specifications can change often in the Agile SDLC since the client and software developer will comprehend them. The cost of this model has been discovered to be quite high. As a result of the meeting between the client and the software developer, there will be a greater probability of success. Developers have cost control; if they just buy the requirements they need, they can cover the costs. This paradigm is complex to deploy yet has a low chance of failure.

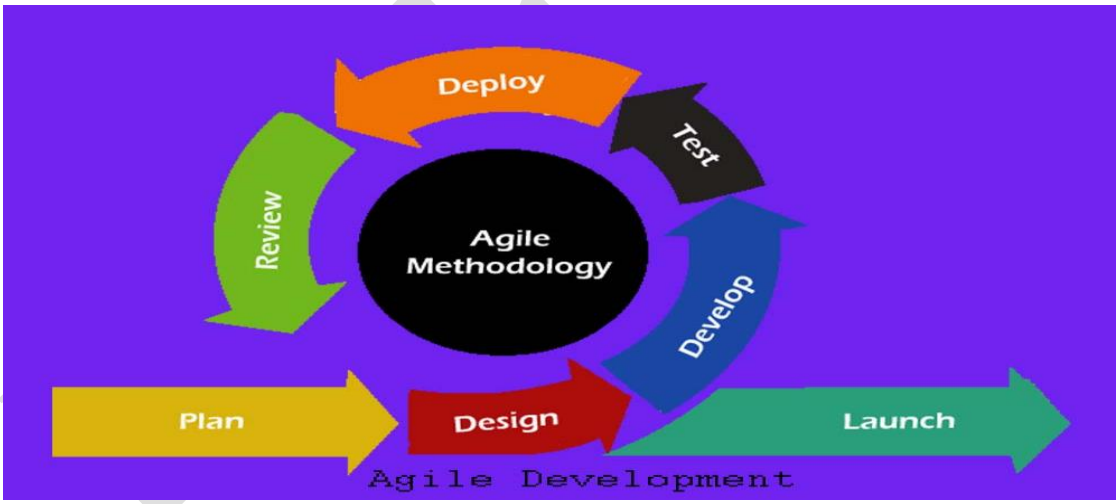

Fig 6. Image: Agile Model

i. ***Advantages:***

- Customer satisfaction is accomplished by the timely and regular delivery of important software.
- People and relationships are more essential than processes and tools. Customers, developers, and testers are all in constant communication.
- Working software is provided on a regular basis (weeks rather than months).
- Face-to-face communication is the most effective mode of communication.

- Every day, business people and developers collaborate.
- Consistent attention to technical and aesthetic quality.
- Constantly adapting to changing circumstances. Even last-minute changes to requirements are encouraged.

ii. Disadvantages:

- Some software deliverable, especially large ones, may be challenging to estimate the labour required at the outset of the software development life cycle.
- The usefulness of critical design and documentation is sometimes overlooked. The project may quickly become derailed if the client representative is unsure about the desired end result.
- Only Expert Developer are capable of making the kinds of judgments needed throughout development. As a result, novice programmers have no place in it unless they are paired with experienced resources.[7]

III. COMPARATIVE TABLE FOR SOFTWARE MODELS

Software development models Struggle with the undefined were first introduced to the software. Development community optimizes and structures the development from the 1950s to the 1960s. Back then, it was beautifully good learning to configure all things, and programming was one of those certain knowledge about the project management processes that had to be planned.

TABLE I. COMPARATIVE TABLE FOR SOFTWARE MODELS

Parameter	waterfall Model	V Model	Prototype Model	Incremental Model	Spiral Model	Agile Model
Clear Requirement Specifications	Initial level	Initial level	Difficult	Initial level	Beginning	Frequently changed
Understanding Requirements	Well Understood	Not Well Understood	Well understood	Well understood	Well understood	Well understood
Cost	Low	Expensive	High	Low	Expensive	Very High
Simplicity	Simple	Intermediate	Intermediate	Intermediate	Intermediate	Complex
Risk Analysis	Only at beginning	yes	No	Yes	Yes	Yes
Flexibility	Rigid	Little Flexible	Flexible	Less Flexible	Flexible	highly
Reusability	Limited	Limited	Yes	Yes	Yes	Use case reuse
Changes Incorporated	Difficult	Difficult	Easy	Easy	Easy	Difficult

IV. ARGUMENT

A software process model is a simplified representation of a software process that is given from a certain point of view. A software process model is a conceptual picture of how a software process works. These actions are included in problem-solving in software:

- Identifying the issue
- Choosing a plot for the solution

- Code that generates the desired result
- Validation of the genuine software

Each movement on account of huge structure can be fairly complex, necessitating the use of procedures and processes to ensure that it is carried out correctly and efficiently.

Moreover, any of the main projects may be so enormous that it cannot be completed in a single phase and must be divided into smaller projects. A complex software structure, for example, is always divided into multiple, distinct design segments, beginning with a high-level design that only describes the system's mechanisms and moving to a thorough project that defines the logic of the procedures.The basic of tasks or elements that must be accomplished in order to develop a software framework are as follows

- System Requirements' Purpose
- System Design & Analysis
- Software development and coding
- End-user testing of the system
- Setup and maintenance of the system

V. CONCLUSION

In-depth analysis of the software engineering process and software models is covered in the reference article. The quality of project management and the failure portions of the software models process are very thoroughly examined by examining the many issues associated to the software project model. The majority of project models are typically based on the software development life cycle, which includes providing necessary for design and development stages. As a conclusion, the main project models are explained in the article. The benefits of software engineering as well as the key aspects of software engineering are discussed. [5]

If the needs change frequently and the project is small, the agile methodology can be used to develop a product in a short period of time with skilled employees. We shall adopt the Waterfall approach if the demand is apparent and the project is substantial.

We may apply the V-Model if the requirements change, the project develops larger, suitable evaluation is necessary at each step, and experts are involved in the early stages of development [6].

REFERENCES

[1] Khan, R. A., Khan, S. U., Alzahrani, M., & Ilyas, M. (2022). Security Assurance Model of Software Development for Global Software Development Vendors. IEEE Access.

[2] Moyano, C. G., Pufahl, L., Weber, I., & Mendling, J. (2022). Uses of business process modeling in agile software development projects. Information and Software Technology, 107028.

[3] Chugh, M. (2022). An Empirical Study on Factors Affecting Selection of Software Development Life Cycle Models. In Proceedings of 3rd International Conference on Machine Learning, Advances in Computing, Renewable Energy and Communication (pp. 149-158). Springer, Singapore.

[4] Chugh M. An Empirical Study on Factors Affecting Selection of Software Development Life Cycle Models. InProceedings of 3rd International Conference on Machine Learning, Advances in Computing, Renewable Energy and Communication 2022 (pp. 149-158). Springer, Singapore.

[5] Pal, K. (2020). Markov Decision Theory-Based Crowdsourcing Software Process Model. In Crowdsourcing and Probabilistic Decision-Making in Software Engineering: Emerging Research and Opportunities (pp. 1-22). IGI Global.

[6] Pal K. Markov Decision Theory-Based Crowdsourcing Software Process Model. InCrowdsourcing and Probabilistic Decision-Making in Software Engineering: Emerging Research and Opportunities 2020 (pp. 1-22). IGI Global.

[7] Udousoro, I. (2020). Effective requirement engineering process model in software engineering. Software Engineering, 8(1), 1.

[8] Krüger J, Mahmood W, Berger T. Promote-pl: A round-trip engineering process model for adopting and evolving product lines. InProceedings of the 24th ACM Conference on Systems and Software Product Line: Volume A-Volume A 2020 Oct 19 (pp. 1-12).

A Short Review on Latest Technologies for the Pretreatment of Lignocellulosic Biomass

Ammarah Batool [1, a], Khurram Shahzad Baig [2,b], Aasia Farrukh [2, c], Fadia Ali Khan [3, d], Aisha Akbar Awan [3, e], *Aqsa Khan Jadoon [4, f]*

[1]*Department of Polymer Engineering, National Textile University, Sector 30 KorangiIndustrial Area, Karachi - 74900, Pakistan*
[2]*Department of Chemical Engineering, Wah Engineering College, University of Wah, Quaid Avenue, Wah Cantt, Pakistan.*
[3]*Department of Mechatronics Engineering, Wah Engineering College, University of Wah, Quaid Avenue, Wah Cantt, Pakistan.*
[4]*Department of Chemical Engineering, University of Karachi, Main University Road,Gulshan-e-Iqbal, Karachi-75270, Pakistan.*

*Correspondence: ammarahbatool@ntu.edu.pk

Email address: [b)] khurram.shahzad@wecuw.edu.pk, [c)] afarrukh@wecuw.edu.pk [d)], fadia.sohail@wecuw.edu.pk, [e)]aisha.akbar@wecuw.edu.pk, [f)] aqsak5002@gmail.

***Abstract*—Due to the depletion of fossil fuel resources in gasoline as well as the developing issue with atmospheric carbon dioxide levels and related warming developments, it is becoming increasingly important to produce the next generation of renewable liquid transportation fuels. The most readily accessible bioresource is lignocellulosic biomass, which may be produced on a global scale at a rate of up to 1.3 billion tonnes per year. Various natural acids, phenols, and aldehydes, as well as a variety of reducing sugars that are highly prized in the production of biofuels like bioethanol and biogas, are released during the hydrolysis of lignocellulosic biomass. The majority of lignocellulosic biomass is made up of organic polymers notably cellulose, hemicellulose, and lignin that are strongly linked to one another using covalent and hydrogen bonds, creating a very sturdy structure. Numerous pretreatment strategies are developed as a way to decorate the separation of these interlinked components to take most enjoy the constitutes of the lignocellulosic biomasses. maximum commonplace pretreatment methods consist of bodily, chemical, physicochemical and biological processes. This evaluation's goal is to examine the various pretreatment strategies now in use and provide an outline of the way they are applied.**

Keywords—Energy, Biofuels, Pretreatment, Lignocellulosic Biomass, Cellulose, Lignin, Reducing Sugars, structure

I. INTRODUCTION

The enthusiasm in developing indispensable kinds of power is burgeoning due to bilateral perquisites within the subject of fiscal system and terrain. Because the impact of backwaters, videlicet crude oil painting, at the eco-device, the turbulence inside the charges of gas and because of elevating fitness enterprises, the conception of farther refinement in the coffers of power is farther adjoined [1].

As a renewable, generous on-edible raw material, lignocellulosic biomass has garnered more and more attention over the former couple of decades. It considerably exists in woody factory, herbaceous factory, submarine factory, forestry and agrarian remainders, marketable

and external strong waste, and so forth, and several studies have proven that lignocellulose may be converted to biofuels and cost- introduced chemical substances and accoutrements in biorefinery procedure. With reactionary gas because the number one source, 80% of the electricity demand around the world is fulfilled through the consumption of petroleum products [2].In keeping with the sector strength outlook from global strength business enterprise, 1 by way of 2040, worldwide strength demand will boom through about 40% [3].

The worldwide strength company estimates that worldwide biofuel manufacturing will grow by way of over 16 between 2016 and 2022 [4].Global bioenergy stocks are more than enough to meet expected biofuel and biomass deliveries without putting food products in direct competition. Lignocellulosic biomass can be obtained from a variety of sources, including shrubby foliage, herbaceous flowers, agrarian waste (such as sludge stover, sludge cob, wheat stover, carbohydrates club bagasse, and so forth.), wooded area waste (such as sawdust, and so forth.), marketable and external stable waste (such as Office waste paper, waste review, chipboard paper tinderbox, and numerous others.[5].Growing the mass consumption of fossil energies reasons force reduction, air adulterants, global rainfall trade, and irrevocable detriment to the surroundings. Greater conduct are centered on the renewable power for a sustainable increase of the public to drop the worldwide environmental troubles[6][7] .In addition, biofuels have the capacity to give other environmental blessings inclusive of upgrades in soil first- class, water affable, sustainability, and biodiversity [8].The green use of biomass coffers is essential for the urgency in dwindling or ending the use of fossil energies, particularly for those far off areas where the progeny admission to other power sources is not possible [9].Thermochemical biofuels may be constantly produced regionally at the same time as perfecting alternate balance and country wide security [7].It has been projected that lignocellulosic biomass could make up 442 billion liters of bioethanol and that overall crop leftovers and lost foliage might create 491 billion liters of bioethanol in a year, or about 16 percent more than the current global bioethanol output. [10].Due to its global void and enormous potential for its transformation into sugars, essential energy, and chemical feedstocks, the declination of cellulosic textile has drawn increasing attention from researchers. [11].Alcohol is a versatile feedstock used to create colored natural chemical compounds and their derivatives, and it is also utilized as a cleanser. Alcohol is produced piecemeal from a volition to gas. Soupy, stiff, and cellular ingredients are the abecedarian basic materials for the fermentation of ethanol. Since agrowastes are located outside of them and are readily available, cellulosic raw materials are becoming the main exploration thrust. The production of energy and chemicals from lignocellulosic biomass involves a variety of processes, including feedstock selection, pretreatment, separation, enzymatic hydrolysis (saccharification), processing, product restoration, and waste management. [11]

II. CLASSIFICATION OF LIGNOCELLULOSIC BIOMASS

Since they are readily available throughout the year, the four most significant (agricultural wastes. Rice straw, wheat straw, corn straw, and bagasse) are the best resources for the synthesis of bioethanol. [12]

A viable renewable resource for producing several types of biofuels and bio-based industrial chemicals is lignocellulosic biomass materials, which make up the majority of sustainable carbon tissue organization.[13].

The high resistance of lignocellulosic biopolymers to microbial or enzymatic disruption, however, amounts to outlandishly high prices for biorefinery designs. In specifically, the conversion of lignocellulosic biomass into biofuels (such as bioethanol) involves five operational steps: instruction of raw resources, pretreatment, enzymatic hydrolysis, fermentation, and product purification (e.g. separation and distillation).[12].Sugars, oils, starches, and lignocelluloses are the main types of plant biomass used for commercial purposes [14].Easy sugars from saccharide biomass, oils from oleaginous biomass, amylaceous compounds from starchy biomass, and cellulose, hemicellulose, and lignin from lignocellulosic biomass are all included in this group, which alludes to the active molecules created upon their decomposition [15].However, it requires a specific model based on value-competitive, sustainable, and biorefining production methods in order to ensure a hit utility. [16].

Therefore, the idea of utilizing green chemistry concepts in biorefineries for supply, fabric efficiency, energy enhancement, minimizing toxicity and waste generation, as well as increasing the reusability of products after their lifespan has ended, has garnered various concerns and discussion.[12].First generation ethanol production has been correctly commercialized the use of starch-based totally feedstock [17].There may be increasing hobby in converting lignocellulosic biomass to ethanol because of its low environmental influences, first-rate useful resource availability, aggressive feedstock rate with oil at $20/barrel, and capacity to reduce the usage of food for gasoline manufacturing [18].

III. PRETREATMENT OF LIGNOCELLULOSIC BIOMASS

It is crucial to have a fundamental grasp of the chemical makeup and material composition of lignocellulosic biomass in order to better understand how it reacts in pretreatment processes for the formation of fermentable sugars. The house has a massive effect on the pretreatment conditions employed as well as its effectiveness [19].Figure 1 shows the schematic treatment of lignocellulosic biomass .

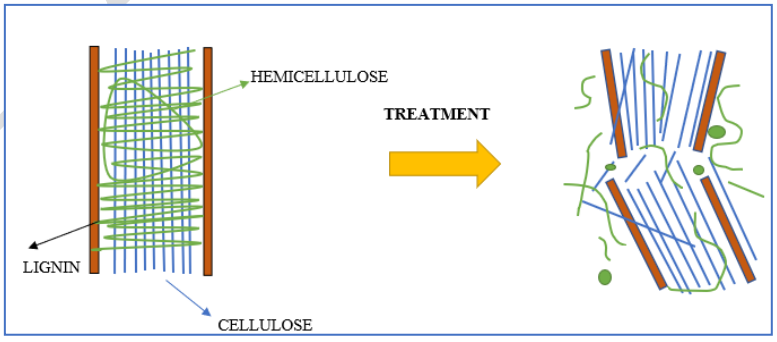

Fig 6. Schematic of Treatment of lignocellulosic biomass

The three polymers cellulose, hemicellulose (a carbohydrate polymer), and lignin (a phenolic polymer) make up the majority of biomass, with trace amounts of pectin, proteins, extracts, and ash. The type of biomass can affect this composition[20] .

TABLE 1 EFFECTS OF TREATMENT

Physical	Chemical	References
Reducing size of materials	Breaking of lignocellulosic bond using solvents	[20]
Amplify the surface area	Depolymerization	[20]

Protracted compounds must be depolymerized into monomers that serve as starting materials for other packaging because these polymers are only occasionally used.[9]. Utilizing three distinct processes—biomass pretreatment, hydrolysis, and fermentation—lignocellulosic biomass is organically converted into biofuels or specific compounds. To breakdown local plant biomass resistive systems and increase sugar yield, pretreatment is necessary.[21].

Breaking the lignocellulosic link, increasing the porosity of lignocellulosic materials, and reducing cellulose crystallinity are the goals of the treatment. [22]. Hexoses (glucose, mannose, and galactose), pentoses (xylose, arabinose), uronic acids (glucuronic acid, methyl glucuronic acid, and galacturonic acid), and deoxyhexoses are all found in hemicellulose, an amorphous polysaccharide (rhamnose, fucose). Cellulose is an extremely stable polysaccharide comprised of a linear arrangement of molecules with hydroxyl groups in equatorial affiliations and more than 10,000 glucose subunits connected by (-1-4)-glycosidic connections. Cellobiose, a glucose dimer, is actually the cellulose's monomeric unit. [23].

Lignin bonds with cellulose and hemicellulose and offers mechanical energy and chemical resistance to the cellular wall [24].Phenylpropanoid biopolymer, which composes lignin, gives plants their strength. The cellulose and hemicellulose that make up the total biomass are securely bound to the lignin molecules by covalent and hydrogenic linkages, giving the structure tremendous strength and resistance to pretreatment techniques.[25].The lignin substance is well-known as the second-best indestructible herbal natural polymer, conveying the best active ingredient of all the aforementioned compounds, enabling vegetation to build impervious chemical systems, and providing a chance for the hydrolysis of cellulose and hemicellulose in lignocellulosic biomass [26]. The quantities of various polymeric constituents within the cell wall structures of feedstocks vary depending on a variety of parameters, including the kind of feedstocks, the growth environment, the time of year, the activity of harvesting and collecting, the handling of materials, storage, etc. [24].

IV. CONVERSION OF LIGNOCELLULOSIC BIOMASS

Conversion of lignocellulosic biomass consist of hydrolysis of biomass then fermentation process to produce alcohol and finally the product after purification

V. CLASSIFICATION OF PRETREATMENT TECHNIQUES

Pretreatment techniques usually consist of physical, chemical, physico-chemical and biological methods that are further summarized in the table 2

TABLE 2 PRETREATMENT TECHNIQUES

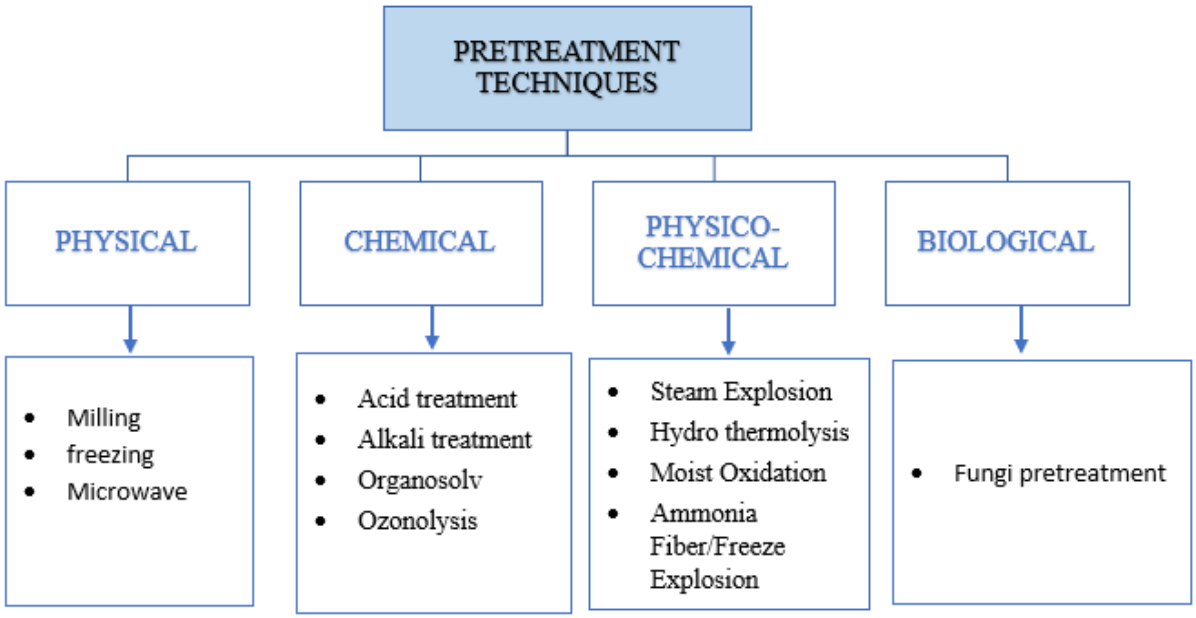

A. Physical Pretreatment

The changes in the biomass's particular floor area, particle sizes, particle density, or level of polymerization are caused by a bodily preparation. By avoiding the use of chemical substances, physical preparation reduces the production of waste and barriers for later reactions [26]. A variety of research works have used specially designed (dry/wet, centrifugal, jet, and vibratory) roller milling and pressure milling alone or in combination with various techniques (acid, enzyme, and irradiation) to make material handling easier in subsequent processing in the past [27]. Biomass that has undergone physical pretreatments such as milling, grinding, and freezing can expand its ground area. Wet disc milling and ball milling are commonplace pretreatments for body parts. The most important disadvantage of milling is immoderate electricity requirement. It has been cautioned the wet disk milling can reduce strength requirement evaluating to specific milling pretreatment strategies, however alternatively, ball milling has been said to offer a higher glucose and xylose yield after enzymatic hydrolysis[1].

Extrusion is each different common bodily method. Extrusion motives depolymerization of cellulose, hemicellulose, lignin, and protein[27].

As a novel technique, cryogenic pretreatment is now being researched. This strategy is based on the idea that during the freeze-thaw process, the bulk of the hydration layer around the macromolecules in the wood molecules may be disturbed. Crystallization at the point of freezing also produces a breaking force. This strain degrades various lignocellulosic systems. The freezing pre-treatment is an environmentally friendly and cost-effective method because it doesn't utilize any chemicals or catalysts. [28].

Additionally, there is a lot of interest in microwave (MW) radiation as a potential processing technique to improve the extractability of biomass materials. Pretreating lignocellulosic materials using a microwave has been used extensively. Woody materials are microwave-irradiated for a brief amount of time during microwave pretreatment. The possibility of MW pretreatment has been demonstrated to be effective in dismantling complicated systems and rupturing natural molecules, which is essential for the release of both intracellular and extracellular material, which in turn will boost the accessibility and bioavailability of a substrate.[29].

B. Chemical Pretreatment

a) Acid Treatment

The lignocellulosic structure can be ruptured by the acid treatment approach, which transforms polysaccharides into oligomeric and monomeric sugars. The most popular concentrated acids for treating with cellulosic biomass were sulfuric acid and hydrochloric acid, respectively. For hydrolysis of cellulose, it is effective. However, they are hazardous, corrosive, and poisonous, necessitating the use of corrosive-resistant reactors and the recovery of concentrated acid following hydrolysis in order to make the treatment practicable. Consequently, Lignocellulosic materials have been properly pretreated using diluted acid hydrolysis. A wide variety of feedstocks, such as wastepaper, municipal strong waste, softwood, hardwood, grassland crops, and agricultural residues, have been used in its combination. With the majority of biomass materials, it functioned properly. Hydrochloric acid, nitric acid, phosphoric acid, and sulfuric acid were all examined for use in biomass pretreatment. The preferred acid is frequently diluted sulfuric acid. When hemicellulose is mixed with biomass, it becomes solubilized, improving the accessibility of the cellulose inside the biomass. This mixture can be heated both concurrently and indirectly through the vessel walls or with steam, as in steam pretreatment.[22]

b) Alkali Treatment

One of the most extensively investigated processes is alkali treatment, which includes use of a series of bases, including aqueous ammonia, ammonia hydroxide, sodium hydroxide, potassium hydroxide, calcium hydroxide (lime), and a mixture of those bases with hydrogen peroxide.. [30]

Alkaline pretreatment chemicals, such as sulfite and sulfuric acid, are far less caustic than their acidic counterparts. Alkaline pretreatments are finished in kinder conditions, some of

them even at cellar temperature, as demonstrated by soaking in sodium hydroxide or ammonium hydroxide. With these techniques, the requirement for premium alternatives and unique designs to handle rusting and harsh reaction conditions can be eradicated. [31]. Lignin and hemicellulose dissolution as well as the de-esterification (saponification) of intermolecular ester bonds are the two main reactions that occur during the alkaline pretreatment process. Moreover, they adjust the DP (monomeric units) of each issue and alter the physical properties of treated solids. These modifications might also include changes to the porosity, crystallinity, and position of the ground.

c) Organosolv

The organosolv approach has been widely utilized to extract significant amounts of lignin. Again, the cellulose fibers in the biomass become accessible to hydrolytic enzymes when the lignin is eliminated, and the absorption of cellulolytic enzymes to the lignin is decreased, resulting in a better conversion of the biomass. Ethanol, methanol, ethylene glycol, and acetone are the solvents that can be used most frequently and extensively. An acid, a base, or a salt are used as enzymes.[22]

d) Ozonolysis

Lignin content can be diminished in lignocellulosic wastes by using ozone treatment. The pattern's moisture content, the particle period, and the ozone consciousness inside the gas drift are the three essential criteria in ozonolysis. As an added benefit, the method no longer results in the creation of any inhibitory compounds and is completed under normal stress conditions at room temperature. Ozonolysis, however, costs a lot of money because it uses a lot of ozone. [30]. The nonlinear triatomic molecule ozone is incredibly reactive and nonlinear, and it is found in compounds with double bonds and other beneficial companies that have high electron densities. Consequently, due to its high quantity of double bonds, lignin is more likely to be oxidized during this process.[32].

TABLE 3 ADVANTAGES AND DISADVANTAGES OF CHEMICAL TECHNIQUES

CHEMICAL TECHNIQUES	ADVANTAGES	DISADVANTAGES	References
Acid Treatment	Gain excessive response	Formation of degradation products	[33]
	Significantly enhance hemicellulose and cellulose hydrolysis	More costly than others	[12]
		Corrosive for reactors	[34]

Alkali Treatment	Requires lower condition of temperature and pressure	Less effective	[35]
	Less degradation	Conversion of alkali into irrecoverable salts	[36]
Organosolv	Effective to remove lignin	Costly	[19]
	Doesn't require size reduction	Hazardous	[20]
Ozonolysis	Effective to remove lignin	It is expensive as large amount of ozone required	[20]
	Works at normal conditions		[37]

C. Physiochemical Pretreatment

Physicochemical strategies are pre-treatment techniques that use a balanced method to affect the physical parameters (stated previously) as well as their reaction mechanisms (bond cleavage) and intermolecular interactions. In these techniques, elements such as temperature or pressure are used in conjunction with a chemical procedure.[36]. Figure shows a typical schematic illustrating the effects of fast decompression on a porous community; this graphic omits the various aspect reactions that could take place when using Co2 or ammonia.

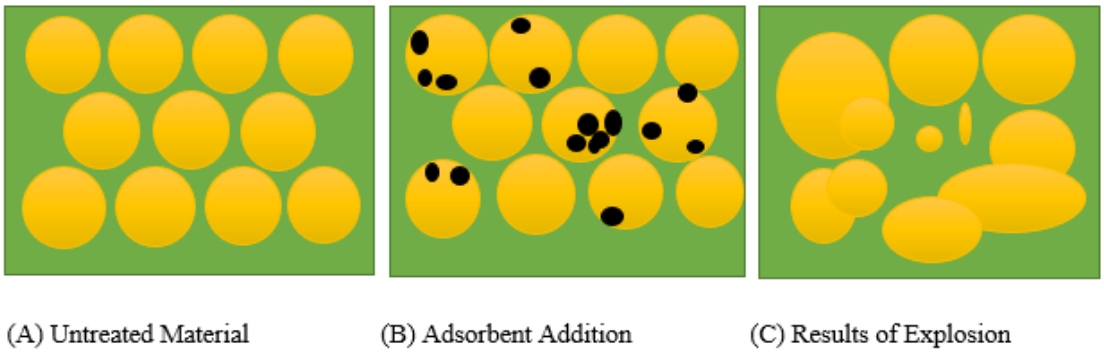

Fig 2. Representation of porous network of lignocellulose waste and the pressure induced explosion pretreatment

a) Steam explosion

One of the most popular pretreatment methods is steam explosion, which disrupts the lignocellulosic fabric's shape through both chemical and physical methods. [34]. Steam explosion breaks down lignin and hemicelluloses while also softening the cellulose in the biomass by combining physical ripping with chemical high-temperature frying. [38]. In this operation, biomass is first chipped, ground, or definitely uncooked preconditioned, then physically treated with high-strain saturated steam at pressures between 0.7 and 4.8 MPa and temperatures of around 160-240 °C. To encourage hemicellulose hydrolysis, the strain is held for a short while up to three minutes before being released. High temperatures used in the process result in the breakdown of hemicellulose and the transformation of lignin, which increases the capacity of cellulose hydrolysis..[22]

As has already established, this process successfully destroys the lignocellulosic structure by a combination of chemical and physical interactions. As part of the chemical pretreatment, the hemicellulose and cellulose forms are hydrolyzed to liberate their glycosidic bonds and to remove or redistribute lignin. The conversion of those acetyl agencies into acetic acid as well as the acidic nature of the water at high temperatures will promote a similar hydrolysis of the hemicellulose. Approximately during the brief decompression of the device, the physical preparation takes place. As a result of this quick growth, the molecular connections are broken, the saturated water inside the fibrils is evaporated, and a powerful lignocellulosic matrix is produced.

b) Hydro-Thermolysis

Hydro thermolysis is a process that uses liquid water under pressure at high temperatures. Other names for the process are strain-cooking in water, autohydrolysis, and hydrothermal remedy. It has typically been used in investigations involving annual plants and hardwood lignocellulosic materials.[39].

This technique uses heated water pressure to cook biomass at a high temperature in water. During pretreatment, water might enter the biomass cell form, hydrating cellulose, solubilizing hemicellulose, and scarcely removing lignin. As a result, it has been widely employed to increase the output of biogas from a variety of lignocellulosic feedstock, such as biomass wastes and every crop used for electricity generation (such as sunflower stalks and sugarcane bagasse). It is a useful technique for increasing cellulose's degradability and expanding its vulnerable floor location (paper residuals, municipal strong wastes)[40].

c) Wet Oxidation

Wet oxidation (WO) is an aqueous excessive temperature excessive stress pretreatment technique, that makes use of oxidative marketers. The mechanism lies on customary hydroxyl radicals, and automobile catalyzing thru fashioned natural acids[37]. The solubilization of the acidic hemicellulose components, desertification of the acetate companies at the hemicellulose, and oxidation are the usual ways that acids are produced. The pH decreases and the acid attention increases, which favors hydrolytic reactions. More and more of the hemicelluloses are fragmented into smaller, water-soluble particles with lower molecular weights. This reaction also effects the cellulose and lignin fractions in addition to the hemicelluloses. After

moist oxidation, cellulose undergoes a significant increase in the rate of acid hydrolysis, which increases the material's accessibility.[41].

d) Ammonia Fiber/Freeze Explosion

The biomass material is exposed to liquid anhydrous ammonia at high pressures and low temperatures in the ammonia fiber/freeze explosion (AFEX) equipment before being immediately depressurized. In contrast to steam explosion preparation, this procedure. As a result, there is a lot less energy input and regular process costs because the low temperatures (60°C to 100°C) are so much lower than those of the steam explosion method.[34]. Ammonia has a significant impact on ions (cations and anions), specific solvating properties, thermal and chemical stability, non-flammability, and low vapor strain. [30]. AFEX pretreatment alters the form of biomass, improving its capacity to retain water and its digestibility. [42].

TABLE 4 ADVANTAGES AND DISADVANTAGES OF PHYSIOCHEMICAL PRETREATMENT

Physiochemical pretreatment	Advantages	Disadvantages	References
Steam explosion	Requires low energy	Incomplete breakage of lignin bonds	[37]
	Less use of chemicals	Formation of degradation product	[20]
Hydrothermolysis	Less formation of degradation products Low cost	Requires high energy	[20]
Wet oxidation	Treatment for waste	High cost	[30]
Ammonia Fiber/Freeze Explosion	Sugar yield increased	Costly	[35]

D. Biological Pretreatment

The Biological pretreatment is regarded as an effective, environmentally secure, and low-power method among this type of pretreatment that also includes physiological, chemical, and physicochemical processes. To decompose hemicellulose, lignin, or remove particular additives, such as antimicrobial compounds through microbe's oxidation of the substrate, lignocellulosic biomass is subjected to biological pretreatment. The removal of lignin and hemicelluloses from solid wastes during this process involves the use of several microorganisms in addition to brown, white, and smooth-rot fungi, however the rate of decay during this process is often quite slow. While white- and smooth-rot fungi both target cellulose

and lignin, brown-rot fungi frequently target cellulose. Over the course of the movement, lignin is broken down with the help of white-rots traces. of the peroxidases and laccase lignin-degrading enzymes. Over the course of the movement, lignin is broken down with the help of white-rots traces. of the peroxidases and laccase lignin-degrading enzymes.[43]

The white-rot fungi Phanerochaete chrysosporium, Ceriporia lacerata, Cyathus stercolerus, Ceriporiopsis subvermispora, Pycnoporus cinnarbarinus, and Pleurotus ostreaus are frequently used for pretreatment. With the exception of the fact that those various basidiomycetes species have also been investigated for the degradation of numerous lignocellulosic feedstocks. Bjerkandera adusta, Fomes fomentarius, Ganoderma resinaceum, Irpex lacteus, Phanerochaete chrysosporium, Trametes versicolor, and Lepista nuda are some of the species that have been well investigated. [33]. Some white-rot fungi have the capacity to break down lignin concurrently. When combined with a particular white-rot fungus, provisional and polysaccharides, which result in the loss of carbohydrates, can selectively break down lignin. Involved extracellular enzymatic systems in bacteria include one ligninolytic system and two hydrolytic systems. The hydrolytic apparatus breaks down the cellulose and hemicelluloses, whereas the ligninolytic apparatus breaks down the lignin. Lignin can be broken down by using enzymes produced by many organisms, of which white-rot fungus has been found to be the simplest. Fungi are typically isolated from soil, developing plants, or agricultural waste.[44]

E. Diverse Combos of Pretreatment Techniques

As a result of continual growth of research and development. Pretreatment techniques can now be developed that are more effective, economical, and eco-friendly thanks to a plethora of technological advancements. The fact that not enough research has been done to decide which technique among these tactics is the most successful means that some of them are still able to realize their aspirations from those times. Therefore, to overcome the current shortcomings of each, a combination of two or three pretreatment techniques may be effective. Pretreatment techniques that are both physical and chemical include planetary milling, organosolv, chemically aided mechanical, ozonolysis, and ball milling, as well as physical and organic (organosolv and dilute sulfuric acid) (fungal and milling pretreatment),both chemical and (dilute sulfuric acid and sodium hydroxide , sodium hydroxide and ionic liquid), Examples of chemical and physical reactions, organic and chemical reactions, and natural and physical reactions include white/brown rot fungi and mild acid, white rot fungi and diluted sulfuric acid, white rot fungi and sodium hydroxide, white rot fungi and hydrogen peroxide, and steam explosion and hydrogen peroxide (white-rot fungi and steam explosion)[44]

VI. CONCLUSION

The hemicellulose and lignin matrix combine to produce a solid lignocellulosic biomass structure. Pretreatment is therefore an important stage in the conversion of lignocellulosic biomass into sugars as well as in the creation of bioproducts and biofuels that are necessary for the industrial sector. Numerous studies have examined how different pretreatment techniques affect lignocellulosic composition and sugar yield. We conclude after evaluating a number of methods that each one has advantages and disadvantages. Physical pretreatment can decrease crystallinity and boost reactivity by shortening particle length, but it cannot get rid of lignin.

Consequently, lignin can nevertheless serve as a barrier and restrict cellulose's access to the subsequent processing. For the conversion of lignocellulose cloth, chemical pretreatment methods like the use of solvents or a mixture of them have a number of disadvantages, including the corrosivity of acids and bases. Physicochemical pretreatment like WO, hydro thermolysis, and steam explosion coverts the lignocellulosic substances into monosaccharides through manner of enhancing the elimination of lignin and developing the overall performance of the hydrolysis gadget but they as steeply-priced and need enhancement to have end up viable. Organic pretreatment is considered due to the fact the bottom fee and environmentally excellent technique. However, in maximum organic pretreatment processes, the fee of hydrolysis might be very low. As a consequence, thinking about all the techniques greater studies and development desired on the way to make greater appropriate techniques, device, and structures for pretreatment of lignocellulosic substances.

REFERENCES

[1] E. Shirkavand, S. Baroutian, D. J. Gapes, and B. R. Young, "Combination of fungal and physicochemical processes for lignocellulosic biomass pretreatment - A review," *Renew. Sustain. Energy Rev.*, vol. 54, pp. 217–234, 2016, doi: 10.1016/j.rser.2015.10.003.

[2] W. H. Chen, B. J. Lin, M. Y. Huang, and J. S. Chang, "Thermochemical conversion of microalgal biomass into biofuels: A review," *Bioresour. Technol.*, vol. 184, pp. 314–327, 2015, doi: 10.1016/j.biortech.2014.11.050.

[3] F. Birol, L. Cozzi, A. Bromhead, T. Gould, and M. Baroni, *World Energy Outlook 2014*. 2014.

[4] W. Li, A. Ghosh, D. Bbosa, R. Brown, and M. M. Wright, "Comparative Techno-economic, Uncertainty and Life Cycle Analysis of Lignocellulosic Biomass Solvent Liquefaction and Sugar Fermentation to Ethanol," *ACS Sustain. Chem. Eng.*, vol. 6, no. 12, pp. 16515–16524, 2018, doi: 10.1021/acssuschemeng.8b03622.

[5] F. Hu and A. Ragauskas, "Pretreatment and Lignocellulosic Chemistry," *Bioenergy Res.*, vol. 5, no. 4, pp. 1043–1066, 2012, doi: 10.1007/s12155-012-9208-0.

[6] Y. D. Singh, P. Mahanta, and U. Bora, "Comprehensive characterization of lignocellulosic biomass through proximate, ultimate and compositional analysis for bioenergy production," *Renew. Energy*, vol. 103, pp. 490–500, 2017, doi: 10.1016/j.renene.2016.11.039.

[7] S. X. Tan, S. Lim, H. C. Ong, and Y. L. Pang, "State of the art review on development of ultrasound-assisted catalytic transesterification process for biodiesel production," *Fuel*, vol. 235, no. July 2018, pp. 886–907, 2019, doi: 10.1016/j.fuel.2018.08.021.

[8] A. Bauen, J. Howes, L. Bertuccioli, and C. Chudziak, "Review of the potential for biofuels in aviation: Final report For CCC," *Fuel*, no. 284, pp. 6021–6025, 2009.

[9] Y. Huang *et al.*, "Fundamental Advances in Biomass Autothermal/Oxidative Pyrolysis: A Review," *ACS Sustain. Chem. Eng.*, vol. 8, no. 32, pp. 11888–11905, 2020, doi: 10.1021/acssuschemeng.0c04196.

[10] S. Kim and B. E. Dale, "Global potential bioethanol production from wasted crops and crop residues," *Biomass and Bioenergy*, vol. 26, no. 4, pp. 361–375, 2004, doi: 10.1016/j.biombioe.2003.08.002.

[11] S. Hari Krishna and G. V. Chowdary, "Optimization of simultaneous saccharification and fermentation for the production of ethanol from lignocellulosic biomass," *J. Agric. Food Chem.*, vol. 48, no. 5, pp. 1971–1976, 2000, doi: 10.1021/jf991296z.

[12] N. Sarkar, S. K. Ghosh, S. Bannerjee, and K. Aikat, "Bioethanol production from agricultural wastes: An overview," *Renew. Energy*, vol. 37, no. 1, pp. 19–27, 2012, doi: 10.1016/j.renene.2011.06.045.

[13] K. P, B. D.M, D. M.J, and S. P, "Methods for pretreatment of lignocellulosic biomass for efficient hydrolysis and biofuel production," *Ind. Eng. Chem. Res.*, vol. 48, no. 8, pp. 3713–3729, 2009.

[14] S. Vaz, "Biomass and the green chemistry principles," *Biomass Green Chem. Build. a Renew. Pathw.*, pp. 1–9, 2017, doi: 10.1007/978-3-319-66736-2_1.

[15] V. Faraco, "Lignocellulose conversion: Enzymatic and microbial tools for bioethanol production," *Lignocellul. Convers. Enzym. Microb. Tools Bioethanol Prod.*, no. March 2013, pp. 1–199, 2013, doi: 10.1007/978-3-642-37861-4.

[16] S. K. Brar, G. S. Dhillon, and C. R. Soccol, "Biotransformation of waste biomass into high value biochemicals," *Biotransformation Waste Biomass into High Value Biochem.*, vol. 9781461480, no. January 2016, pp. 1–504, 2014, doi: 10.1007/978-1-4614-8005-1.

[17] E. Warner, K. Moriarty, J. Lewis, A. Milbrandt, and A. Schwab, "2015 Bioenergy Market Report BIOENERGY TECHNOLOGIES OFFICE," no. February, 2013.

[18] M. Wang, J. Han, J. B. Dunn, H. Cai, and A. Elgowainy, "Well-to-wheels energy use and greenhouse gas emissions of ethanol from corn, sugarcane and cellulosic biomass for US use," *Effic. Sustain. Biofuel Prod. Environ. Land-Use Res.*, pp. 249–280, 2015, doi: 10.1088/1748-9326/7/4/045905.

[19] M. Jędrzejczyk, E. Soszka, M. Czapnik, A. M. Ruppert, and J. Grams, *Physical and chemical pretreatment of lignocellulosic biomass*. 2019. doi: 10.1016/B978-0-12-815162-4.00006-9.

[20] S. Rahmati *et al.*, "Pretreatment and fermentation of lignocellulosic biomass: Reaction mechanisms and process engineering," *React. Chem. Eng.*, vol. 5, no. 11, pp. 2017–2047, 2020, doi: 10.1039/d0re00241k.

[21] J. Zhang, X. Zhang, M. Yang, S. Singh, and G. Cheng, "Transforming lignocellulosic

biomass into biofuels enabled by ionic liquid pretreatment," *Bioresour. Technol.*, vol. 322, p. 124522, 2021, doi: 10.1016/j.biortech.2020.124522.

[22] S. Briefs and I. N. Molecular, *SPRINGER BRIEFS IN MOLECULAR SCIENCE Pretreatment of Lignocellulosic Biomass for Biofuel Production*.

[23] P. A. Julien, T. Fri, and P. Julien, "Deconstruction of lignocellulosic biomass with ionic liquids," *Green Chem.*, no. 207890, pp. 2729–2747, 2017.

[24] S. Naik, V. V Goud, P. K. Rout, K. Jacobson, and A. K. Dalai, "Characterization of Canadian biomass for alternative renewable biofuel," *Renew. Energy*, vol. 35, no. 8, pp. 1624–1631, 2010, doi: 10.1016/j.renene.2009.08.033.

[25] V. K. Ponnusamy *et al.*, "A review on lignin structure, pretreatments, fermentation reactions and biorefinery potential," *Bioresour. Technol.*, vol. 271, pp. 462–472, 2019, doi: 10.1016/j.biortech.2018.09.070.

[26] U. Wietelmann and M. Steinbild, "Lithium and Lithium Compounds," *Ullmann's Encycl. Ind. Chem.*, pp. 1–38, 2014, doi: 10.1002/14356007.a15_393.pub2.

[27] M. Hjorth, K. Gränitz, A. P. S. Adamsen, and H. B. Møller, "Extrusion as a pretreatment to increase biogas production," *Bioresour. Technol.*, vol. 102, no. 8, pp. 4989–4994, 2011, doi: 10.1016/j.biortech.2010.11.128.

[28] V. Rooni, M. Raud, and T. Kikas, "The freezing pre-treatment of lignocellulosic material: A cheap alternative for Nordic countries," *Energy*, vol. 139, pp. 1–7, 2017, doi: 10.1016/j.energy.2017.07.146.

[29] F. M. Pellera and E. Gidarakos, "Microwave pretreatment of lignocellulosic agroindustrial waste for methane production," *J. Environ. Chem. Eng.*, vol. 5, no. 1, pp. 352–365, 2017, doi: 10.1016/j.jece.2016.12.009.

[30] S. Behera, R. Arora, N. Nandhagopal, and S. Kumar, "Importance of chemical pretreatment for bioconversion of lignocellulosic biomass," *Renew. Sustain. Energy Rev.*, vol. 36, pp. 91–106, 2014, doi: 10.1016/j.rser.2014.04.047.

[31] J. S. Kim, Y. Y. Lee, and T. H. Kim, "A review on alkaline pretreatment technology for bioconversion of lignocellulosic biomass," *Bioresour. Technol.*, vol. 199, pp. 42–48, 2016, doi: 10.1016/j.biortech.2015.08.085.

[32] A. R. Mulakhudair, J. Hanotu, and W. Zimmerman, "Biomass and Bioenergy Exploiting ozonolysis-microbe synergy for biomass processing : Application in lignocellulosic biomass pretreatment," *Biomass and Bioenergy*, vol. 105, pp. 147–154, 2017, doi: 10.1016/j.biombioe.2017.06.018.

[33] A. K. Kumar and S. Sharma, "Recent updates on different methods of pretreatment of lignocellulosic feedstocks : a review," *Bioresour. Bioprocess.*, 2017, doi: 10.1186/s40643-017-0137-9.

[34] G. Brodeur, E. Yau, K. Badal, J. Collier, K. B. Ramachandran, and S. Ramakrishnan, "Chemical and physicochemical pretreatment of lignocellulosic biomass: A review," *Enzyme Res.*, vol. 2011, no. 1, 2011, doi: 10.4061/2011/787532.

[35] Y. L. Loow *et al.*, "Recent Advances in the Application of Inorganic Salt Pretreatment for Transforming Lignocellulosic Biomass into Reducing Sugars," *J. Agric. Food Chem.*, vol. 63, no. 38, pp. 8349–8363, 2015, doi: 10.1021/acs.jafc.5b01813.

[36] M. J. Taylor, H. A. Alabdrabalameer, and V. Skoulou, "Choosing physical, physicochemical and chemical methods of pre-treating lignocellulosic wastes to repurpose into solid fuels," *Sustain.*, vol. 11, no. 13, 2019, doi: 10.3390/su11133604.

[37] M. Badiei, N. Asim, J. M. Jahim, and K. Sopian, "Comparison of Chemical Pretreatment Methods for Cellulosic Biomass," *APCBEE Procedia*, vol. 9, no. Icbee 2013, pp. 170–174, 2014, doi: 10.1016/j.apcbee.2014.01.030.

[38] S. Meenakshisundaram, A. Fayeulle, E. Leonard, C. Ceballos, and A. Pauss, "Fiber degradation and carbohydrate production by combined biological and chemical/physicochemical pretreatment methods of lignocellulosic biomass – A review," *Bioresour. Technol.*, vol. 331, no. March, p. 125053, 2021, doi: 10.1016/j.biortech.2021.125053.

[39] M. Galbe and O. Wallberg, "Pretreatment for biorefineries: A review of common methods for efficient utilisation of lignocellulosic materials," *Biotechnol. Biofuels*, vol. 12, no. 1, pp. 1–26, 2019, doi: 10.1186/s13068-019-1634-1.

[40] nguyen thi Lieu, "No Title空間像再生型立体映像の 研究動向," *Nhk技研*, vol. 151, no. 5, pp. 10–17, 2015.

[41] V. B. Agbor, N. Cicek, R. Sparling, A. Berlin, and D. B. Levin, "Biomass pretreatment: Fundamentals toward application," *Biotechnol. Adv.*, vol. 29, no. 6, pp. 675–685, 2011, doi: 10.1016/j.biotechadv.2011.05.005.

[42] I. Method and C. Reagents, "Ammonia , Free." pp. 1–4.

[43] A. Manuscript, "Reaction Chemistry & Engineering," 2020, doi: 10.1039/D0RE00241K.

[44] J. Baruah *et al.*, "Recent trends in the pretreatment of lignocellulosic biomass for value-added products," *Front. Energy Res.*, vol. 6, no. DEC, 2018, doi: 10.3389/fenrg.2018.00141.

Gender Classification Using Novel Acoustics Deviated Local Ternary Patterns

Azmat Hayat [1, a*], M. Munwar Iqbal [1, b], Hafsa Ilyas [2, c], Ali Javed [2, d]
[1]*Computer Science Department, University of Engineering and Technology, Taxila, Pakistan*
[2]*Software Engineering Department, University of Engineering and Technology, Taxila, Pakistan*

Email address: [a)] azmat.hayat@uettaxila.edu.pk, [b)] munwar.iq@uettaxila.edu.pk, [c)] hafsailyas97@gmail.com, [d)] ali.javed@uettaxila.edu.pk

***Abstract*—Speech plays an important role in human-computer interaction and can be used in many applications like automatic speech recognition, forensic voice verification, speaker recognition, mobile banking, and shopping. Gender identification through voice has been a challenging task in the field of speech recognition and is considered as one of the crucial tasks for such applications. The extraction of useful and optimal features, presence of background noise, signal distortion, and variation in pitch and frequency, makes gender classification through speech very difficult. To overcome such challenges, we proposed a novel acoustic deviated local ternary patterns (DLTP) to represent the audio signal. DLTP features have the capability to capture the distinct speech attributes (pitch and frequency) of the male and female voices. The extracted features are then employed to train the k-nearest neighbor algorithm (KNN) for the accurate classification of gender. The proposed approach is evaluated on fluent speech commands and common voice datasets. The classification accuracy of 97% on common voice and 98.3% on fluent speech commands dataset demonstrate the effectiveness of our proposed method.**

Keywords— Automatic gender classification, acoustics deviated local ternary pattern, K-nearest neighbor.

I. INTRODUCTION

Voice biometrics are commonly used these days for user authentication to automate homes and different businesses due to the advancement in digital voice assistants and benefits over other modes of biometrics i.e., facial recognition. The human speech contains useful information including gender, age, emotion, and other distinctive traits of speaker. Gender detection from the speech is essential in human-computer interaction to improve e-commerce applications (i.e., Amazon, eBay), and also reduces the computation time during online gender-based search [1]. The mutual process for gender identification through voice is somewhat easy but it is challenging for automated systems to accurately identify the gender due to the presence of various artifacts such as environmental noise in the audio [2]. For classifying a gender using voice, it is essential to extract the unique features in term of frequency and pitch as each speaker has different voice depending on vocal cord.

In literature, researchers have explored different acoustic feature descriptors and used them with either machine learning or deep learning algorithms for voice-based gender classification. In [3], the optimal features were extracted from noise free and smooth acoustical data, using the two layers. In the first layer, fundamental frequency, spectral entropy, spectral flatness, mode frequency was computed while the second layer extracted mel-frequency cepstral coefficients (MFCC) features. The extracted features were then classified using k-nearest

neighbor (KNN) and support vector machine (SVM). In [4], two algorithms YIN and MFCC were utilized to classify gender through voice. Livieris et al. [5] introduced self-labeled ensemble-based algorithm called iCST-voting for recognizing gender through speech. This approach ensembled three self-labeled methods including tri-training, co-training and self-training for classifying gender and attained good preliminary results on deterring and voice gender datasets. Tursunov et al. [6] presented a convolution neural network (CNN) with multi attention module (MAM) for gender and age classification. MAM consists of frequency and time attention blocks that extracted important spatial and temporal features. This approach attained 96% accuracy for gender classification on common voice (CV) dataset. The method [6] provides the high recognition rate for males as compared to the females.

However, the detection of gender using acoustic features is still a challenging task due to the presence of background noise, speech signal distortion, varied pitch and frequency, age factor, etc. Moreover, the extraction of critical and optimal acoustic features is also very essential for accurate gender classification via voice. So, we proposed novel acoustics deviated local ternary patterns (DLTP) that extract useful features from voice samples for gender classification. The DLTP features are then classified using the subspace-KNN classifier. The key contributions of our work are:

- We propose novel acoustic deviated local ternary patterns for effectively capturing the unique and varying attributes of male and female voices for the classification of gender.
- We performed extensive experiments on two datasets to signify the effectiveness of our proposed framework for the identification of gender using speech samples.

II. PROPOSED METHODOLOGY

The detailed architecture diagram of the proposed method is shown in Fig. 1.

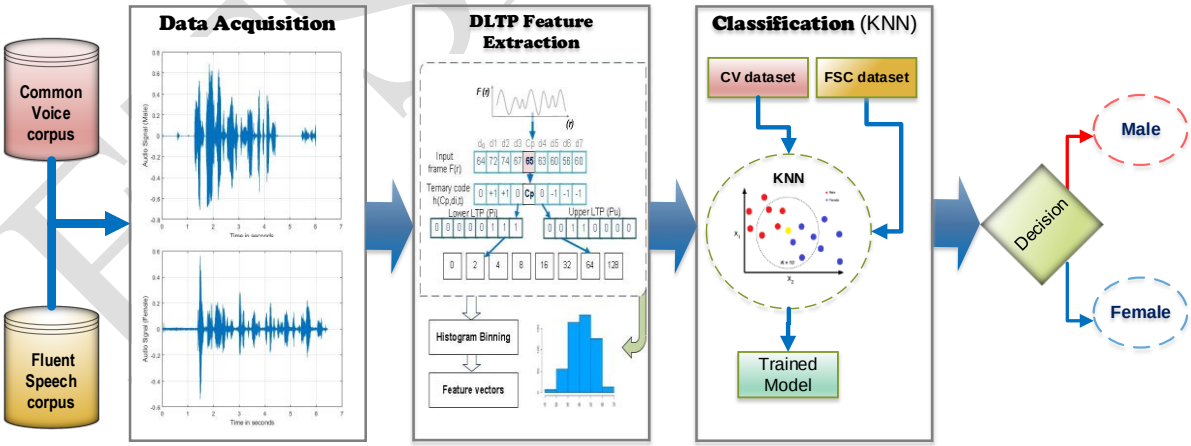

Fig 1. Architecture diagram of the proposed method

A. Acoustic Deviated Local Ternary Pattern

Audio features of the voice sample S[t] are extracted using the proposed deviated local ternary patterns. Every frame Fp of audio sample S[t] is encoded to locally compute the acoustic local ternary patterns (LTP). In order to calculate the LTP, we calculate the difference

between central sample Cp and its neighboring samples di which is the ith neighboring sample and belongs to neighborhood Fp centered at Cp, where i = 0,1, ... ,7. After assigning different tenderness threshold values, we finally compute the threshold value t as the half of the standard deviation $\boldsymbol{\sigma}$ of each audio signal. The calculation of $\boldsymbol{\sigma}$ and t is given by:

$$\sigma = \sqrt{\frac{1}{N}\sum_{i=1}^{n}(x_i - \mu)^2} \quad (1)$$

$$t = \frac{\sigma}{2} \quad (2)$$

The sample values are quantized to zero which are within the range of ±t around the central sample Cp. The sample values above Cp+t are set to 1 and below Cp-t are set to -1. So, the audio signal h(Cp, di, t) representation using three valued ternary pattern is given as:

$$h(C_p, d_i, t) = \begin{cases} 0 & (C_p + t) < d_i < (C_p - t) \\ +1 & d_i - (C_p + t) \geq 0 \\ -1 & d_i - (C_p - t) \leq 0 \end{cases} \quad (3)$$

The ternary patterns are further divided into upper patterns hu and lower patterns hl. In the hu pattern, all other values are replaced with zero except the +1 values. Similarly, in hl , except -1 values, all other values are replaced with 0. The upper and lower patterns are computed as:

$$\boldsymbol{h_u(C_p, d_i, t)} = \begin{cases} \mathbf{1} & \boldsymbol{h(C_p, d_i, t) = +1} \\ \mathbf{0} & \boldsymbol{otherwise} \end{cases} \quad (4)$$

$$\boldsymbol{h_l(C_p, d_i, t)} = \begin{cases} \mathbf{1} & \boldsymbol{h(C_p, d_i, t) = -1} \\ \mathbf{0} & \boldsymbol{otherwise} \end{cases} \quad (5)$$

To obtain optimal and most of the traits of audio sample, uniform patterns are very important. So, to obtain the lower uniform patterns and upper uniform patterns, we encode the decimal values of lower and upper patterns in hu and hl respectively, as in (6) and (7). After that, two histograms are computed from lower and upper codes and then concatenated to obtain the final 20-dimentional feature vector.

$$G_{F_p}^{(u)} = \sum_{i=0}^{7} h_u^{uni}(C_p, d_i, t) \quad (6)$$

$$G_{F_p}^{(l)} = \sum_{i=0}^{7} h_l^{uni}(C_p, d_i, t) \quad (7)$$

B. Classification

For classifying the voice samples of males and females, we trained the subspace-KNN classifier on acoustic DLTP feature vectors. For training the subspace-KNN, we set the number of learners and dimensions to 30 and 10, respectively. Training data consists of N pairs (yi, zi) where yi is the m-dimension feature vector and zi $\in\{0,1\}$ represents the class labels (male or female). From the set of features, random features are selected, and based on selected features,

random samples are taken from training data. For the given sample, k-nearest neighbors are computed among the randomly selected subspaces and the label of nearest neighbors is appended to list L, at each iteration. Finally, a frequently occurred label in L is assigned to the given sample.

III. EXPERIMENTS AND RESULTS

A. Datasets

We used the common voice [8] and fluent speech commands (FSC) dataset [9] to evaluate the efficacy of the proposed method. The FSC dataset comprises 52 male (14,837 voice samples) and 49 female (11,786 voice samples) speakers, each having 300-400 voice recordings of 1-3 seconds in different environments. Common Voice is a publicly available multilingual speech dataset containing audio samples of 3-7 seconds in mp3 format. We utilized the English subset of the CV dataset consisting of 775,989 audio samples (578,600 male and 197,389 female). For both datasets, 80% of the data is used for training and 20% is used for testing.

B. Performance Evaluation of the Proposed Approach

We designed an experiment to measure the performance of our approach on CV and FSC datasets to show its effectiveness while classifying gender via voice samples. For this purpose, we used the proposed DLTP features to train and test the subspace-KNN algorithm for the CV and FSC datasets individually.

Our approach attained an accuracy of 97%, precision of 93.5%, and sensitivity of 100% on the CV dataset. Whereas on the FSC dataset, we achieved 98.3% accuracy, 100% precision, and 97.9% sensitivity. However, the equal error rate (EER) value of 0.034% and 0.017% is achieved on the CV and FSC datasets respectively. It can be concluded from the results that our proposed DLTP feature descriptor can accurately capture the distinct characteristics of male and female voices such as pitch, frequency, etc. Thus, enables the classifier to accurately identify the gender of a person using voice.

C. Performance Evaluation on Different Classifiers

The objective of this experiment is to show the effectiveness of our DLTP descriptor against different classifiers while classifying gender via speech. For this, we extracted DLTP features set of audio samples from both datasets (CV and FSC) separately and evaluate on different classifiers.

The results for different classifiers are presented in Table I for both datasets. For the gender classification, subspace-KNN classifier attained the best results on both datasets (CV and FSC). Whereas cubic-SVM achieved the lowest accuracy and highest EER value on CV dataset. Likewise, for FSC dataset, fine-gaussian SVM attained highest EER and lowest accuracy. It can be concluded that proposed DLTP features performed best with subspace-KNN classifier. Thus, we utilized subspace-KNN for gender classification using the DLTP features of voice samples.

TABLE I. COMPARISON OF OUR DLTP FEATURES ON DIFFERENT CLASSIFIERS.

Algorithms	CV dataset (80-20)				FSC dataset (80-20)			
	EER	***Precision***	***Sensitivity***	***Accuracy***	***EER***	***Precision***	***Sensitivity***	***Accuracy***
Fine Gaussian-SVM	0.116%	82%	97%	91%	0.118%	100%	85.8%	88.2%
Cubic-SVM	0.148%	77.4%	99%	81%	0.019%	99.7%	97.9%	97.9%
Cubic-KNN	0.114%	82.3%	98%	88.4%	0.062%	99.7%	92.8%	94%
Subspace-KNN	**0.034%**	**93.5%**	**100%**	**97%**	**0.017%**	**100%**	**97.9%**	**98.3%**

D. Comparison with Existing Methods

We designed a comparative analysis experiment based on accuracy to evaluate the effectiveness of our proposed approach against other existing methods. We compared the performance of our method with these [6, 7, 10] on common voice dataset. Methods [6], [7] and [10] reported the accuracy of 96%, 96.4% and 91%, respectively. While our method attained an accuracy of 97% and average accuracy gain of 2.5% over contemporary methods. Thus, comparatively our method achieves the highest accuracy and can be effectively used for the classification of gender via voice samples.

IV. CONCLUSION

This paper has presented a gender classification approach based on voice using the novel DLTP feature descriptor. More specifically, we have proposed a novel deviated local ternary patterns and train the subspace-KNN classifier on 20-dimensional DLTP features for the classification of gender. The performance of our method is evaluated on two datasets named as fluent speech commands and common voice dataset. The experimental results indicated the good performance of our approach and revealed that our proposed feature descriptor can capture the discriminative and optimal features of male and female voice samples. In the future, we will extend our approach for the classification of gender using the multilingual speech samples.

REFERENCES

[1] O. Keyes, "The misgendering machines: Trans/HCI implications of automatic gender recognition," Proceedings of the ACM on human-computer interaction, vol. 2, no. CSCW, pp. 1-22, 2018.

[2] M. M. Nasef, A. M. Sauber, and M. M. J. A. A. Nabil, "Voice gender recognition under unconstrained environments using self-attention," vol. 175, p. 107823, 2021.

[3] M. A. Uddin, M. S. Hossain, R. K. Pathan, and M. Biswas, "Gender recognition from human voice using multi-layer architecture," in 2020 International conference on

innovations in intelligent systems and applications (INISTA), 2020: IEEE, pp. 1-7.

[4] M. Ardiana, T. Dutono, and T. B. Santoso, "Gender Classification Based Speaker's Voice using YIN Algorithm and MFCC," in 2021 International Electronics Symposium (IES), 2021: IEEE, pp. 438-444.

[5] I. E. Livieris, E. Pintelas, P. J. M. L. Pintelas, and K. Extraction, "Gender recognition by voice using an improved self-labeled algorithm," vol. 1, no. 1, pp. 492-503, 2019.

[6] A. Tursunov, J. Y. Choeh, and S. J. S. Kwon, "Age and Gender Recognition Using a Convolutional Neural Network with a Specially Designed Multi-Attention Module through Speech Spectrograms," vol. 21, no. 17, p. 5892, 2021.

[7] S. R. Zaman, D. Sadekeen, M. A. Alfaz, and R. Shahriyar, "One Source to Detect them All: Gender, Age, and Emotion Detection from Voice," in 2021 IEEE 45th Annual Computers, Software, and Applications Conference (COMPSAC), 2021: IEEE, pp. 338-343.

[8] Common Voice Dataset: Common Voice (mozilla.org), Accessed on September 26, 2022.

[9] Fluent Speech Commands Dataset: https://www.kaggle.com/datasets/tommyngx/fluent-speech-corpus, Accessed on September 26, 2022.

[10] A. A. Alashban and Y. A. Alotaibi, "Speaker Gender Classification in Mono-Language and Cross-Language Using BLSTM Network," 2021 44th International Conference on Telecommunications and Signal Processing (TSP), 2021, pp. 66-71, doi: 10.1109/TSP52935.2021.9522623.

Organized By:

Sponsored By:

HSK ENGINEERING

Bank Alfalah
The Way Forward

University of Wah,
Quaid Avenue,
Wah Cantt

Contact us: +92-51-9157000,
+92-51-905525256-7

Email: info@uow.edu.pk
http://uow.edu.pk